An Experimental Study of the Propagation of Equivalence Ratio Oscillations on their Effect on Combustion Instabilities

by

Joshua Glenn Walker

A thesis submitted to the Graduate Faculty of
Auburn University
in partial fulfillment of the
requirements for the Degree of
Master of Science

Auburn, Alabama
May 4, 2019

Keywords: combustion instabilities, chemiluminescence,
equivalence ratio, photomultiplier tube

Approved by

David Scarborough, Chair, Assistant Professor of Aerospace Engineering
Brian Thurow, Department Chair of Aerospace Engineering
Roy Hartfield, Professor of Aerospace Engineering

Abstract

Lean premixed combustors have become a promising method in gas turbine engines to operate more efficiently and within the regulatory standards for emissions. However, this lean premixed operation is susceptible to combustion instabilities within the combustor. These instabilities are a coupling between the heat release and pressure oscillations which is impacted by many factors, one of which is the fuel oscillations. This study analyzed the way in which fuel oscillations propagate through the mixing chamber and combustor utilizing optical diagnostics. A swirl combustor was designed and fabricated to be the test bed for these optical diagnostics to measure the equivalence ratio both before and in the flame. The first was the development and implementation of a helium-neon laser probe to measure equivalence ratio in the mixing chamber of the combustor. The second was a photomultiplier tube system that was utilized to measure chemiluminescence data that has shown to correlate well with equivalence ratio within the flame. These two optical diagnostics provided information about the fuel mixture before the flame and in the flame itself. The results showed that acoustic forcing increased the mixing both axially and radially. Furthermore, there was a drop in equivalence ratio oscillations across the swirler under acoustic forcing and under controlled oscillating conditions. Finally, the photomultiplier tube system proved accurate under lean steady state conditions but needs further verification under controlled oscillating conditions and acoustic forcing conditions.

Acknowledgments

I would like to thank Dr. Scarborough for providing me with this project and guiding me through the process of conducting useful and interesting research. Without his support and that of Auburn University I would not have been able to conduct this research. I am a much better engineer because of the faculty and staff that have taught and assisted me through graduate school.

I would also like to thank my wife, Ellie, and her support of me through graduate school. You have worked hard to get us to this point, and I am incredibly thankful for that. Lastly, I would like to thank my friends and family who have encouraged me through this process, it has meant so much along the way.

Table of Contents

List of Tables

List of Illustrations

List of Abbreviations

α	Absorption coefficient
c	speed of sound
HeNe	helium-neon
I	Measured absorption intensity
I_0	Initial absorption intensity
InAsSb	indium-arsenide-antimonide
k	bond force
L	Path length
n_f	moles of fuel
n_a	moles of air
P	Pressure
PMT	photomultiplier tube
ppm	parts per million
SLM	Standard Liter per Minute
x_f	Mole fraction
λ	fundamental vibration wavelength
μ	mass of the hydrogen atom

Chapter 1: Introduction

Gas turbine engines have become a widely used option for producing energy in situations that require power in remote places or during high load times. This includes situations such as combined cycle power plants, power in undeveloped nations, power in remote locations, and even power on ships. This is due to a number of advantages that gas turbine engines possess over conventional power generating systems. For instance, their size allows them to be transported easily and have large power densities. This allows for gas turbines to be used on mobile platforms as well as in remote areas. Furthermore, certain power generating gas turbine engines are designed to operate on over 50 gases and liquids.[1] This allows them to be utilized in undeveloped nations. Gas turbine engines can also produce power from around 30 MW to roughly 600 MW which makes them ideal for a large number of situations. Additionally, gas turbine engines can be used in combined cycle power plants to produce extremely efficient power generation. GE and EDF recently unveiled a combined cycle power plant in Bouchain, France that achieved 62.22% efficiency.[2] Ultimately, the advantages of quick power up, highly customizable platforms, and high efficiencies make gas turbine engines a promising source of power generation for future needs.

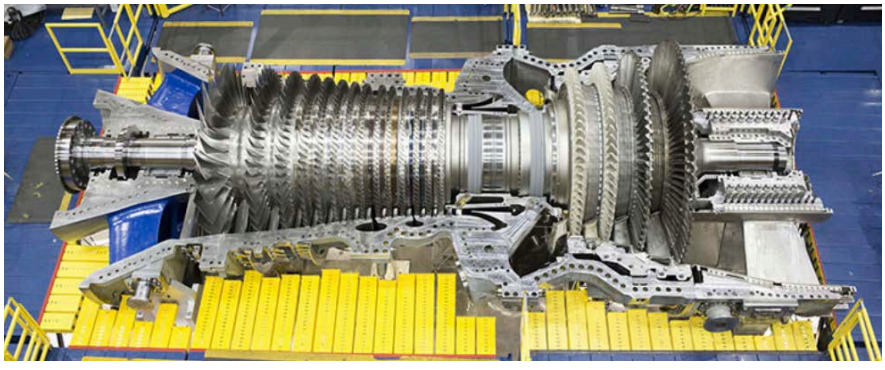

Figure 1. GE high efficiency H-class gas turbine engine [2]

As a result of the harmful byproducts produced from the combustion process within gas turbine engines, it is of utmost importance to reduce the harmful emissions that they create. Nitrous oxide or NOx is particularly harmful as it is a direct contributor to acid rain, smog, and other harmful health issues. This has led to strict regulatory standards limiting the amount of NOx emissions in gas turbine engines to double digit parts per million, ppm, NOx. However, innovation and modernization have allowed gas turbine engine designers to reach single digit ppm NOx. To do this, an understanding of the conditions in which NOx and other emissions are created is needed. The variation of carbon monoxide, CO, and NOx with temperature is shown in Figure 2 [3], which shows that the CO and NOx emissions are simultaneously minimized over the region between 1700 to 1900 K. Therefore, gas turbine engine designer endeavor to keep the combustor maximum temperature in this range.

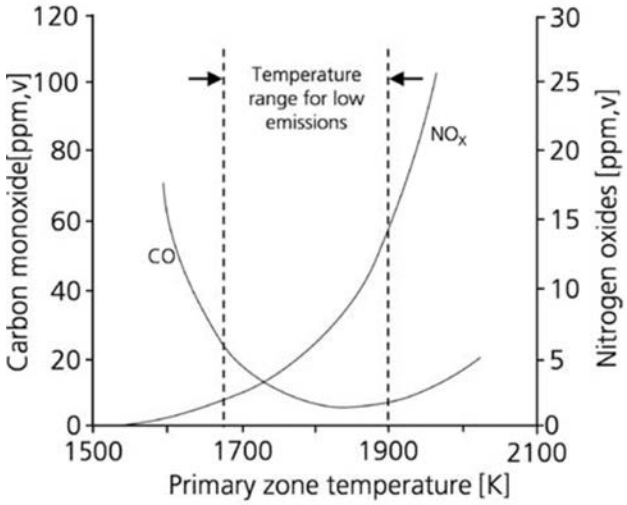

Figure 2. Nonlinear relation between NOx, CO, and temperature [3]

One method for reducing NOx emissions and meeting regulatory requirements is lean, premixed combustion technology. In fact, lean, premixed, swirl-stabilized combustion is the low emissions combustion technology of choice for combustion of gaseous fuels in air, especially in gas turbine engines. In lean, premixed, swirl-stabilized combustion, fuel is injected into and allowed to mix with the combustion air before entering the combustion zone creating a very nearly uniform mixture of fuel and air for combustion. The amount of fuel injected into the air

stream is controlled so that the “flame temperature” is within the range indicated in Figure 2. In lean, premixed combustion, the engine operates with less fuel than required for stoichiometric combustion, which serves to reduce the combustion temperature to the range required for low emissions. For gas turbine engines with a compression ratio of 30:1, the inlet air temperature is nearly 800 K, and achieving an equilibrium flame temperature of 1700 K requires an air-fuel ratio of about 43. Therefore, the fuel-air ratio is very “lean”, resulting in low flame speeds. In order to stabilize the flame in the relatively high velocity combustion zone, measures must be taken to stabilize the flame. One method commonly utilized for flame stabilization is to utilize a swirler or other device designed to impart an azimuthal velocity component, i.e., swirl, to the flow. This swirl creates a complicated three-dimensional flow field within the combustor that serves to stabilize the lean flame in the high velocity flow field.

Unfortunately, lean, premixed combustors suffer from problems with combustion instabilities as well as lean blowout. High amplitude combustion instabilities, which are characterized by high-amplitude acoustic pressure and heat release oscillations, can cause significant damage to engines and lead to catastrophic failure in some instances.

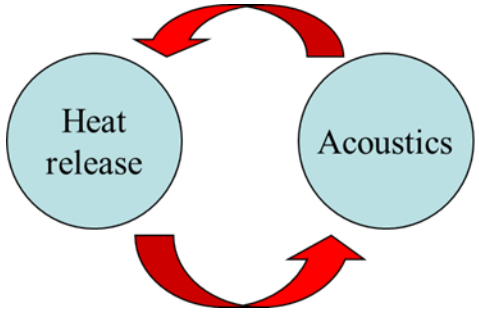

Figure 3: Illustration of the coupling between heat release and acoustic oscillations. [4]

Combustion instabilities develop as a result of the coupling between the unsteady heat release and acoustic pressure oscillations in the combustor. This cyclical relation is better depicted by Figure 3. According to Rayleigh’s criterion, when the heat release is in phase with the acoustic pressure oscillations, energy is added to the acoustic field and the amplitude of the

oscillations increases until nonlinear processes take over to limit the amplitude. The resulting high-amplitude acoustic pressure oscillations can lead to hot spots and high cycle fatigue, ultimately leading to damage to combustor components, resulting in costly repairs and downtime.

Combustion instabilities are particularly distressing in that they often arise unexpectedly. For example, a combustion system that is stable during testing and commissioning can suddenly exhibit a combustion instability when fielded. In addition, historically stable combustors can suddenly become unstable when operating conditions or ambient conditions change or due to component wear as the engine system ages. Also, a seemingly minor modification of combustion system hardware can result in unstable operation. Modifications as simple as moving fuel injection location, changing fuel injector hole size, or moving a perforated plate or swirl vane can cause a combustor to become unstable.

In an effort to maximize the efficiency of gas turbine engines, designers are pushing to reduce the pressure drop across many flow components, such as combustor liners, diffusers, and combustor to turbine transition pieces. This is usually done by changing the effective flow area of these parts by enlarging or increasing the number of holes in the part. However, these seemingly minor changes frequently result in stability problems in part because reducing steady flow pressure drop also tends to reduce acoustic damping, which is critical to the stability margin. A lack of understanding about how a given design change may affect engine stability is often sufficient to deter the designer from implementing efficiency improving modifications.

Combustion instabilities create challenges for the reliable, safe operation of gas turbines engines. In most cases, gas turbine engines cannot operate over their entire operating regime

without encountering problems with combustion instabilities. Therefore, significant effort is expended commissioning new engines to identify and mitigate or avoid combustion instabilities.

In an effort to eliminate combustion instabilities, significant effort has gone into thermo-acoustic modeling of these systems. Unfortunately, at present it is not possible to model the response of the heat release to acoustic oscillations. Further, the acoustic response of many engine components is not well understood. Therefore, experimental results such as those in Figure 4 are relied on to design engines.[4] These limitations are due to a lack of fundamental knowledge about combustion instabilities as well as a lack of quantitative information about these instabilities. Therefore, computer modeling is not yet capable of modeling all of the mechanisms that cause these instabilities and, in most cases, relies on flame transfer models for the combustor in question. This leads to in-field modifications of combustors which can be costly for both time and budget on a project. Consequently, it is important to develop understand the causes of combustion instabilities and how they can be mitigated.

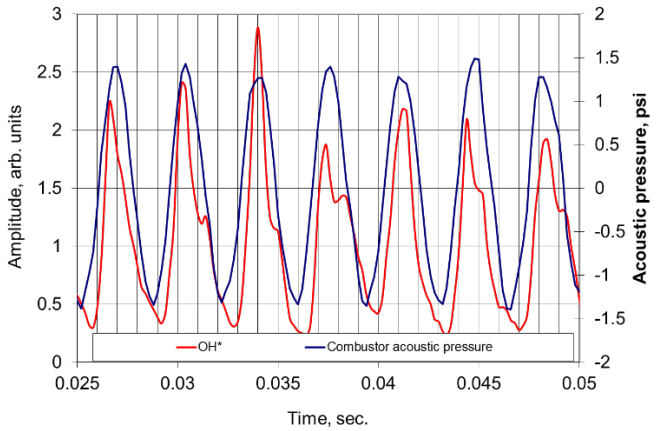

Figure 4: Plot of acoustic pressure and heat release oscillations vs time for an unstable, premixed combustion system. [4]

Predicting combustion instabilities requires an understanding of the physical mechanisms that cause them. This has led to a significant number of theories and research conducted to define these mechanisms. The following mechanisms have been theorized as the most influential in causing combustion instabilities. One mechanism is the flame surface area fluctuations driven by

acoustic velocity oscillations. This theory predicts instabilities through the Strouhal number which is the ratio of the dominant frequency times the tube radius to the laminar burning velocity. [5], [6] Another mechanism is the large scale, coherent vortical structures that develop in the combustion process that can lead to combustion instabilities.[7], [8] Furthermore, the flame wall interaction has been studied for its impact on anchoring the flame and impacting the instabilities.[9] Additionally, several authors have studied the impact inlet velocity perturbations induced by acoustic waves have on flame instabilities.[10]–[12] Finally, a number of studies have been conducted on the impact of equivalence ratio (ER) oscillations on combustion instabilities. [13]–[16] Overall, each mechanism plays a role in causing combustion instabilities and due to this complex list of contributing factors there is not yet a concrete model for combustion instabilities. In practice, modelers rely on measurements of the heat release transfer functions to quantify the response of the flame to each of these factors.

Cho and Lieuwen conducted an analysis of the specific ways in which equivalence ratio impacts combustion instabilities. They focus on the direct relationship with heat release oscillations. They concluded that the heat release is controlled by the superposition of three mechanisms: heat of reaction, flame speed, and flame area. The heat of reaction and flame speed are directly controlled by the equivalence ratio oscillations. Whereas, the flame area is indirectly controlled by equivalence ratio oscillations through the flame speed oscillations.[16] The relationship of the three is more clearly shown in Figure 5. Furthermore, this figure shows how significant the equivalence ratio oscillations are on the heat release oscillations over things such as velocity perturbations.

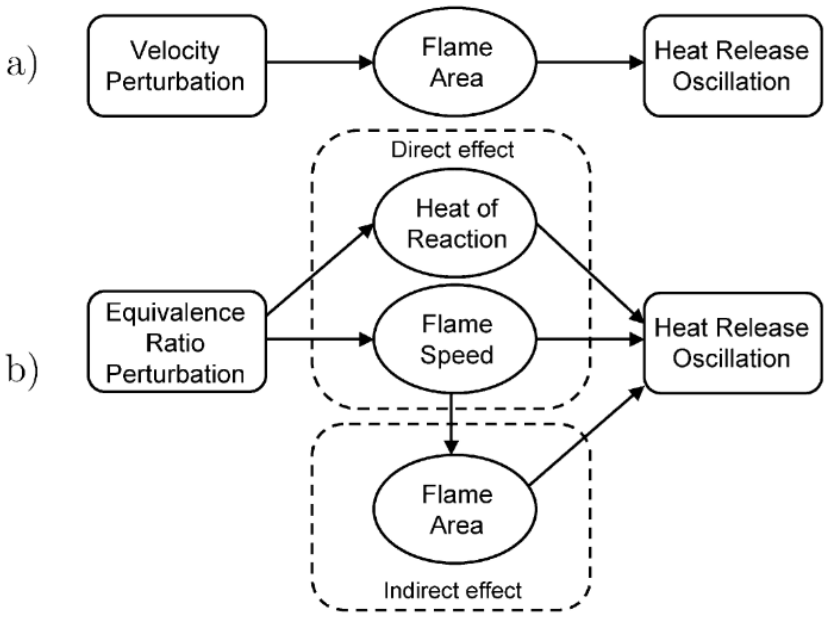

Figure 5. a) Impact of velocity perturbations on flame response b) Equivalence ratio perturbation impact on flame response [16]

This study focuses on equivalence ratio and how they propagate through a combustor. In particular, this study focuses on how equivalence ratio oscillations formed at the fuel injection site propagate through a swirl combustor by measuring equivalence ratio oscillations at several locations in the combustor and measuring equivalence ratio oscillations in the flame. A helium-neon, HeNe, laser probe was constructed and utilized to determine the equivalence ratio oscillations upstream of the combustion process. High speed measurements of CH* and OH* chemiluminescence in the flame was used to measure equivalence ratio oscillations within the flame. The acoustic pressure and velocity oscillations were determined using dynamic pressure measurements upstream of the flame. These data provide information on how equivalence ratio oscillations propagate from the fuel injector to the flame and how the flame responds to acoustic pressure, velocity, and equivalence ratio oscillations.

The following chapter presents the background and theory used in the development of the optical diagnostic probes and experiments to follow. This begins with the work conducted to

develop the HeNe equivalence ratio probes and the fundamental theories behind them. Next, the work and current research utilizing chemiluminescence measurements to define flames are outlined. The following chapters present the development of the experimental setup, the data reduction process, validating the experiment, the results of the study, and finally a brief conclusion.

Chapter 2: Background and Theory

This chapter presents the background and theory used to develop the experimental setup discussed in the following chapter. This includes theory regarding combustion instabilities, the research conducted to develop the HeNe laser probe, and the theories behind the chemiluminescence measurements.

2.1 Combustion Instabilities

Combustion instabilities are a coupling between the dynamic heat release and pressure oscillations within a combustor. Under normal operating conditions there are a large number of factors that can affect both of these variables. This can include acoustic effects, entropy oscillations, or turbulent vortex shedding to list a few.[5]–[14] The large number of these disturbances that can cause heat release or pressure oscillations becomes the primary difficulty in understanding combustion instabilities. Although all of these factors impact whether a combustion instability occurs, there are two criteria for a natural combustion instability to occur. The first is the Rayleigh criterion which follows[17]:

$$\int_t \iiint_V p'(x,t)q'(x,t)dVdt - \int_t \int_{V,S} \Psi(x,t) = G \tag{2.1}$$

The first integral represents the driving term with both the pressure and heat release oscillations integrated over the volume of the combustion location. The second integral represents the damping term which is integrated over either the surface or volume depending on where the losses are assumed to be. When the gain, G, is positive the system is unstable and when the gain is zero or negative it is stable.[17] The second criteria that must be satisfied for a combustion instability to occur is that the rate of energy addition must surpass the energy dissipation within the combustor. Without this, the combustor will damp naturally.[15] It has been theorized that a

significant factor in causing these two conditions is the equivalence ratio oscillations as it is a direct factor in the heat release oscillations.

Equivalence ratio oscillations have been conjectured as a major factor in causing combustion instabilities because of the direct impact they have on flame properties. Equivalence ratio impacts the flame speed, flame thickness, and heat of reaction. By this, the equivalence ratio directly affects the heat of reaction and flame speed, and then indirectly affects flame area through the flame speed.[16] Furthermore, these properties are increasingly sensitive to equivalence ratio oscillations as the combustor operates in leaner conditions.[13]

With the conclusion that equivalence ratio oscillations play a significant role in causing combustion instabilities, it naturally follows to determine the formation of the equivalence ratio oscillations. While natural equivalence ratio oscillations occur due to factors such as turbulent mixing, there must be significant oscillations due to pressure and heat release for a combustion instability to mature. This closes the feedback loop mentioned between pressure and heat release. It has been speculated that a significant portion of these equivalence ratio oscillations come from the inlet lines for fuel and oxidizer. This relation is better represented in Figure 6. It illustrates how the equivalence ratio oscillations impact heat release which causes oscillations within the inlet lines and completes the combustion instability feedback loop. [15]

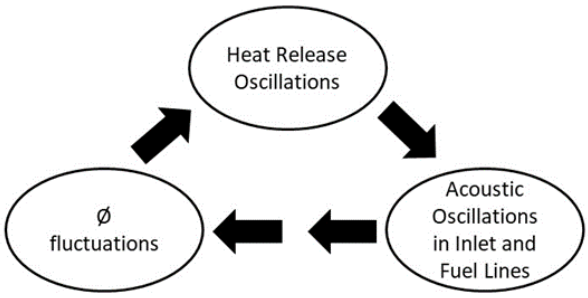

Figure 6. Possible feedback loop for combustion instabilities caused by equivalence ratio oscillations [15]

These oscillations in the inlet lines can cause significant equivalence ratio oscillations. The relationship between inlet oscillations and equivalence ratio oscillations can be determined from the definition of equivalence ratio and defined by:

$$\frac{\phi'}{\overline{\phi}} = \frac{\frac{\dot{m}'_f}{\overline{m}_f} - \frac{\dot{m}'_o}{\overline{m}_o}}{1 + \frac{\dot{m}'_o}{\overline{m}_o}} \tag{2.2}$$

where the subscripts for f and o represent fuel and oxidizer respectively, ϕ represents the equivalence ratio, m represents the inlet mass flowrate, the prime terms represent the oscillating variables, and $\overline{m}$ represent the mean flowrates.[15] With this equation it can be shown that with a choked fuel inlet ($\dot{m}'_f = 0$) and acoustic oscillations of 1% of the mean value, equivalence ratio oscillations are experienced of 20%.[15] This leads to the conclusion that inlet conditions play a significant role in driving equivalence ratio oscillations.

Finally, with the observation of the significant affect inlet conditions have on equivalence ratio oscillations, it follows to consider how these inlet conditions propagate to the combustion zone. Previous research has determined the time scales for the delay of inlet to combustion chamber but not much work has been conducted on the actual measurements of observing equivalence ratio propagation through a combustor. Consequently, this work will focus on investigating the propagation of ER oscillations in the combustor premixing section, the swirler/dump plane, and the combustor. These studies will be conducted under both cold flow and hot conditions. The next section will outline the optical diagnostic technique of using a HeNe laser to measure equivalence ratio. The theory behind this probe are explained and variables for propane combustion are given.

2.2 HeNe Laser

As concluded previously, it is of importance to measure the equivalence ratio in the mixing section of a lean premixed combustor. This has been proven possible through the use of HeNe lasers and their resulting absorption measurements. This section outlines the theory behind this spectroscopy method. Then the researchers that applied this measurement to equivalence ratio are discussed. Finally, the current work that researchers are conducting with this technique are briefly discussed.

Helium-neon lasers were used for hydrocarbon spectroscopy as early as the 1960's. One of the possible emission lines for the Helium-neon laser has a wavelength of 3.39 micrometers which is close to the fundamental vibrational frequency of the bond between carbon and hydrogen atoms. This can be determined from the force in the C-H stretching bond, the mass of the hydrogen atom, and the speed of sound. The force for C-H stretching bonds varies from 480-600 N/m^2. The mass of a hydrogen atom is roughly 1.6×10^{-27} kg. Finally, the speed of sound is nearly 3×10^8 m/s.[18] Using the following correlation for fundamental vibration:

$$\lambda = 2\pi c\left(\frac{\mu}{k}\right)^{\frac{1}{2}} \tag{2.3}$$

where λ is the fundamental vibration wavelength, c is the speed of sound, μ is the mass of the hydrogen atom, and k is the bond force.[18] This results in a value between 3.1~3.4 μm which is the wavelength emitted from certain HeNe lasers. This result allowed for the correlation between this lasers emissions to the absorption by certain hydrocarbons. This technique requires analysis of the way in which both temperature and pressure impact this absorption.

Although it has been shown that in general hydrocarbons which exhibit various forms of C-H bonds should absorb light from a HeNe laser, each fuel must be analyzed to understand their specific absorption trends. This could include trends based on pressure and temperature. Tsuboi et al. conducted shock tube experiments to measure the decadic molar extinction coefficient of various hydrocarbons. They found that propane exhibited almost no temperature dependence. They theorized this was due to the light being absorbed by the ground state of the molecules. Furthermore, they found that propane had little pressure dependence either. The results for the temperature dependence are shown in Figure 7. Each of the data sets represents various molar fractions and diluent species.[19]

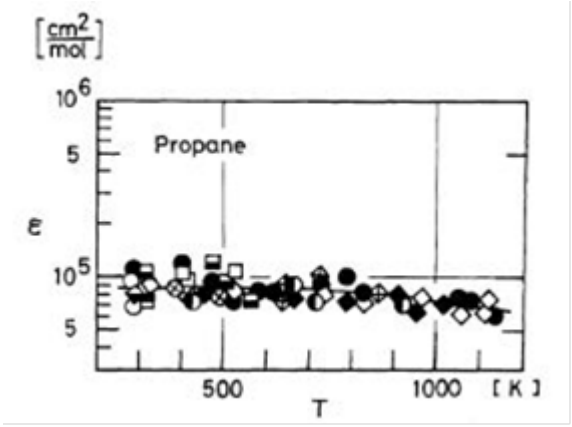

Figure 7. Temperature dependence for propane on the molar absorption coefficient [19]

The Beer-Lambert Law for light absorption may be used to determine the fuel concentration in a flow. The Beer-Lambert law relates the radiant intensity of the light source to the length of the light in the absorbing medium and also to the concentration of absorbing species as follows:

$$\frac{I}{I_0} = \exp(-\alpha \cdot L \cdot P \cdot x_i) \tag{2.4}$$

where I, I_0, α, L, P, and x_i are absorption intensity, initial absorption intensity, the absorption coefficient, path length, mean pressure, and mole fraction, respectively. This can be applied to fuel flows to determine the equivalence ratio through the definition of the mole fraction and equivalence ratio which will be explored in Chapter 4.

Researchers have developed optically accessible experiments to measure the equivalence ratio using the relationship between the absorption of hydrocarbons by HeNe lasers to equivalence ratio. This was accomplished by designing combustors with quartz tube mixing chambers or fiber optic probes. Mongia et al. at UC Berkeley was one of the first groups to demonstrate this capability. They measured acoustic pressure oscillations, wall temperature at various axial locations, and equivalence ratio oscillations in a lean, premixed combustor. Also, their fuel injector could be positioned at different axial locations in the premixing duct. This allowed them to locate the fuel injector at an acoustic pressure node, antinode, or any other point in the acoustic field. They found that the equivalence ratio oscillations matched the phase of pressure fluctuations. In addition, they found that better fuel air mixing did not always guarantee lower pressure oscillations.[20] Santavicca et al. constructed a similar lean premixed combustor. However, they added a swirler near the dump plane between the premixing section and the combustion section to more accurately simulate realistic gas turbine engine combustors. Furthermore, they measured the heat release oscillations using PMT's to measure flame chemiluminescence. This research led to insights in to how equivalence ratio oscillations oscillate with heat release oscillations. They found that the heat release and pressure oscillations exhibited similar harmonics whereas the equivalence ratio exhibited higher harmonics. [14], [21] Ultimately, these two groups of researchers demonstrated the ability to measure equivalence ratio oscillations in an experimental lean, premixed combustor.

With this fundamental work in the field of combustion instabilities, work has progressed to determining the impact equivalence ratio oscillations have on heat release which directly impacts flame transfer functions. This can be important in producing more accurate computer models.[22] To further this research, the way in which equivalence ratio oscillations propagates

through a mixing chamber can be influential in determining significant factors related to the flame transfer functions.

2.3 Chemiluminescence Measurements

In addition to measuring the equivalence ratio within a flame, the heat release is an important factor in determining combustion instabilities. This fact is defined by the Rayleigh criteria stated previously. Consequently, prior to the equivalence ratio measurements, chemiluminescence was used to measure qualities of flames. This began by correlating chemiluminescence measurements to reactions in the flame front or to heat release and has now even been correlated to equivalence ratio within the flame. The light emission from the flame can provide a significant amount of data about the combustion process.

Researchers have demonstrated that local chemiluminescence measurements of OH* and CH* can provide details of the combustion in a turbulent premixed flames.[23]–[27] This led to the relationship between CH* and heat release. Furthermore, it has been shown that time series chemiluminescence can determine the timescale of reaction and the flows at the flame front.[23] These relationships can provide the information needed for heat release to understand the relationship between heat release and pressure oscillations within a combustor.

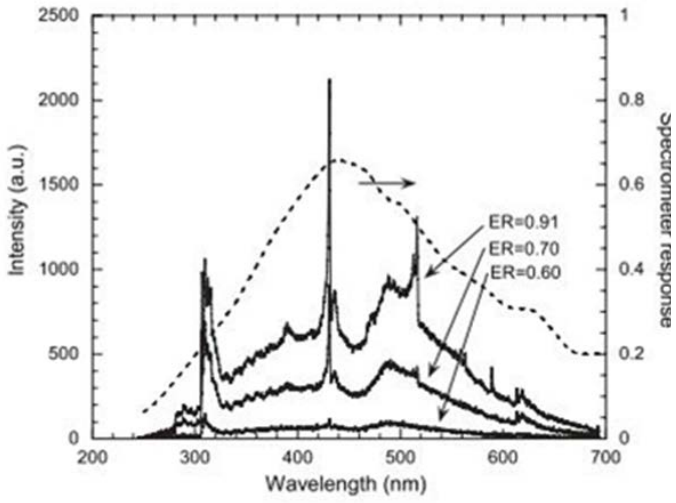

Figure 8. Example light spectroscopy for multiple equivalence ratios [4]

For this study, the work done to correlate chemiluminsescence measurements with equivalence ratio will be utilized. The theory

behind this method came from observing light emissions from multiple premixed flames such as the relationship observe in Figure 8. This shows how as the equivalence ratio is increased, there is more light measured at specific wavelengths. Ratios of certain wavelengths can be directly correlated to equivalence ratio. An example of such work is shown in Figure 9 which shows the relationship of CH/OH, C2/CH, and C2/OH for a methane flame at various power settings. This demonstrates that this relationship can be correlated to equivalence ratio even at different power conditions. This type of work will be followed to measure the various ratios for the propane flame analyzed in this study.

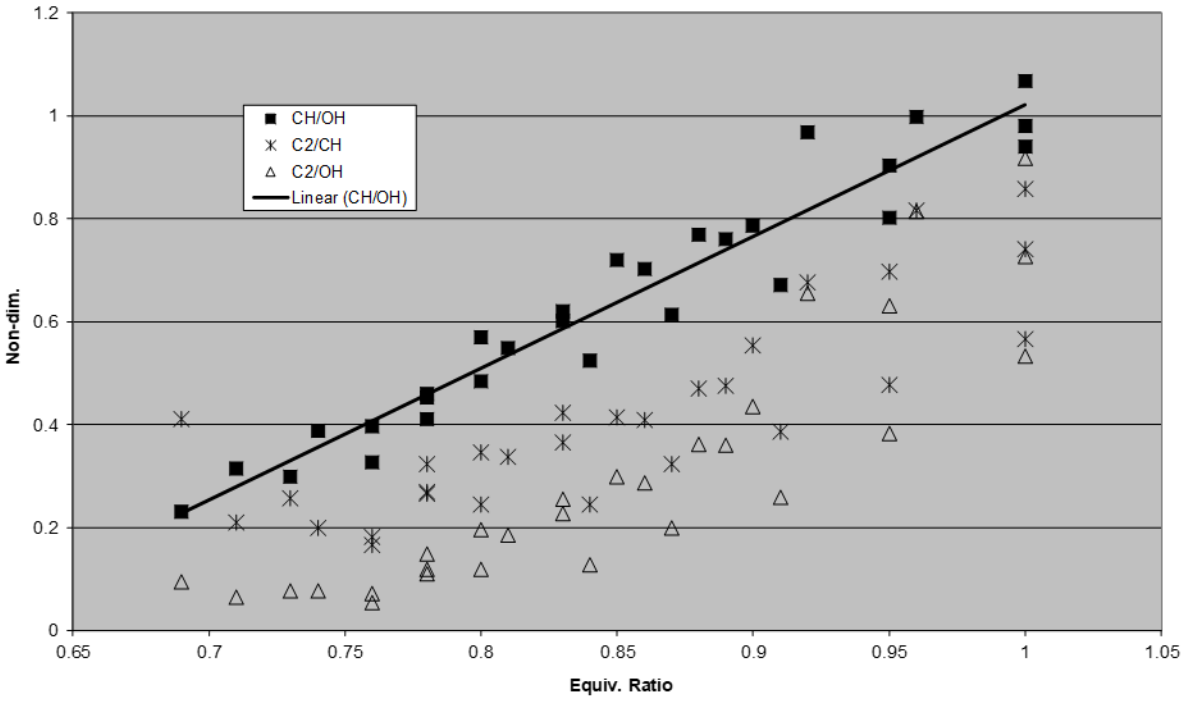

Figure 9. Variation of CH/OH, C2/CH, C2/OH vs Equivalence Ratio [4]

It has been found that the relation between CH*/OH* correlate well with equivalence ratio for methane flames. [28]–[32] This work was furthered to include strain rate dependence and analyzing the background noise floor. It was found that strain rates did not have a significant impact on these ratios in determining equivalence ratio. Furthermore, it was found that CO2*

was a better background floor measurement than C2*. [33] Muruganandam et al. determined that this ratio was not sensitive to moderate changes in flowrate, air preheating, or fuel composition. [34] Overall, work has been conducted to demonstrate the relationship between chemiluminescence imaging and equivalence ratio measurements. However, little work has been done to combine the measurements with the HeNe laser probe and the optical measurements within the flame. This study will look to analyze the correlation between the oscillations within the combustor to the oscillations in the flame.

The next chapter will outline the development of the experimental setup for this study. This begins with the initial burner which leads to the development of the swirl burner used in the final studies. In addition, the data acquisition system is outlined.

Chapter 3: Experimental Setup

This section describes the experimental facilities, instrumentation, and data acquisition and control equipment used in this investigation. First, this chapter will describe the initial experimental combustor used to develop the diagnostic probes. This includes the burner design, flow control, diagnostic measurements, and operation of the burner. Next, the design and fabrication of the swirl combustor used in the following experimental studies is outlined. This focuses on the addition of the swirl portion of the combustor which simulates gas turbine engines better than the initial burner. Finally, the data acquisition software developed is described.

3.1 Design 1: Modified Bunsen Burner

This section describes the Bunsen burner type combustor, instrumentation, and data acquisition equipment used in the experiment. The design of the modified Bunsen burner was chosen because of its simplicity and ease of use. This first design has major advantages for being a simplified burner but lacks realistic gas turbine combustor capabilities. It was mainly used as a preliminary test bed for the optical diagnostic techniques.

The schematic for this design is shown in Figure 10. It consists of two aluminum blocks that house the speakers, pressure gauge, pressure transducer, and inlet ports for the fuel and oxidizer. The burner operates with a cone flame atop the glass tube similar to that of a laboratory Bunsen burner. It operates on propane but can be switched to methane or other gaseous hydrocarbons if desired for testing.

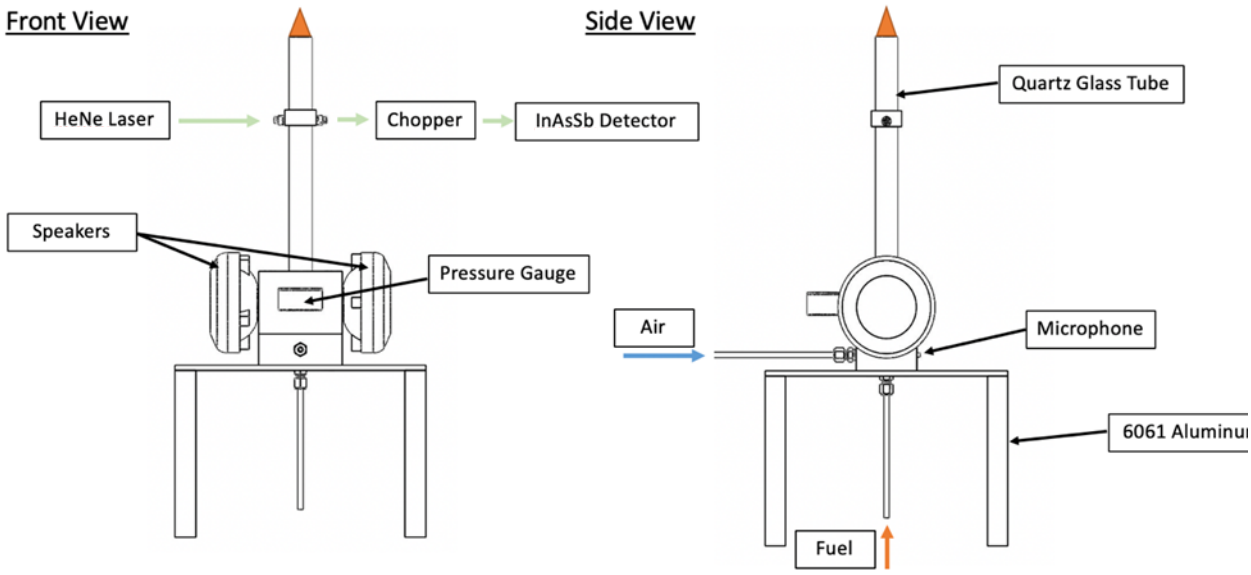

Figure 10. Modified Bunsen burner schematic

3.1.1 Flow Control

Oxidizer and fuel are input into the burner through 6.35 mm tubing axially and radially into the base. The oxidizer and fuel flows are controlled by Omega FMA5400A/5500A series mass flow controllers (MFC) that operate up to 100 SLM and 20 SLM respectively. The MFCs are shown in Figure 11. The 20 SLM MFC operates with +/- 1% full scale error over its entire operating regime. The 100 SLM MFC operates with +/- 1.5% full scale error from 20 to 100% of range and +/- 3% full scale error from 0 to 20% of range. The oxidizer MFC will operate in the 20 to 100% range for most of the testing which keeps it in the +/- 1.5% error. The gas flow schematic is shown below in Figure 12. Both MFCs require feed pressure

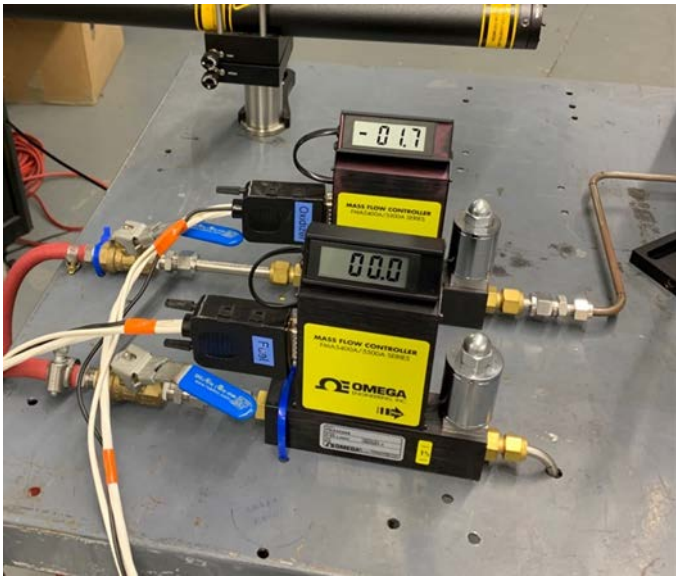

Figure 11. Fuel and oxidizer MFC from front to back

between 137 kPa and 345 kPa, so the pressure regulators are set at 310 kPa to account for pressure drop in the lines for both flows.

Furthermore, ball valves are situated above the tanks and before the test rig to allow safe setup and operation of the experiment. The air is supplied by a shop air compressor and the fuel is supplied by a standard 20 lb. propane tank. Upon entering the burner, the flows are mixed in the base block and through a sintered disc that is specified to remove particles down to 40 microns. This disc acts as a flashback resistor and to create a pressure drop that stabilizes the flow before being acoustically driven by the speakers. It is used in certain test conditions to create a uniform flow in the mixing chamber, but can also be removed to allow unsteady mixing in this chamber.

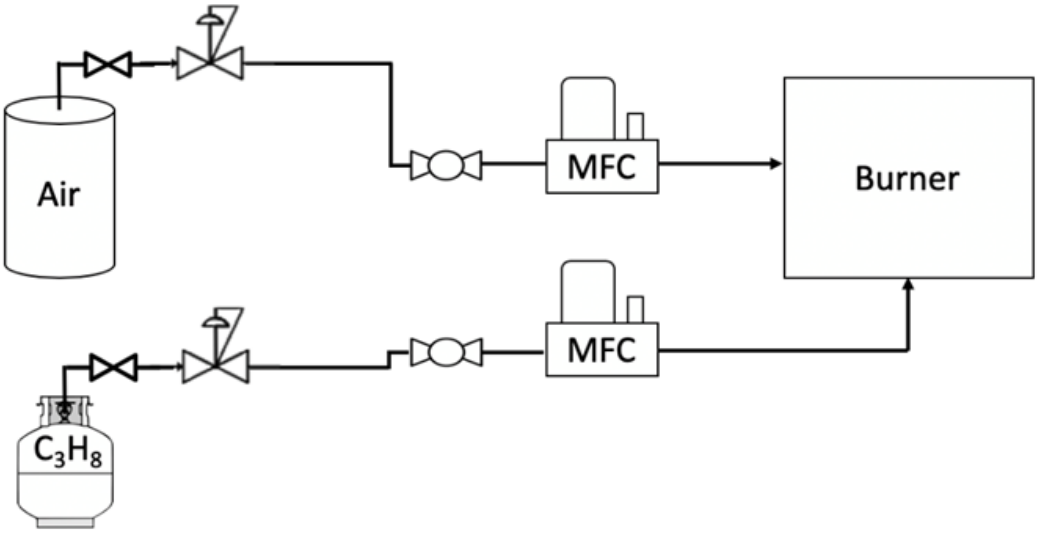

Figure 12. Oxidizer and Fuel Flow P&ID

3.1.2 Acoustic Forcing

After the gas is mixed in the base of the burner and before it flows into a quartz tube, the experiment can be acoustically driven by two speakers. The speakers are 100 Watt speakers driven by a 1000 watt amplifier. The amplifier is a Pyle Pro PTA1000 amplifier which supplies power to the speakers and can create various types of waves in the mixing tube. The internal schematic of the combustor is shown to the right in Figure 13. This shows the chamber created to allow mixing and then acoustic forcing before entering the quartz tube. The speakers can create sound pressure levels up to 175 dB in the mixing chamber. This provides the needed forcing for equivalence ratio oscillations in the mixing chamber.

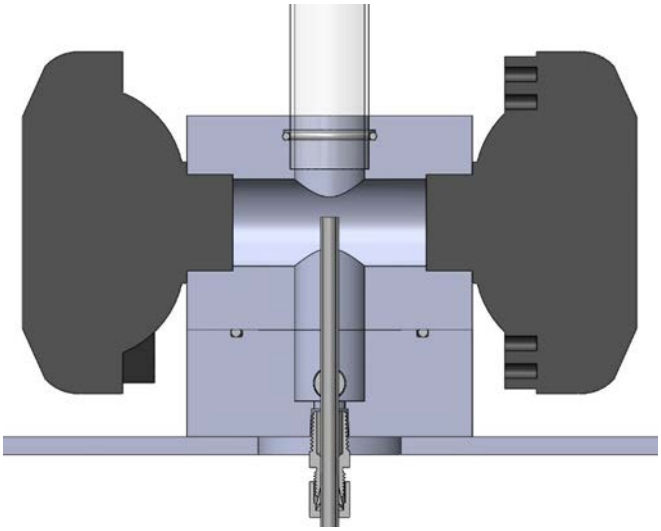

Figure 13. Internal CAD of burner

3.1.3 Burner Tube

The premixed flow that is created in the aluminum base of the burner is passed into a quartz glass tube and up to the flame. This quartz glass tube allows the optical accessibility required for the laper probe. The transmission percentage is shown in Figure 14 [35], which indicates around 80% transmission near 3,390 nm. This allows the use of the laser probe discussed

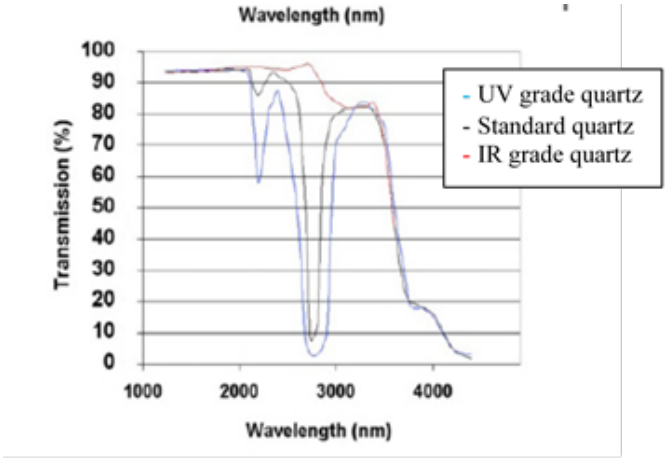

Figure 14. Quartz glass transmission percentage [35]

in the next section. In addition to allowing optical accessibility for the laser probe, quartz glass will be used later for the combustion chamber as it allows for chemiluminescence imaging on the flame.

3.1.4 Dynamic Pressure Transducer

In order to measure the acoustic pressure oscillations in the burner, a dynamic pressure transducer (DPT) is mounted in the base of the mixing block. The DPT is a quartz sensing element Kistler 211B6. It has a pressure range of 50 psi and a resolution of 0.0005 psi (rms). The nominal sensitivity for the sensor is 100 mV/psi. In addition, the sensor has a rise time from 10 to 90% of 2 microseconds. This sensor allows accurate collection of the pressure oscillations in the burner.

3.1.5 Infrared Absorption System

To measure equivalence ratio oscillations in the mixing chamber a laser probe was constructed. The laser probe consists of a helium-neon (HeNe) laser and optical detector that measures light intensity. The laser is a Research Electro-Optics 32172 helium neon laser that operates at 3390 nanometers. It is a 2.0 mW polarized laser with a 2.02 mm beam diameter and less than 0.05 mrad long term beam drift. The light is passed through the quartz glass on the burner and into a photodetector. The detector is a Thorlabs PDA10PT with an indium-arsenide-antimonide detector element. It is a thermoelectrically cooled detector that maintains -30C to minimize the thermal contributions to the output signal. At 3390 nm the detector has a sensitivity of roughly 1.10 A/W. In addition, the detector has a variable gain amplifier that can amplify from 100 V/A to 10,000 V/A which allows for detectable output voltages. The InAsSb detector has an internal bandwidth filter set to 25 kHz.

The detector requires a pulsed or chopped signal so after the light passes through the burner, it passes through a variable speed optical chopper. This optical chopper has the capability to pulse the light from 120 Hz to 6 kHz. It was determined based on previous research and combustor design that analysis up to 500 Hz was desired. This resulted in a measuring frequency of at least 5,000 Hz due to the Nyquist criteria. In addition, due to the data reduction process discussed in the next chapter, a frequency that results in sets of 10 for each averaging section was desired. Furthermore, the data acquisition system measured data at 51,200 Hz. Consequently, a chopper frequency of 5,120 Hz was chosen to satisfy both the desired combustion instability measurement regime and the data acquisition requirement.

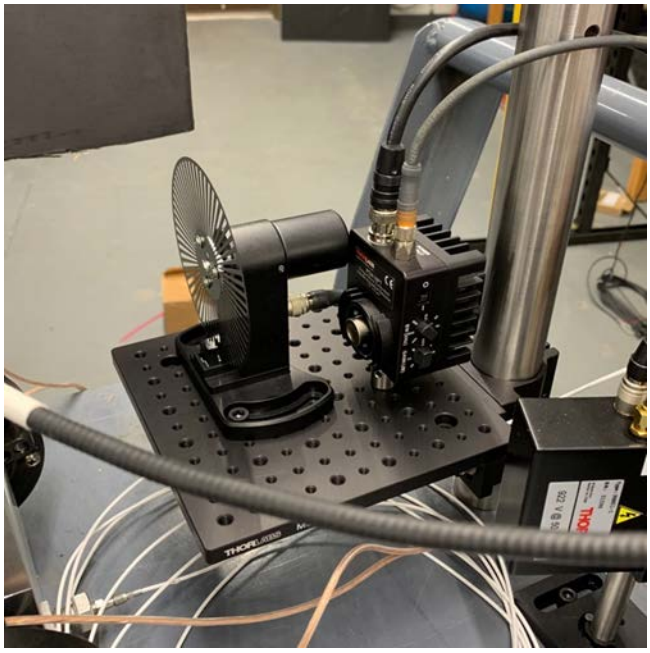

Figure 15. Optical chopper and InAsSb detector on the optical post

The optical chopper and InAsSb detector are shown in Figure 15 mounted to a plate on an optical post. This allowed the detector to be translated vertically to measure signals at various heights. The laser is mounted on a similar optical post to allow vertical translation as well. This combination of laser, chopper, and detector will be referred to as the InfraRed Absorption System (IRAS).

The IRAS measures the line of sight integrated fuel concentration in a 2 mm diameter cylinder oriented transversely through the combustor. Consequently, the measured ER is the local ER averaged along the line of sight rather than the global ER for a given radial cross section. In order for the IRAS to accurately measure the global ER at a given combustor cross-section using a single measurement, the fuel and air must be homogeneous over that cross-sectional area. If the fuel-air mixture is not homogenous at a given cross-section, measurements must be made at a number of transverse locations as shown in Figure 16. These measurements must then be area averaged in order to obtain the global ER at that axial cross-section Figure 16(a) shows that in an unmixed scenario this measurement at location 1 would show no fuel in the mixture but at location 3 would show a large amount. Figure 16(c) shows that as this flow becomes fully mixed each location would show the same amount of fuel-air, corresponding to the global ER. The ER will be measured with the IRAS at location 3 on this schematic which can represent the local or global ER depending on the mixture.

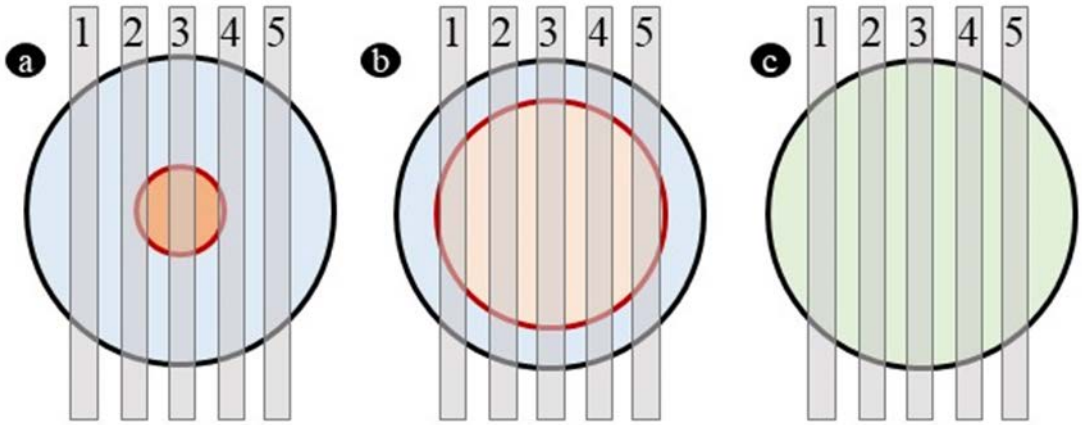

Figure 16. Cross-section of combustor mixing section with multiple IR absorption locations

a) Unmixed fuel-air mixture b) Partially mixed fuel-air mixture c) Fully mixed fuel-air mixture

To further understand how this line of sight measurement impacts the study, a schematic of the combustor discussed in the next section with the laser measurements is represented in Figure 17(a). The three red lines represent the fuel propagation in mixing scenarios and the orange lines show the location of the laser measurements. For instance, the laser at location 1 is measuring a well stirred mixture for the solid line. However, for both dashed lines, the fuel jet is still mixing and thus the laser measures more fuel in its location centered in the fuel jet than it would otherwise in a fully mixed location. This then provides a local ER measurement that is higher than the representative global ER. Figure 17(b) shows an illustration depicting this phenomenon. For the measurement at location 1 at an unmixed cross-section, most of the fuel is in the center of the flow. Therefore, there is more fuel along the line of sight than for the total volume element. This corresponds to a higher local ER measurement. However, at location 3 in this scenario, the mixture has finished mixing and would consequently show the same local and global ER as the fuel is evenly mixed in the chamber. Consequently, the IRAS measurements in the following studies must be prefaced with this information. Certain mixtures will provide information about the global ER and others will provide information about the local ER. This can be beneficial in that this provides information about the way in which the fuel-air flow mixes in both the radial and axial directions.

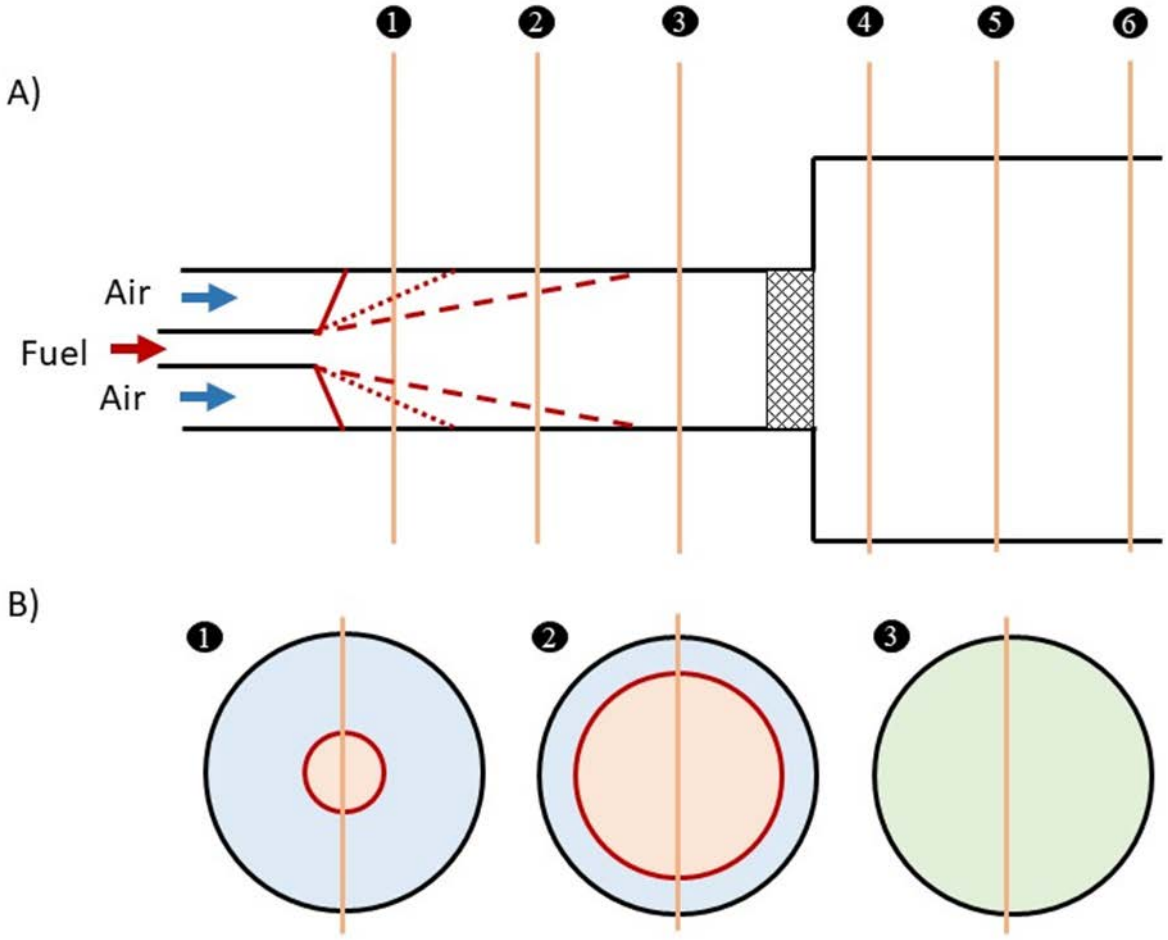

Figure 17. A) Fuel and air inlet schematic for different fuel mixing lengths with laser measurement location B) Cross-sectional views of locations 1, 2, and 3 for a representative fuel and air mixture in view A.

3.1.6 Photomultiplier Tubes

In addition to the IRAS to measure equivalence ratio, a photomultiplier tube (PMT) system was developed to measure light emissions from the flame. Three PMTs are mounted to the experiment to measure wavelengths of light for heat release and equivalence ratio. The PMTs are Thorlabs PMM01 photomultiplier tubes. They are Bialkali amplified detectors that can measure from 280 to 630 nm. Each PMT requires a bias voltage input up to 1.8 V which is supplied by the NI9264 DAQ module discussed in the next section. Bandpass filters that are specified to allow light within 5 nm of a nominal wavelength are mounted to the front of the

PMTs. The wavelengths chosen were 430 nm, 310 nm, and 515 nm which reflect the light emissions for CH*, OH*, and C2* respectively. These PMTs are then connected together with a fiber optic bundle to be able to measure from the same source in the flame. This bundle is then mounted onto an optical post that allows vertical and horizontal adjustments providing the capability to measure at multiple locations.

In addition to the PMTs, a compact spectrometer is connected to the fiber bundle to verify the full spectrum of light received from the flame. The spectrometer is a Thorlabs CCS200 which measures light from 200 to 1000 nm. It is a Czerny-Turner spectrometer and roughly the size of a portable hard drive. The device requires 2 seconds to measure the light absorption from the propane flame. This length of time is not suitable to measure combustion instabilities but provides insight into the global spectrum of light emitted from the burner. The PMTs and spectrometer are shown in Figure 18.

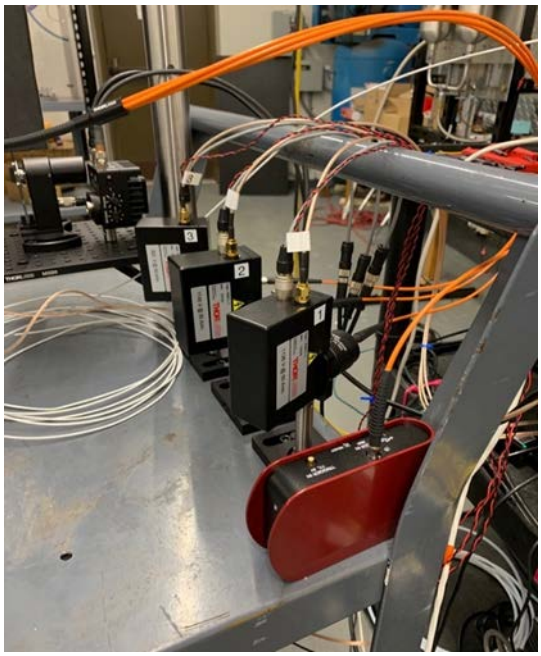

Figure 18. PMT and spectrometer on experimental rig

3.1.7 Operation

Following the successful design and implementation of the burner, test trials were conducted to demonstrate the safe operation of the burner and develop Standard Operating Procedures. The final burner is shown in Figure 19(a) and a normal operating condition is shown in Figure 19(b). Initial testing showed the capability to operate in lean or rich environments,

demonstrate yellow tipping limits, flashback limits, and blowout limits as to be expected with literature about propane burners. These results for the modified Bunsen burner soon led to the desire for a more realistic combustor design.

Figure 19. Modified Bunsen Burner Design a) Final Build b) Normal Operation

3.2 Design 2: Swirl Combustor

This section outlines the modifications conducted to create a swirl combustor with the previously discussed burner. This new swirl burner, while being a simplified version, is a more accurate representation of the burners used in gas turbine engines. It therefore will provide more realistic insights into the way in which combustion instabilities occur in gas turbines.

3.2.1 Swirl Design

With the successful design and completion of the initial burner discussed, the need for a swirl plane to simulate practical gas turbine combustors developed. To limit the need for a

complete redesign, the second burner was designed as a modification of the first burner. The goals for this burner consisted of adding a swirl plane, maintaining optical accessibility for the HeNe laser probe, and providing optical accessibility to the combustion chamber for chemiluminescence imaging. This final redesign consists of everything from the first burner with a swirl plane mounted above the quartz tube. The schematic for this design is shown in Figure 20. Notice as expected that the addition of the swirl plane inverted the flame from the previous design.

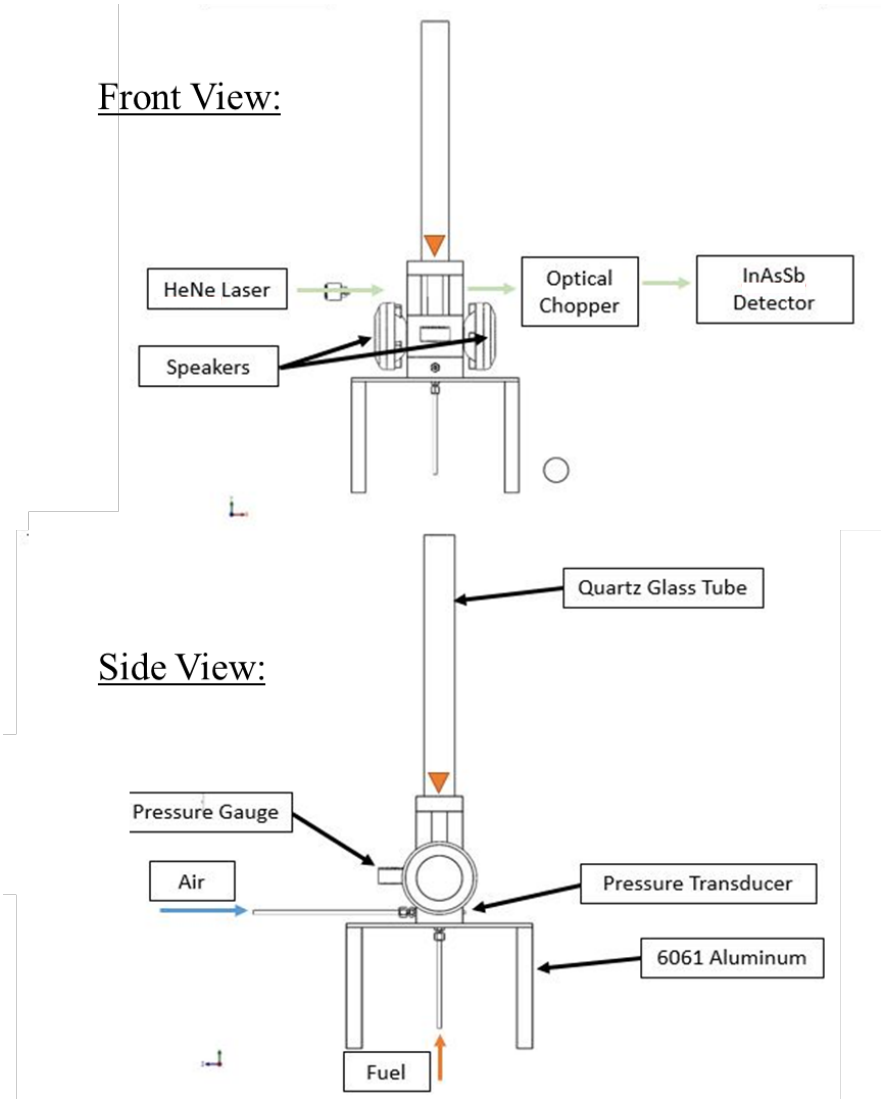

Figure 20. Swirl Burner Schematic

To achieve the stated goals, a swirl plane was mounted on posts above the existing quartz tube. This modification provided the capability to use the previously discussed systems for pressure measurements, equivalence ratio measurements, MFC flow control, and acoustic forcing. The swirl plate holds a swirler that can be interchanged for various swirlers. This allows for different testing conditions purely based on the swirl number of the swirler. In addition to holding the swirler, the swirl plate holds a quartz tube to act as the combustion chamber. The above quartz tube has an inner diameter of 47 mm while the mixing chamber has a diameter of 19 mm. This results in a dump plane area ratio of roughly 2.47. In addition to stabilizing the flame, the quartz tube allows for optical measurements for heat release and ultimately equivalence ratio in the flame. The completed experimental setup is shown in Figure 21(a), with a focus on the dump plane in Figure 21(b).

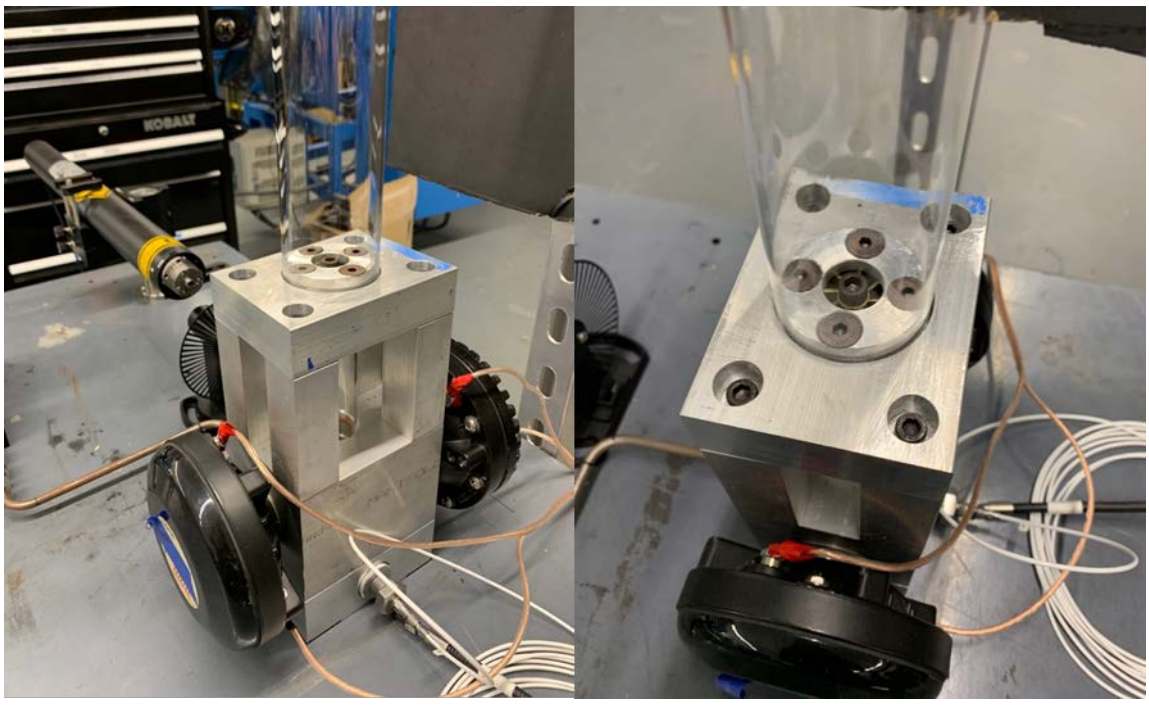

Figure 21. Swirl Burner a) Burner b) Dump Plane

3.2.2 Operation

The swirl burner can be operated under multiple operating conditions. The lean operating regime is shown in Table 1. The table indicates the conditions that initiate blowout, flashback, and unstable flow. The following studies will focus on total flowrates between 50 and 90 SLM and equivalence ratios between 0.6 and 0.8. These conditions simulate a high power and low power mode of operation. As indicated by the table, there are many conditions that can be tested on this burner in the future including rich conditions that are not plotted in this table. While the green area is stable operation, the different locations on the operability map exhibit different types of flames. Some of these flame types will be indicated below on Figure 22.

Table 1. Swirl Burner Operating Regime

Total Flow (SLM)	Equivalence Ratio										
	0.50	0.55	0.60	0.65	0.70	0.75	0.80	0.85	0.90	0.95	1.00
10					1				2		
20		3									
30											
40					4						
50								5			6
60											
70											
80		9									
90			8						7		

The red squares indicate flashback or blowout. The blue squares indicate the beginning of liftoff. The yellow squares indicate unstable burning and finally the green squares indicate stable operation. The numbers indicate the following images on the image matrix in Figure 22.

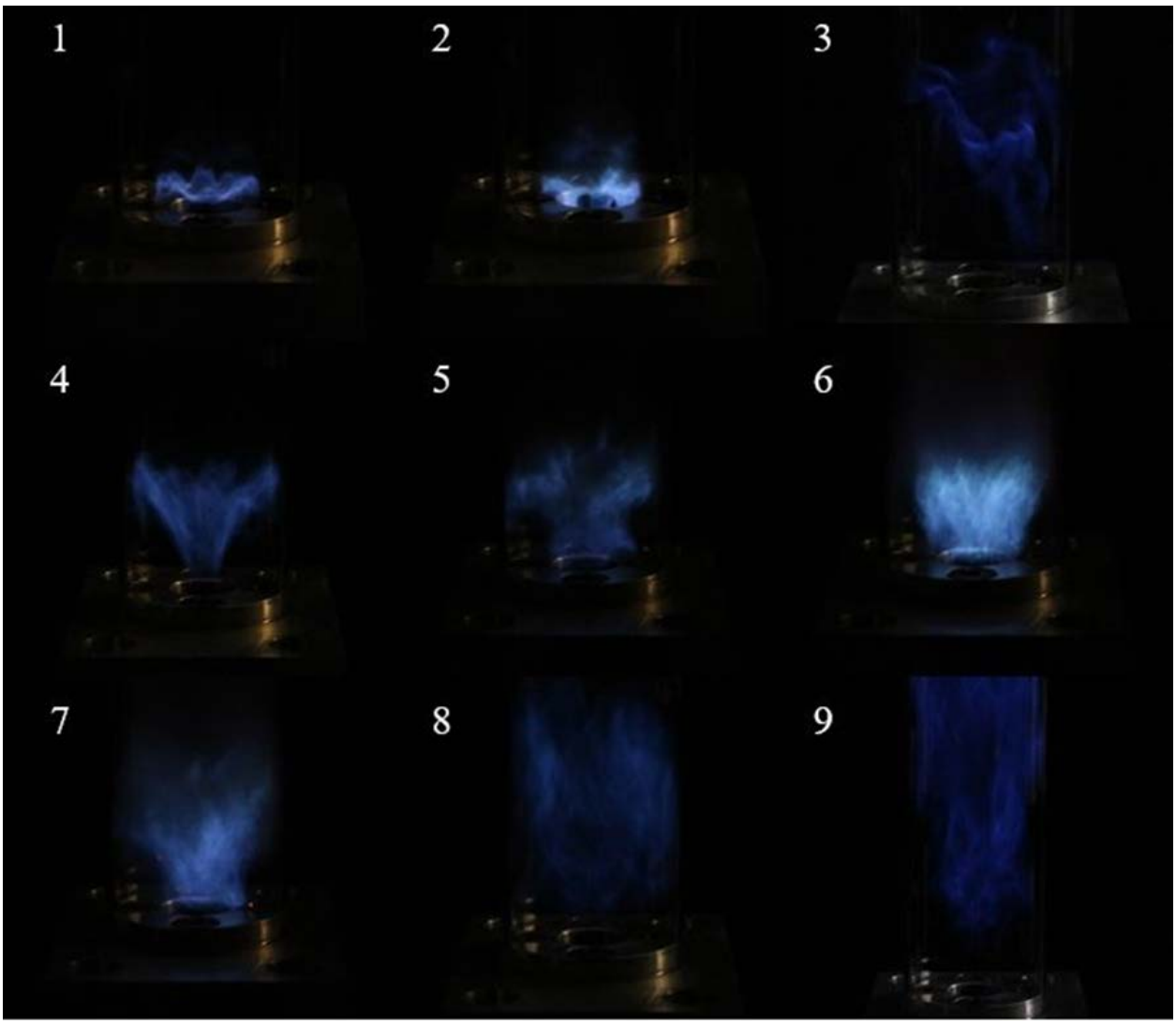

Figure 22. Operability Images

3.3 Data Acquisition and Control

This section describes the data acquisition software and interface utilized in this experiment. LabVIEW was utilized to create the operating program for the experimental facility and interface with the DAQ system.

The LabVIEW program was responsible for operating all aspects of the experiment except for powering on the HeNe laser. The laser was controlled with an interlock and key to ensure safe operation. The control schematic is shown below in Figure 23. Once the software was initiated, the LabVIEW program began sending and reading signals from a cDAQ-9189. These signals were then routed through four DAQ modules to the various components on the experiment. Burner control in the software was designed so that total flowrate and equivalence ratio were the inputs for each test. This can be seen at the top of Figure 23. The specific values for the oxidizer and fuel were calculated based on the stoichiometric mass mixture between fuel and oxidizer. For propane this value is 23.9. Once calculated these values were converted to a voltage based on the full scale voltage of each MFC and sent through a NI9264 to the MFCs. In addition, the code was programmed with safety criteria so that the fuel cannot be on while the

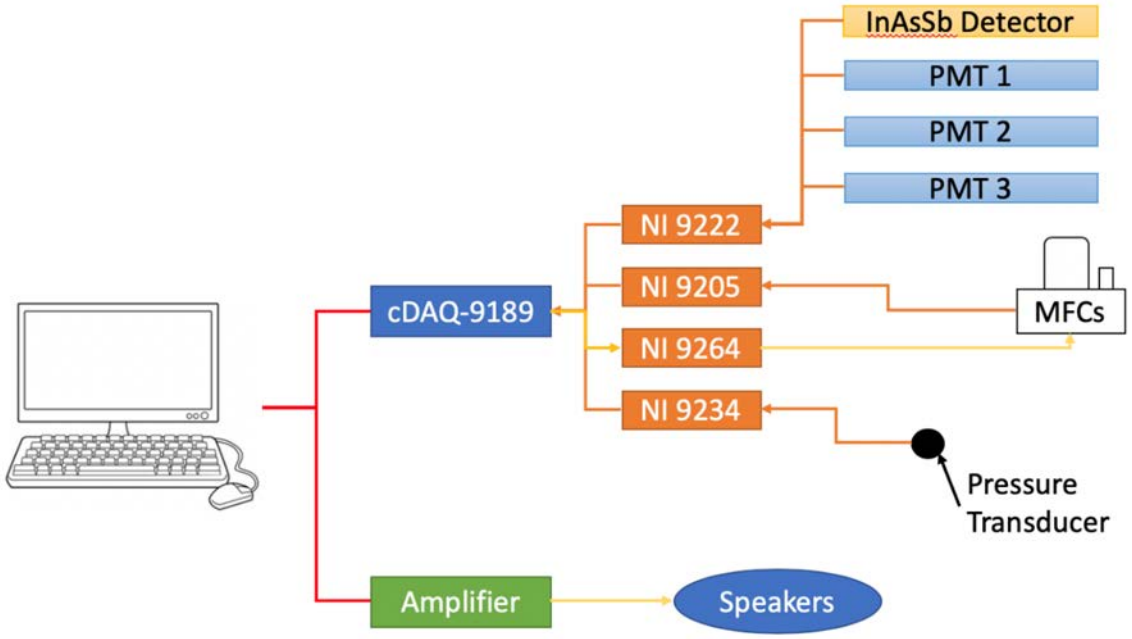

Figure 23. Control Diagram for Data Acquisition

oxidizer is off. This prevents accidentally leaving fuel on without any oxidizer. Once flowrates were selected, the frequency for the experiment was chosen and input into the software. This sound signal was created by the LabVIEW program and output through the sound card in the computer. This signal was fed into the amplifier which then powered the speakers. This created the appropriate frequency wave in the mixing block. Finally, a gain value up to 1.8V was selected for each PMT and output through the NI9264 to each PMT.

Following the output parameters for the test, the program was responsible for reading and recording the data measured in the experiment. An analog input module, NI9222, measured the PMT and InAsSb voltage data. A sound and vibration module, NI9234, measured the DPT data. This module handled the sensitivity and filters required for the Kistler DPT. Both the NI9222 and NI9234 were sampling at 51,200 Hz to allow for maximum accuracy with the PMT, InAsSb, and DPT data. The software records MFC output, InAsSb output, PMT1/2/3 output, and DPT output which were written to a standard text file. This text file was then processed with a MATLAB script that is discussed in the following chapter.

Due to scaling limitations, the LabVIEW control portion of the interface developed is shown below in Figure 24. The full display with output graphs is shown in Appendix I. The input

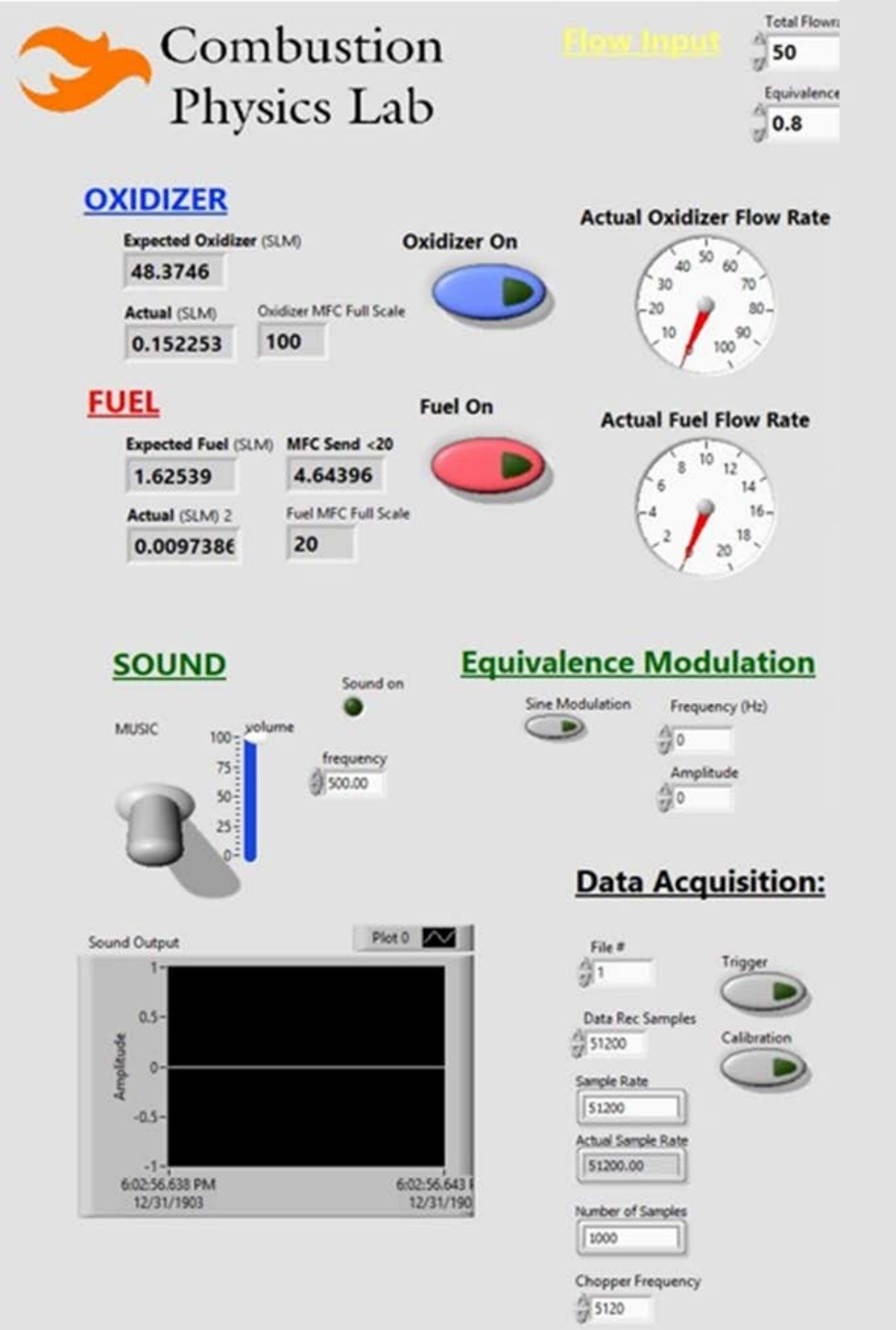

Figure 24. LabVIEW control interface

for total flowrate and equivalence ratio are located in the top right. These inputs then led to the calculation of the values under fuel and oxidizer. Furthermore, both methods of equivalence ratio oscillations are labeled in green, one for the acoustic forcing with speakers and the other for the MFC modulation. For various validation tests, the capability to oscillate the equivalence ratio in the burner without the speakers was needed and programed into the code. This resulted in the ability to sinusoidally oscillate the MFC outputs to create this modulation. This method is limited to low frequencies but can provide accurate oscillatory data without the unknowns created by the speakers. Finally, the trigger and calibration buttons are located at the bottom of the program along with file number and sampling information.

The next chapter discusses the data reduction used by this LabVIEW script and experimental setup. This includes the equations for equivalence ratio and fast Fourier transforms.

Chapter 4: Data Reduction

This section outlines the data reduction procedures used in this study. This focuses on the equivalence ratio calculations for both the IRAS and PMT setup. These algorithms were input into a MATLAB script used to reduce the data systematically.

4.1 Laser Equivalence Ratio

The HeNe laser equivalence ratio is calculated utilizing the Beer-Lambert Law for absorption. This equation follows:

$$\frac{I}{I_0} = \exp(-\alpha \cdot L \cdot P \cdot x_f) \tag{4.1}$$

where I is the measured absorption intensity, I_0 is the initial absorption intensity, α is the absorption coefficient, L is the path length, P is the pressure, and x_f is the mole fraction of fuel. This equation can be rearranged to solve for mole fraction:

$$x_f = \frac{\ln\left(\frac{I}{I_0}\right)}{-\alpha \cdot L \cdot P} \tag{4.2}$$

Then the equivalence ratio can be calculated using the mole fraction definition:

$$x_f = \frac{n_f}{n_f + n_a} \tag{4.3}$$

where n_f is the moles of fuel and n_a is the moles of air and the equation for equivalence ratio:

$$\phi = \frac{\frac{n_f}{n_a}}{\left(\frac{n_f}{n_a}\right)_{stoich}} \tag{4.4}$$

where ϕ is the equivalence ratio.

Combining Eq. 1.2, Eq. 1.3, and using the values for propane results in:

$$\phi = \frac{23.9 x_f}{1 - x_f} \tag{4.5}$$

This equation converts the mole fraction given by the Beer-Lambert law into equivalence ratio and can be easily programmed with the constants for propane. An error analysis was conducted on this process as is located in Appendix III which determined that there was a 7.6% measurement error.

In order to get data from the raw laser output the data must be processed before Eq. (4.5) can be used. An example raw output of the laser is shown below in Figure 25.

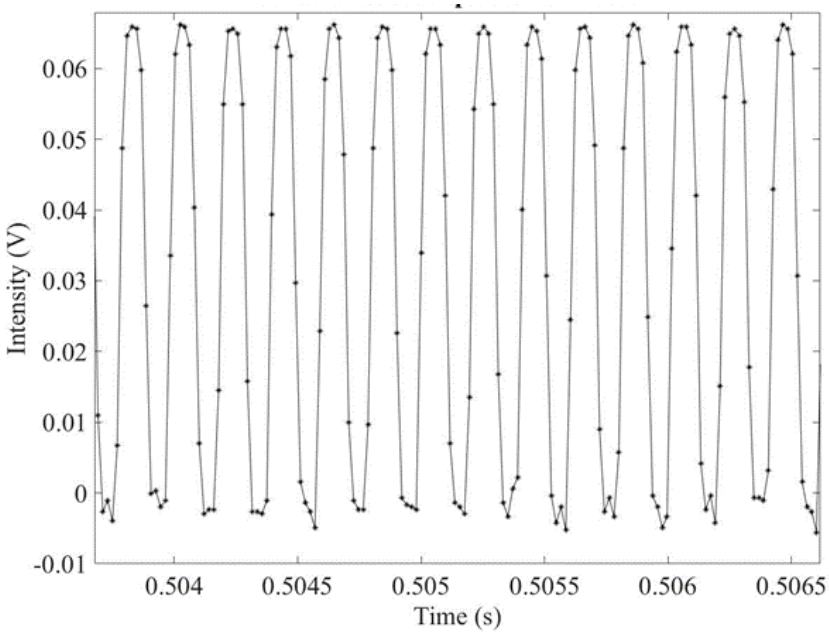

Figure 25. Raw laser absorption data

The output indicates a square wave which should occur due to the optical chopper. However, this data cannot be used as raw data points to calculate the equivalence ratio because it is does not maintain the magnitude of intensity along the curve. Therefore, the data is averaged over every ten data points which was determined from the sampling frequency of 51,200 Hz and the chopper frequency of 5,120 Hz. This was the chosen chopper frequency because it kept the data sets in groups of 10. Furthermore, due to this averaging affect this chopper frequency of 5,120

Hz allows reasonable data sampling up to 500 Hz which is the area desired for analysis. The Fourier transform is conducted on the HeNe equivalence ratio data, PMT equivalence ratio data, and DPT data. It is calculated with MATLAB's built in Fast Fourier Transform (FFT) function.

The laser output was measured with nothing present along its path other than the optical chopper. The resulting equivalence ratio amplitude spectrum shows a 200 Hz oscillation. The laser output was processed through the equivalence ratio reduction in order to understand the magnitude at which this amplitude was occurring. However, the magnitude of all of the results shown are small enough that they do not affect the results observed under acoustic forcing later in the study. Consequently, this frequency of oscillation will be ignored in the following study.

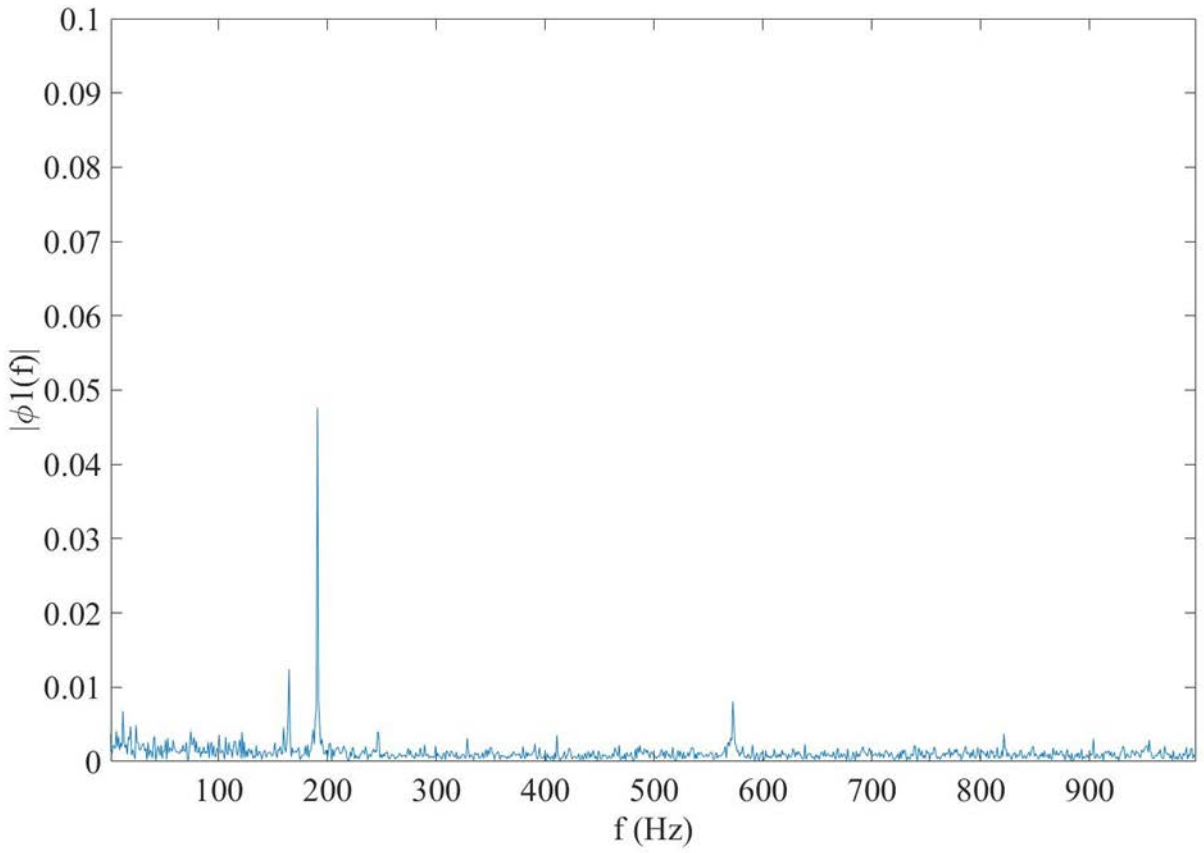

Figure 26. Verification data for no flow vs cold flow measurements

4.2 Flow Characteristics

The flow in the following experiments will be quantified by the total flowrate and ER provided in the operating program. However, with fluid mechanics there are non-dimensional terms associated with these flows that better provide insight into the flow characteristics. These are the Reynolds number and Strouhal number. The Reynolds number provides information about the ratio of inertial forces to viscous forces which can describe the laminar or turbulent characteristics of the flow. The Strouhal number describes oscillating flows and can provide insight into the vortex shedding within the flow. These are calculated with the following equations:

$$\mathrm{Re} = \frac{\rho v L}{\mu} \tag{4.6}$$

where ρ is the density, v is the flow velocity, L is the characteristic length, and μ is the dynamic viscosity.

$$St = \frac{\omega L}{v} \tag{4.7}$$

where ω is the oscillation frequency, L is the characteristic length, and v is the flow velocity.

4.3 PMT Measurements

It has been hypothesized that chemiluminescence measurements can be directly correlated to equivalence ratio. This is done through a calibration series and utilizing the line of best fit from this data to correlate equivalence ratio. The calibration data will be presented in the results of this study.

In order to use the chemiluminescence data, the measurements from the three PMTs must be adjusted for both wavelength and gain. Thorlabs provides this data for the output of the PMM01 PMT used in this study. Figure 27 shows the curve for the spectral response of the PMM01 PMT.[36] This curve will be used to obtain the sensitivity for 310 nm, 430 nm, and 515 nm. Figure 28 shows the gain response for the bias gain used in the experiments.[36] This curve was input into the data reduction software to adjust based on the input value for each PMT in each test.

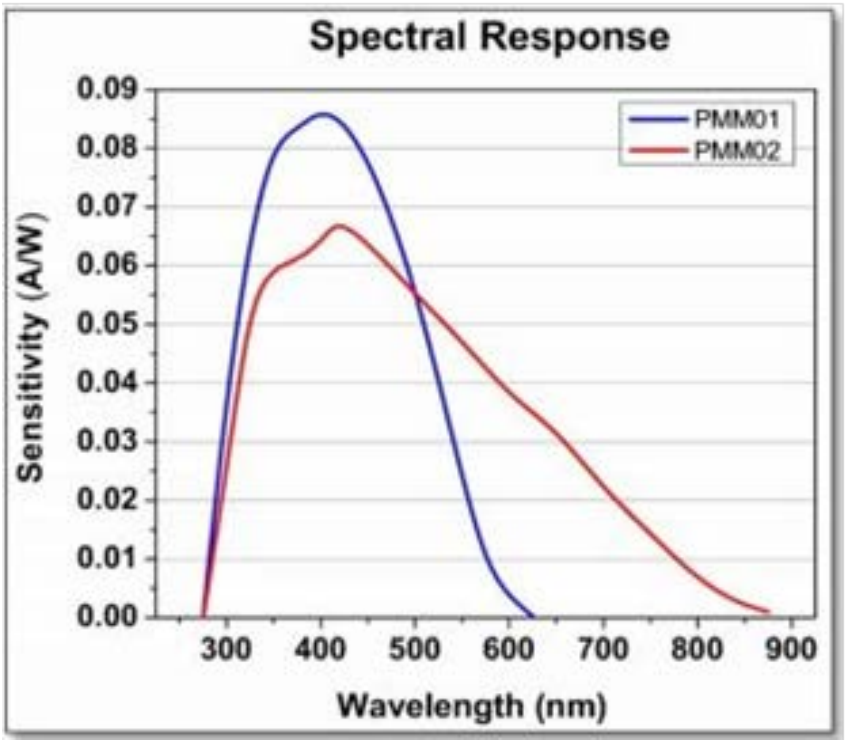

Figure 27. Spectral response for PMM01 PMT [36]

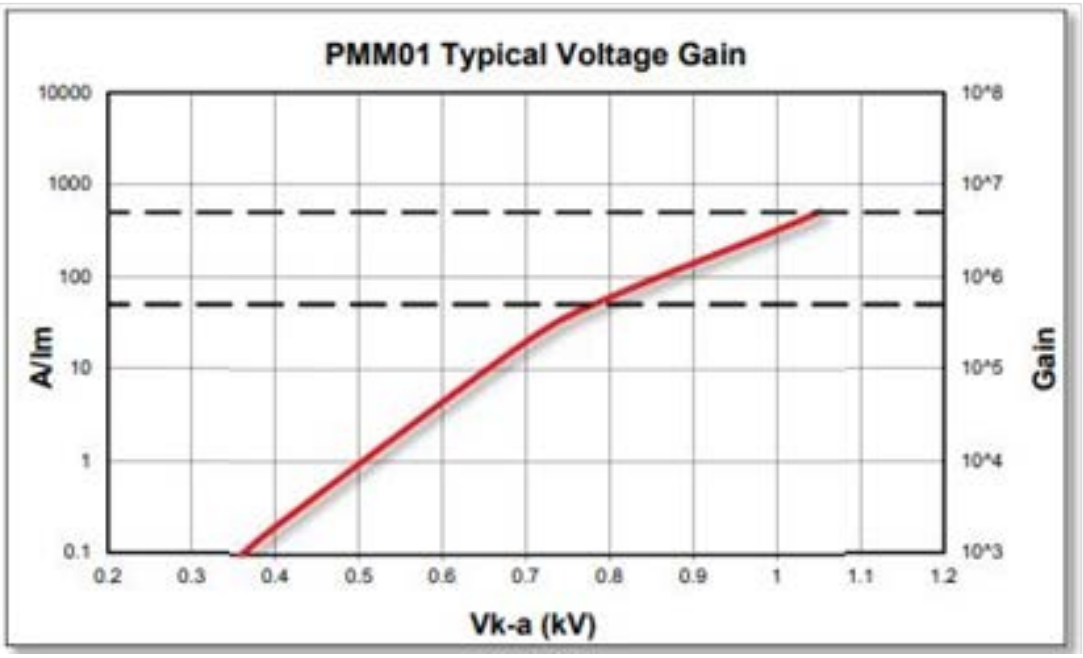

Figure 28. Gain values for PMM01 PMT [36]

Chapter 5: Diagnostic Calibration and Validation

The following chapter discusses the calibration and verification process to validate the experimental setup. The first section consists of the calibration for the IRAS and the DPT. Next, the verification experiments to prove the accuracy of the diagnostic equipment is discussed.

5.1 Component Calibration

This section outlines the calibration for components on the experimental setup. First, this entails calibrating the IRAS. Next, the calibration and verification of the dynamic pressure transducer is outlined. Then the process to determine the acoustic signature of the burner is shown.

5.1.1 HeNe Laser

This section outlines the observations and resulting decisions made for the laser in the IRAS. The HeNe laser operates at a nominal power of 2 mW. It was observed that this power output oscillated with time when taking data. This is crucial for the validity of the experiment as the initial intensity is used to calculate the ER with the Beer-Lambert law discussed previously. Figure 29 shows the maximum raw output value of the HeNe laser over the course of 30 minutes. The top plot shows the first 10 minutes, the middle plot shows the next 10 minutes, and finally the bottom plot shows the final 10 minutes. It can be seen that the laser not only oscillates but changes frequency over the course of a few minutes. This oscillation slows as is shown by the frequency in the bottom plot being less than in the top plot. This trend continues and the frequency continues to reduce but does not completely stop. Therefore, the decision was made to allow the laser to warm up for at least one hour prior to testing so that the oscillations would be minimized and that a calibration file would be taken at intervals no longer than one minute. This ensured that the error would remain within an acceptable limit.

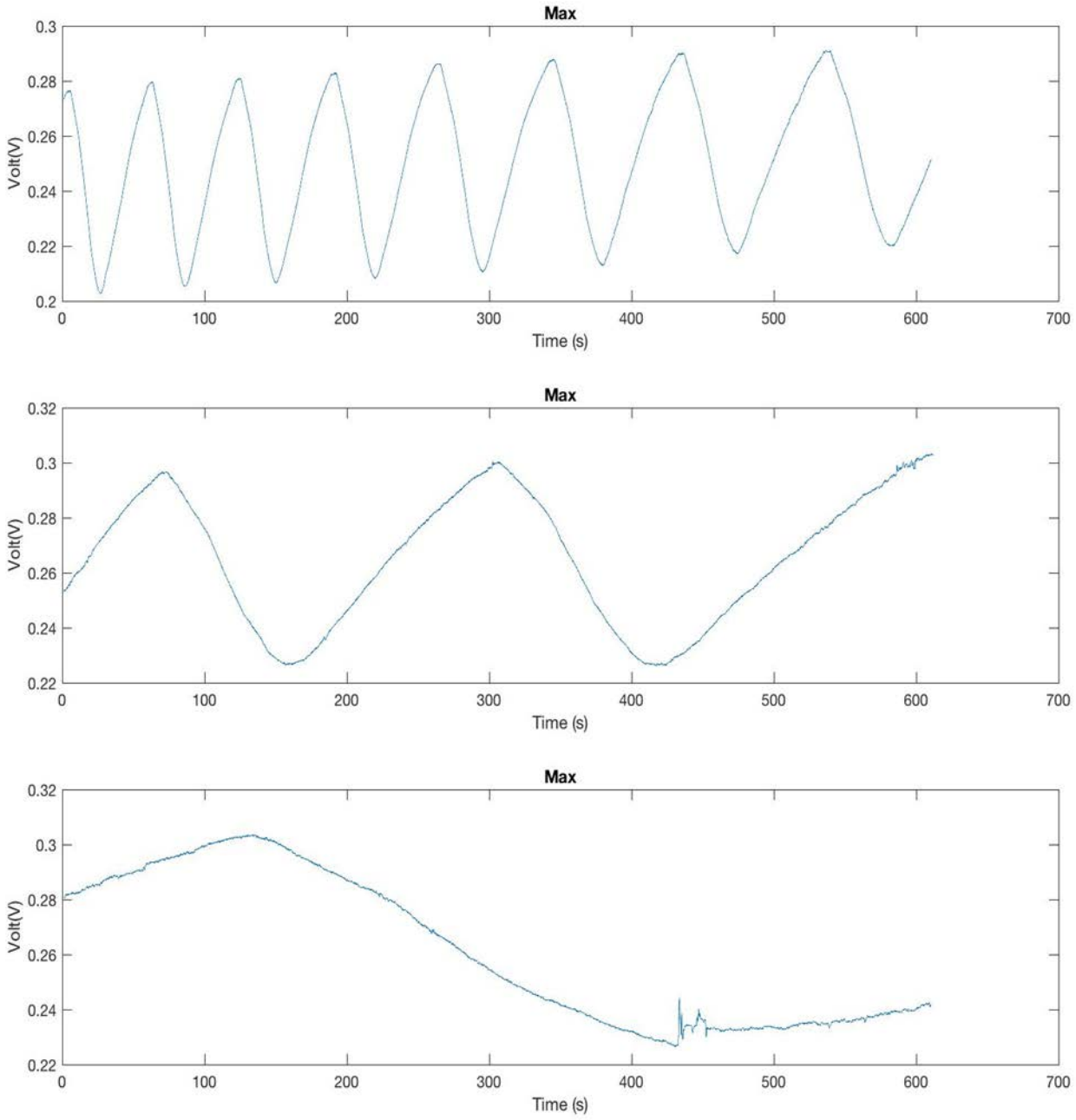

Figure 29. HeNe laser raw output over 30 minutes with 10 minute time intervals

5.1.2 Pressure Transducer Calibration

The DPT was calibrated with a Bruel & Kjaer type 4228 pistonphone. This device is verified to output at 251.2 Hz +/- 1% and 124 +/- 0.2 dB. This correlates to a nominal rms sound pressure level of 31.7 Pa. For the range provided, the low value would be 30.97 Pa and the high value would be 32.44 Pa. The resulting Fourier transform is shown in Figure 30 which indicates a pressure of 40.81 Pa. This gives an rms value of 28.85 Pa which is within 7% of the expected value and deemed acceptable

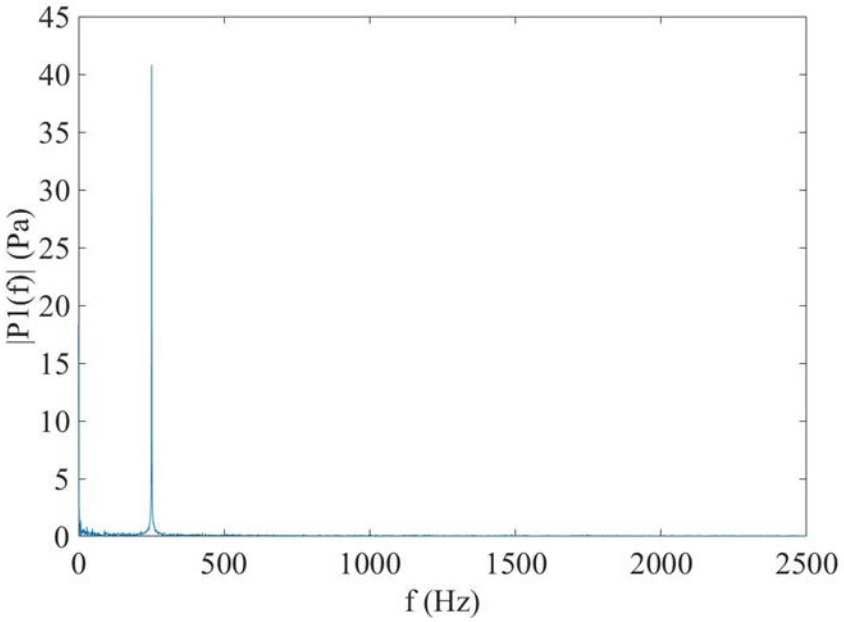

Figure 30. Calibration data for pressure transducer

5.1.3 Burner Acoustic Signature

This section outlines the acoustic signature of the completed burner. To conduct tests at significant pressure oscillations, a frequency sweep was conducted with the speakers at intervals of 5 Hz. First, this process was completed with steady state conditions, i.e. no air flowing nor combustion. Next, the same test was conducted under cold flow airflow. Due to the significant impact of airflow on acoustic signatures, air was run at a condition of 70 SLM which was in the

middle of the conditions tested in the studies. Finally, this same acoustic signature test was conducted with the burner ignited at a flowrate of 70 SLM and ER of 0.8. The results for these tests are shown in Figure 31. They indicate pressure nodes for the cold flow and no flow tests at 150 Hz and 500 Hz. These frequencies will be used along with 400 Hz in the cold flow study as a result of these findings. The burning case dramatically affects the signature at the lower frequencies and shifts the upper node to 540 Hz which agrees with the expected findings that the combustion process modifies the acoustics in the combustion chamber.

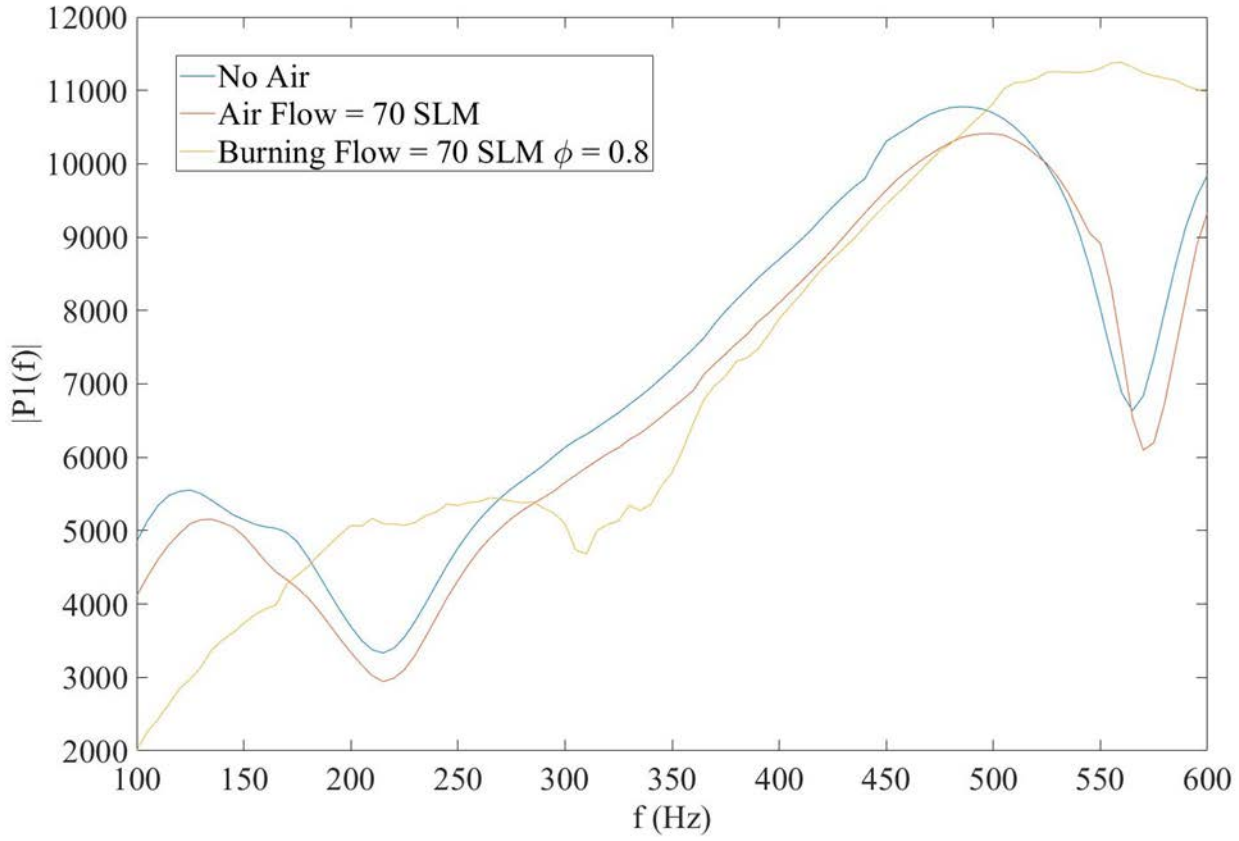

Figure 31. Acoustic pressure overlay for 1) Steady state with no flow 2) Flow at 70 SLM 3) Burning with total flowrate of 70 SLM and ER of 0.8

5.2 Experimental Verification

This section outlines the verification experiments and data used for the various diagnostic probes. In order to assertively conclude results from the experimental setup it must first prove its ability to measure known cases accurately. This began with the steady state flow cases for the IRAS ER measurements. From this data, the probe can confidently determine static ERs at various flowrates. This is followed by quantifiable dynamic tests that show the IRAS is capable of measuring oscillating ERs which is critical for the following studies about combustion instabilities. Using these two sets of data, the validity of the probe to measure unknown frequency oscillations is speculated. Next, experiments showing ER oscillations as well as no oscillations when expected are conducted to verify the burner and acoustic forcing operation. Under certain circumstances even with acoustic forcing, there should not be ER oscillations, and this needed to be verified for both the flow control system and the diagnostic probes

5.2.1 Steady Flow IRAS Equivalence Ratio Validation

This section describes a series of experiments aimed at validating the IRAS under steady state and MFC forced conditions.

For the “steady state” experiments, the ER was measured using the IRAS and the MFC’s for several overall/air flow rates and ER’s ranging from 30 SLM to 90 SLM and 0.6 to 0.9, respectively. For these experiments, the sintered disc was installed at the base of the burner between the two aluminum blocks so that the fuel and air was well mixed by the time it reached the measurement locations. This was done to ensure that the local measurement matched the global ER measured by the MFCs. This verified that the IRAS could measure various amounts of fuel in different flows.

Figure 32 shows the MFC and IRAS measured ER history results for an overall flowrate of 30 SLM and global ER of 0.9. These results show that the average IRAS measured ER closely matches the ER measured using the MFC's. However, the IRAS ER history contains some "noise".

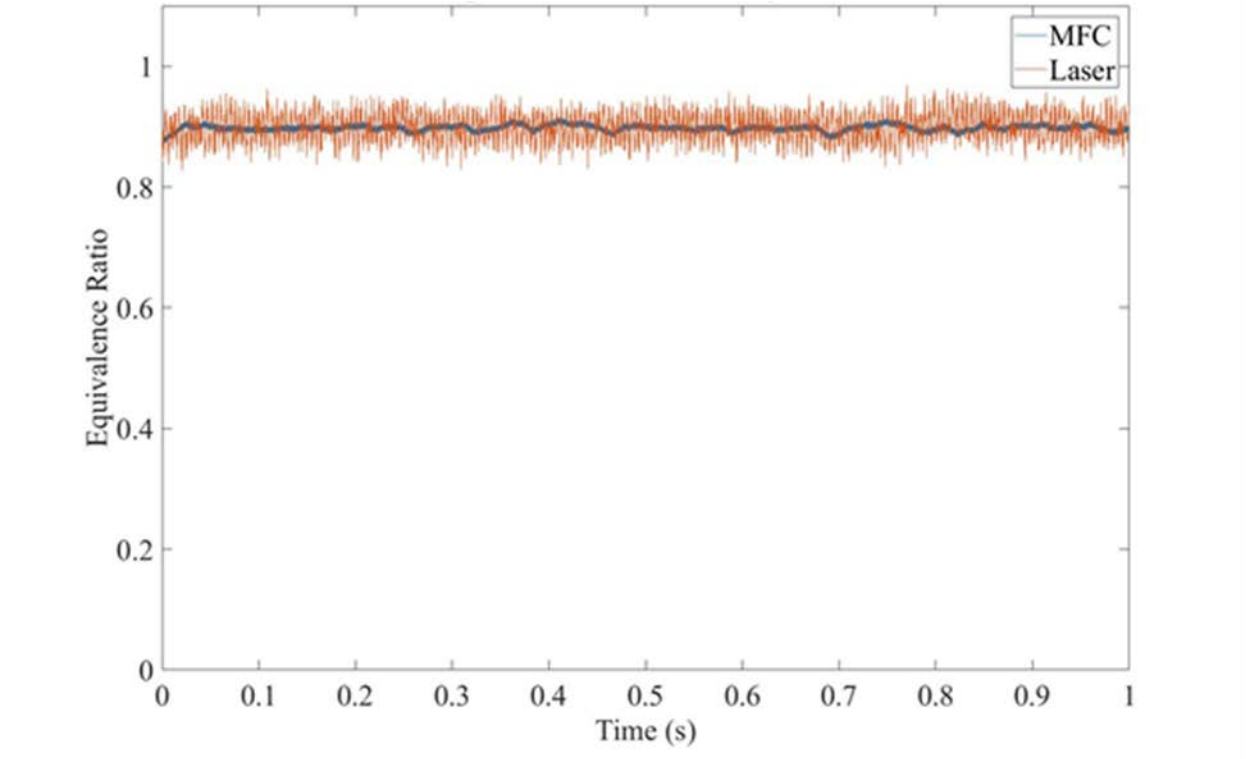

Figure 32. HeNe probe validation at Total Flowrate = 30 SLM and Phi = 0.9

The ER was also measured at different axial locations in the premixing and combustion sections to determine whether or not the IRAS measurements exhibited any dependence on measurement location. As before, these experiments were conducted with the sintered disc installed. The ER was measured using the IRAS at locations 14 cm, 18 cm, 22 cm, 24 cm, and 26 cm from the inlet of the fuel for global ER's from 0.5 to 1.0 at a flowrate of 80 SLM. Figure 33 shows the ER measured by the IRAS at each location divided by the ER measured at location 1. The first number in the legend indicates the ER and the second number indicates the total

flowrate in SLM. These results show that the IRAS measured ER exhibit a maximum difference of +/-10% for all cases. These results verified that the IRAS measured ER was in good agreement with the global ER at all measurement locations, both upstream and downstream of the swirler.

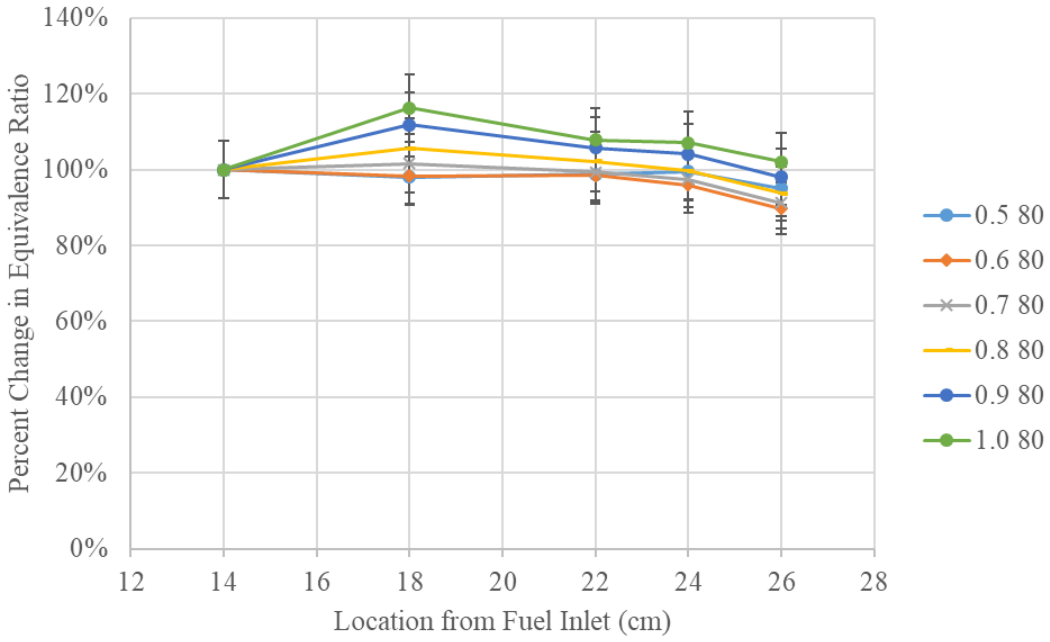

Figure 33. Equivalence ratio measurements along the combustor at 80 SLM

5.2.2 Dynamic IRAS Equivalence Ratio Validation

The previous section established that the laser absorption technique accurately measured the steady ER. The next step was to establish that the IRAS could measure ER oscillations at frequencies up to 500 Hz. Therefore, an ER of known amplitude and frequency was generated using the MFCs. The MFCs were programmed to provide a time varying ER of known amplitude about a set nominal ER. Due to the inherently low frequency response of the MFCs, these tests were limited to frequencies of 5 Hz or less.

The results for a test set at a nominal ER of 1.1 with oscillations of 0.35 amplitude at 1 Hz is shown in Figure 34 and the corresponding spectrum of this test is shown in Figure 35.

These figures show that the IRAS measurement matches the prescribed mean equivalence ratio and equivalence ratio oscillation amplitude accurately with an average error of 0.89% and maximum of 22.8%. Furthermore, the spectrum of this test shows the correct amplitude and frequency of 0.35 and 1 Hz. The nominal value for the equivalence ratio is shown at 0 Hz as 1.1 and an amplitude of 0.35 is shown at 1 Hz.

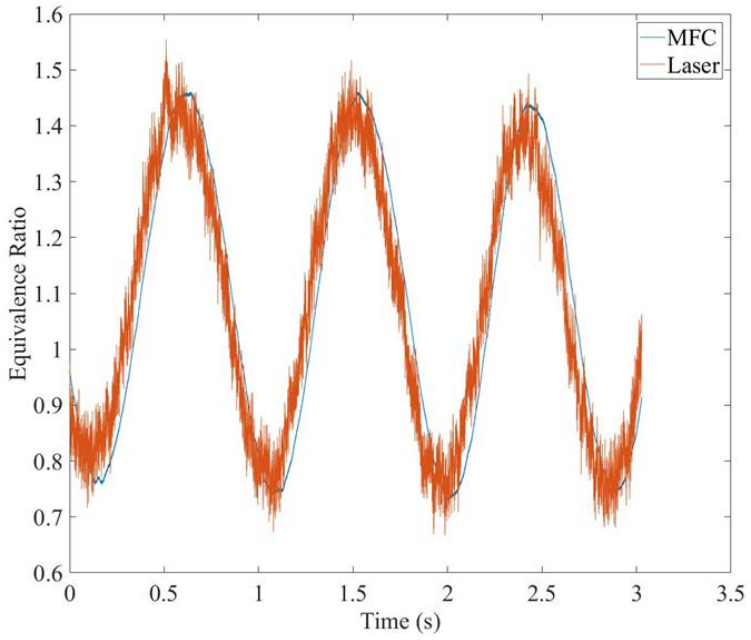

Figure 34. Dynamic verification test for the IRAS with a nominal ER of 1.1 and amplitude of 0.35 at 1 Hz

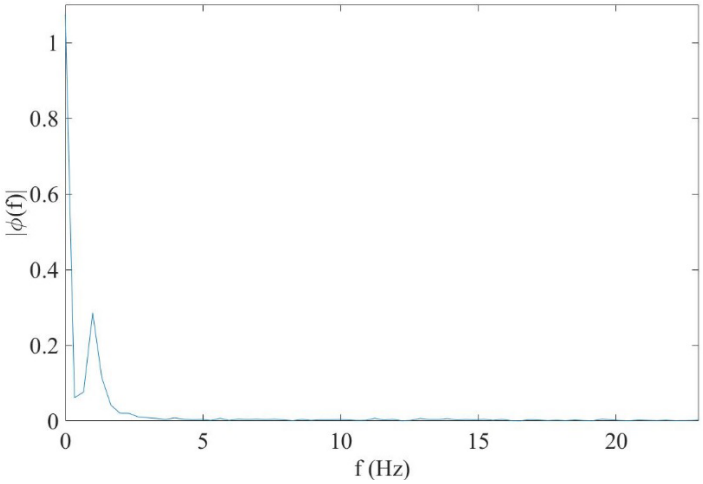

Figure 35. FFT amplitude spectrum of dynamic laser validation experiment for nominal ER of 1.1 and amplitude of 0.35 at 1 Hz

With the results for the steady flow and known dynamic tests, it is conjectured that the IRAS can measure greater frequencies. This assumption is made based on the accuracy of the probe at known values and the detectors ability to measure at frequencies high enough for satisfactory resolution at the desired ER oscillations. This will be crucial as the frequencies desired to measure in the study are up to 500 Hz.

5.2.3 Choked Inlet Conditions

In order to verify that the IRAS measurement aligned with expected results under choked inlet conditions, tests were conducted with and without acoustic forcing with choked fuel and air inlet conditions. The choked inlet conditions guarantee that there should be no ER oscillations regardless of acoustic forcing or combustor operating conditions. For these tests, the fuel and air supply systems were choked and allowed to completely mix before entering the base of the burner. This was conducted with the pipe T and needle valve shown in Figure 36. Furthermore, the oxidizer MFC was set to full open so that the flowrate could be controlled by choking the flow at the needle valve. The fuel MFC remained controlled by the LabVIEW program to maintain control of the ER. Tests were conducted with no flow, cold flow, and under burning conditions.

Figure 36. Needle valve and piping for choked inlet condition experiments

The initial test compared the no flow condition to a cold flow of 50 SLM with ER of 0.8. This amplitude spectrum was expected to show no oscillations as there were no forcing conditions nor natural instabilities. The results are shown in Figure 37, which show an apparent ER oscillation near 200 Hz for both conditions in spite of the fact that there were in fact no equivalence ratio oscillations present.

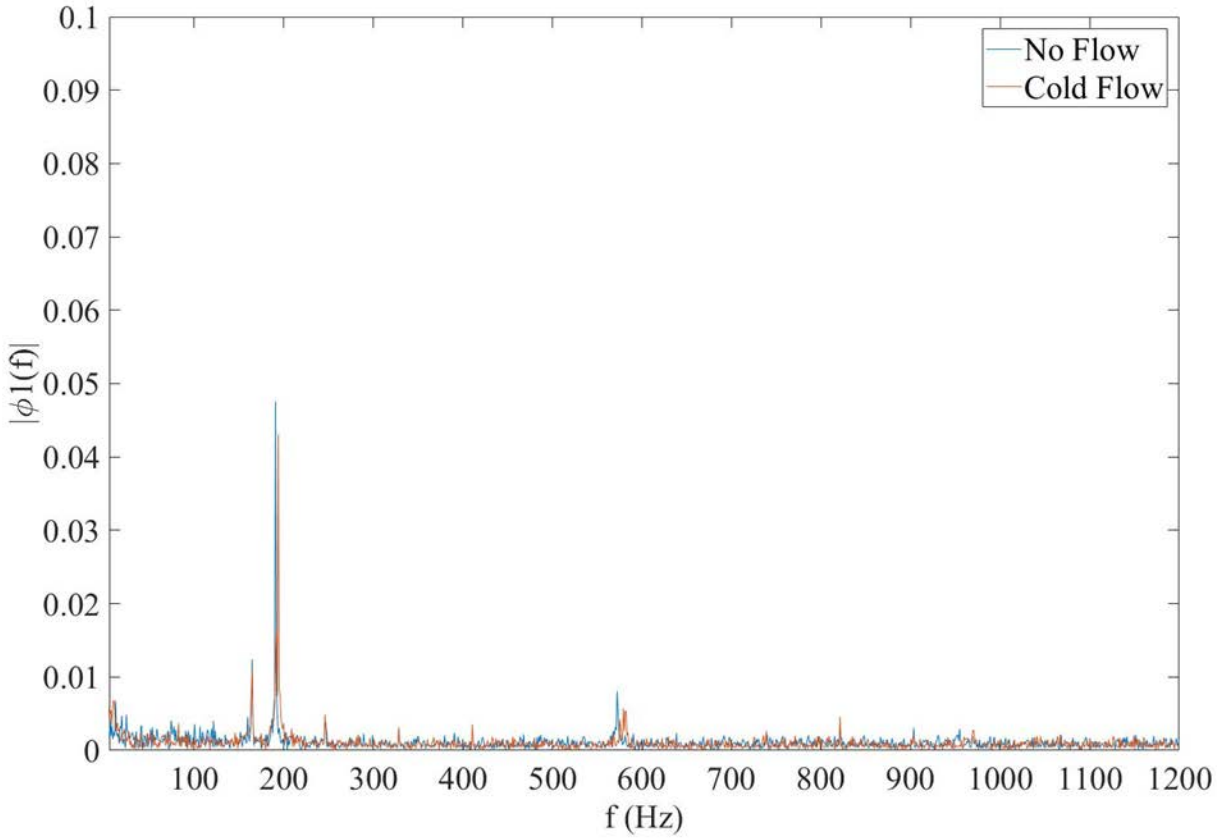

Figure 37. Raw laser output amplitude spectrum

Next, for the same nominal operating conditions the speakers were used to provide acoustic oscillations at frequencies of 100, 300, 500, and 1000 Hz. As before, the choked fuel and air supply systems guarantee there will be no ER oscillations for these tests. Figure 38 shows the amplitude spectrum of the IRAS measured ER oscillations for these tests. As before, the amplitude spectrum reveals an ER oscillation at 200 Hz. However, it does not show any significant oscillations at the driving frequencies which indicates that the inlet choking is working as expected. The most significant oscillation occurs at 500 Hz which is still of a magnitude that is below the oscillations normally driven in the chamber.

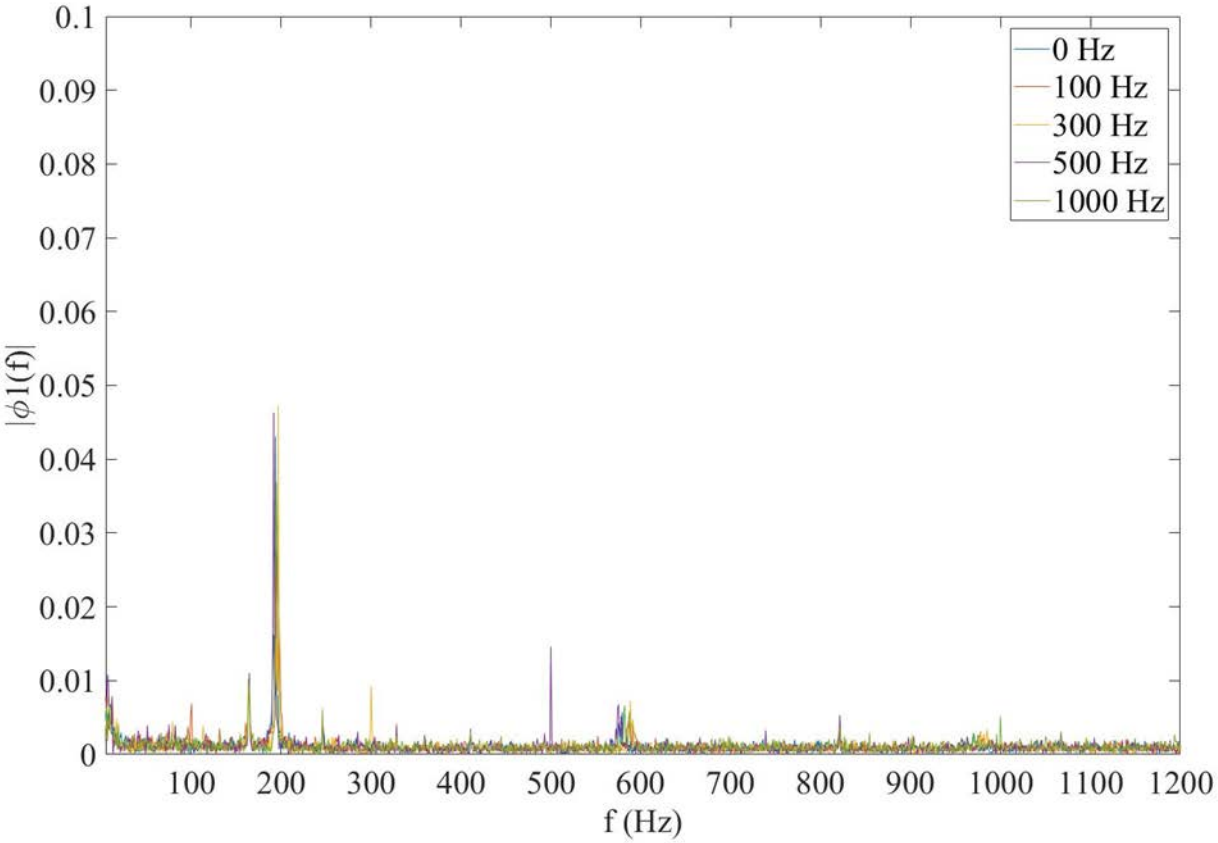

Figure 38. Choked inlet condition frequency sweep

5.2.4 Repeatability Study

Finally, a study was conducted to verify the repeatability of the IRAS measurement. These tests were conducted at a location upstream of the swirler and a location downstream of the swirler. The study consisted of unforced cases and acoustic forcing of 150 Hz and 500 Hz, Global ERs of 0.7 and 0.9, and flowrates of 60 and 80 SLM repeated 5 times. This set of tests is summarized in Table 2.

Table 2. Test matrix for repeatability study

Test Variable	Values Tested
Locations	Upstream, Downstream
Frequency (Hz)	0,150,500
Global ER	0.7,0.9
Flowrate (SLM)	60,80

The results showed that the measurement was repeatable with a maximum average standard deviation between tests of 3.6%. The least deviation between tests occurred for the unforced cases at both locations with roughly the same average standard deviation of 0.6%. All of the forced cases measured roughly 3% standard deviation across all of the forced cases. The complete results are shown in Appendix II with a summary below in Table 3.

Table 3. Repeatability test results

	Condition	AVG St Dev
Location 1	Unforced	0.64%
	Forced 150 Hz	2.78%
	Forced 500 Hz	1.42%
	Forced MFC	1.67%
Location 2	Unforced	0.56%
	Forced 150 Hz	3.14%
	Forced 500 Hz	2.46%
	Forced MFC	3.57%

The following chapter presents the two studies conducted with the experimental setup discussed in Chapter 3. First, the IRAS will be used to measure ER oscillations at several locations throughout the inlet duct and combustor to investigate how the ER oscillations change as they propagate through the system. Next, the PMT system described above will be used to measure ER oscillations in the flame. These measurements will then be compared with the IRAS measured ER oscillations upstream of the flame.

Chapter 6: Results and Analysis

In this chapter, two studies are conducted and analyzed to provide information on ER propagations through a swirl combustor. The first consists of measuring the ER with the IRAS probe at various locations along the burner under cold flow conditions. The second is a study to correlate PMT chemiluminescence to ER oscillations. These studies aim to provide information on how the ER oscillations created at the fuel inlet propagate through the combustor. They will look to analyze the way in which the premixing section, swirler, and dump plane impact the oscillations. This can be valuable in understanding how ER oscillations that begin at the injector reach the flames.

6.1 A Cold Flow Study on Equivalence Ratio Propagation

This section describes the results of an investigation designed to study the manner in which ER oscillations propagate through the premixing section, the swirler, and the combustion chamber under cold flow conditions with and without acoustic forcing. The IRAS was used to measure ER oscillations at 6 locations along the burner including 3 locations upstream of the swirler and 3 downstream.

For the steady flow case, near the injector the fuel is concentrated near the centerline of the premixing duct. As the fuel and air propagate downstream, the fuel mixes radially with the air due to the effects of turbulence. At some point downstream, the fuel and air are completely mixed, and the ER at any radial location is equal to the average, global equivalence ratio as measured using the MFC's. Flow and pressure oscillations in the premixing duct cause the air velocity and fuel injection rate to vary with time resulting in ER oscillations that originate at the fuel injection site and propagate downstream with the convective velocity of the flow. The amplitude of these ER oscillations are expected to decay as the fuel and air mix radially. Further,

axial diffusion may result in further decay in the amplitude of the ER oscillations. The studies described here are intended to quantify the effect of acoustic oscillations on the amplitude of the ER oscillations due to both radial and axial effects.

6.1.1 The effect of acoustic oscillations on equivalence ratio oscillation amplitude

The first portion of this study aimed to observe the impact that acoustic forcing had on both axial and radial mixing. This study was conducted with the second swirl burner previously outlined in Chapter 3. In order to analyze both axial and radial mixing, the fuel was injected 12 cm from the base of the burner which located it at the bottom of the premixing section. This was done to reduce the amount of time for fuel-air mixing upstream of the first measurement location. This provided for maximum ER oscillations in this case. The ER was measured at a total of 6 locations, three below and three above as shown in Figure 39. Distance from the burner base was measured using a laser-target card and ruler. The three locations below the swirler were 3 cm, 5 cm, and 7 cm above the burner base. The three locations above the swirler were 1 cm, 3 cm, and 5 cm above the swirl plane. The fuel was injected 1 cm above the burner base so these locations correspond to 2 cm, 4 cm, 6 cm, 10 cm, 12 cm, and 14 cm above the fuel injection point or location 1, 2, 3, 4, 5, and 6 as indicated on Figure 39. These distances correspond to the locations shown on the following plots. These measurement locations allowed for insights into the way in which the mixing chamber, swirler, and dump plane had on the equivalence ratio oscillations.

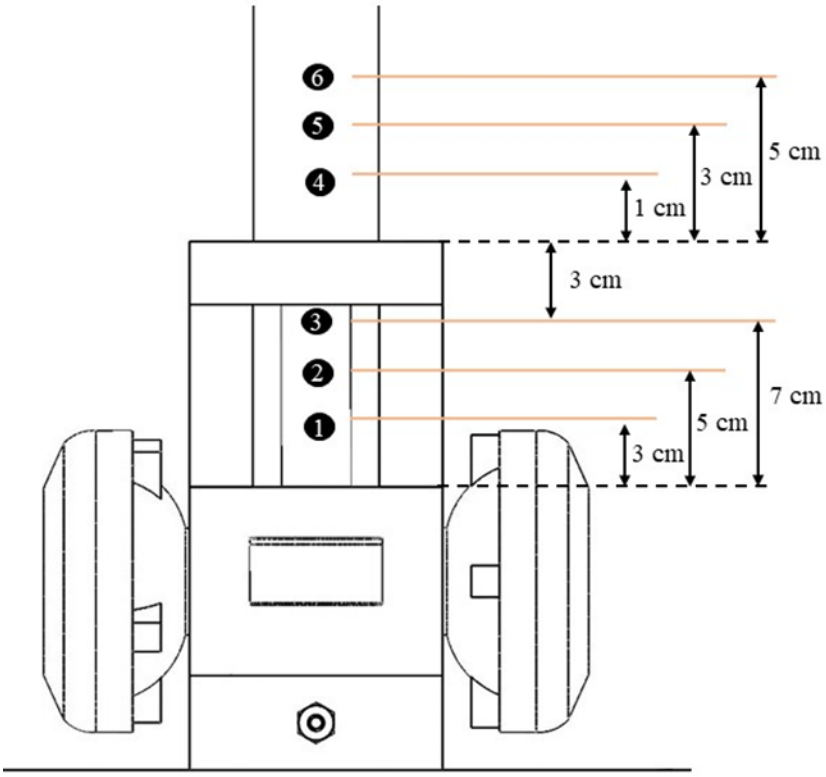

Figure 39. Cold flow laser absorption locations

The study consisted of acoustic forcing of 100 Hz, 150 Hz, 300 Hz, 400 Hz, and 500 Hz, ERs of 0.7, 0.8, and 0.9, and flowrates of 60 SLM, 70 SLM, and 80 SLM repeated at all 6 locations previously discussed. This set of tests is summarized in Table 4. The Reynolds number and Strouhal number for each case are shown in Appendix IV.

Table 4. Test matrix for combined mixing cold flow study

Test Variable	Values Tested
Total Flowrate (SLM)	60, 70, 80
Driving Frequency (Hz)	0,100,150,300,400,500
Global ER	0.7, 0.8, 0.9

The acoustic forcing frequencies of 150 Hz and 500 Hz were chosen to provide for maximum acoustic pressure oscillations based on the acoustic response of the burner shown in Figure 31.

The other forcing frequencies were included to further understand the relationship between forcing frequency and ER oscillations. In order to eliminate amplitude effects, the acoustic pressure amplitude was held constant for the 5 frequencies. This consisted of measuring the pressure amplitude at various power settings for each frequency and amplitude matching them.

The results for a typical condition with a flowrate of 60 SLM, ER of 0.7, and acoustic forcing of 150 Hz are shown in Figure 40. The results are normalized using the steady ER magnitude so that the ER spectrums are represented as a percentage of the nominal ER. As observed on this spectrum, the magnitude of local ER oscillation can reach 40%. The spectrum of the IRAS ER measurements shown in Figure 40 confirmed that the dominant ER oscillation amplitude is at the driving frequency, with secondary peaks at the harmonic frequencies. For this investigation, only the driving frequency will be considered. A close up of the driving frequency for this same test case is shown in the cutout. The first location, located closest to the fuel injector and centered in the fuel stream is expected to have the highest amplitude, as it corresponds to the least mixed location. Furthermore, Figure 40 shows a successive decrease in amplitude for each location, with the three locations above the swirler being only marginally different.

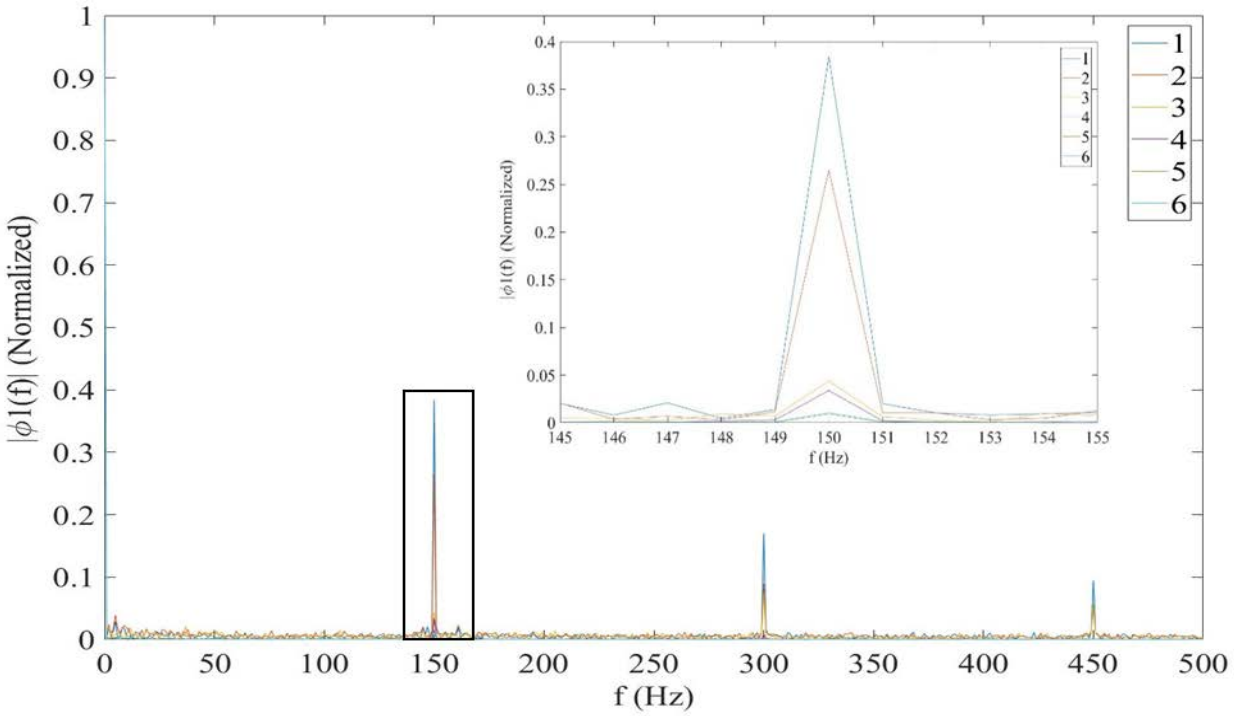

Figure 40. Normalized equivalence ratio spectrum for each location at a total flow of 60 SLM, equivalence ratio of 0.7, and frequency of 150 Hz, with focus on dominant 150 Hz amplitude.

Next, the decay rate was examined by normalizing the ER oscillation amplitude at the driving frequency by the first location's, as shown in Eq. (6.1).

$$\phi\left(f_{driving}\right)_{normalized} = \frac{\phi\left(f_{driving}\right)_i}{\phi\left(f_{driving}\right)_1} \tag{6.1}$$

For the unforced condition, this amplitude is the nominal equivalence ratio, evaluated at $\phi_i(0Hz)$, as there are no oscillations within the chamber. This was then averaged across all flowrates and nominal global ER. The primary interest in this study is the change in magnitude of local ER oscillations from location to location. Since there is radially mixing, as discussed in the previous section, it is expected that the local equivalence ratio measured will decrease as the distance from the fuel inlet increases until it is well mixed. The results for this analysis are shown in Figure 41.

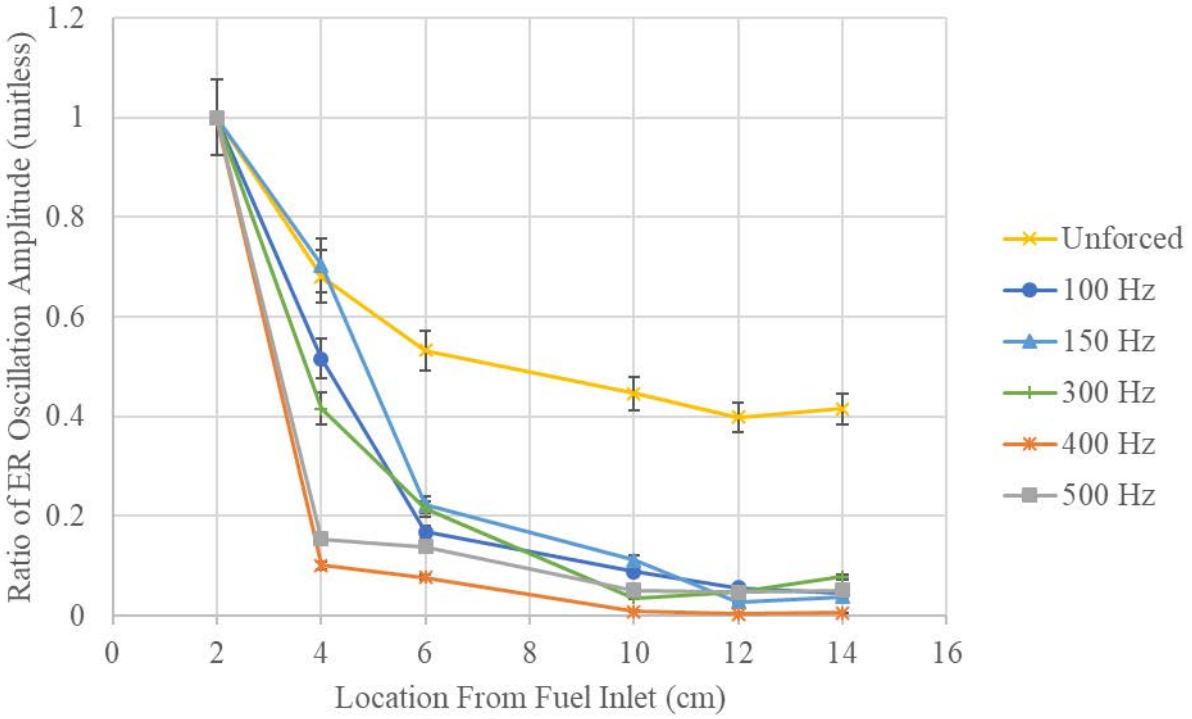

Figure 41. Ratio of ER oscillations to location 1 vs location from fuel inlet at each frequency

These results show that the unforced condition experiences a decrease in local ER with axial location. This follows from the explanation in Chapter 3 in that this is a measurement of the local ER as opposed to the global ER which is held constant in all of the conducted tests. These results show that under unforced conditions the flow has almost mixed completely so that the local ER measurements decreases as it approaches the global ER by location 4. The global ER supplied by the MFCs correspond to roughly 40% of the initially measured local ER from the IRAS. This slope of the unforced case shows that the most significant drop comes in the mixing chamber and is further aided by swirler which is at 9 cm from the fuel injection. Following the swirler the ER flattens which corresponds to the chamber reaching a well-mixed condition. In contrast, the ER oscillation amplitude for all five forced cases decreases much more rapidly as axial location increases. This supports the hypothesis that the acoustic driving is aiding the

mixing upstream of the swirler. Furthermore, the higher frequencies of 400 and 500 Hz exhibit increased mixing upstream of the swirler over the lower frequencies of 100, 150, and 300 Hz. This is observed by the more rapid decrease in oscillation for these cases by location 2. Then all of the forced cases show similar reduction across the swirler and then level out downstream in the combustion chamber.

The decay in ER oscillation amplitude shown is due to the combined effect of radial and axial mixing. The effect of radial mixing can be understood by considering the following. As the flow propagates downstream, the fuel mixes radially with the air reducing the ER at the center and increasing it away from the center as shown in Chapter 3 on Figure 16. At some point downstream of the fuel injector, the fuel is completely mixed with the air as shown in Figure 16(c). At each measurement location in this scenario, the mixture is homogeneous and a single measurement consequently gives the correct global equivalence ratio.

Therefore, the unforced case in Figure 41shows how the fuel and air mix as they propagate downstream from the injection site. The acoustically forced measurements shown in Figure 41 show that the acoustic oscillations dramatically increase the rate of radial mixing as the fuel and air propagate downstream from the injection site. Further, these measurements indicate that the rate of mixing increases with frequency up to 500 Hz.

Focusing on the 150 Hz and 500 Hz cases shown in Figure 42 and Figure 43, respectively, can provide additional insights into the mixing in the chamber. Understanding that these results mainly show the axial mixing, they indicate that the fuel and air axial mixing is dependent on acoustic forcing frequency. The first number in the legend indicates the ER and the second number indicates the total flowrate in SLM. The 150 Hz cases show more variance than the 500 Hz at both upstream locations. This corresponds to standard deviations of 6.0 and 7.7 for

locations 4 cm and 6 cm respectively while the 500 Hz cases exhibit standard deviations of only 4.3 and 2.2 for the same locations. However, as both conditions move from location 6 cm to 10 cm which corresponds to the location of the swirler the variance drops. The 150 Hz case has a standard deviation of 0.9 while the 500 Hz case has a standard deviation of 1.0. This supports the claim that the swirler is aiding the mixing process and therefore reducing the variance in equivalence ratio downstream of the swirler.

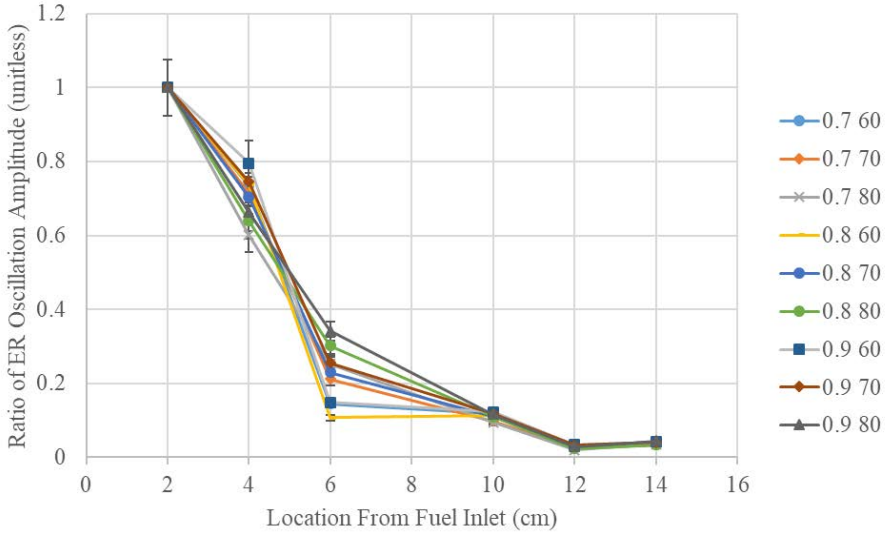

Figure 42. ER oscillation ratio of initial location to each location and operating condition at 150 Hz

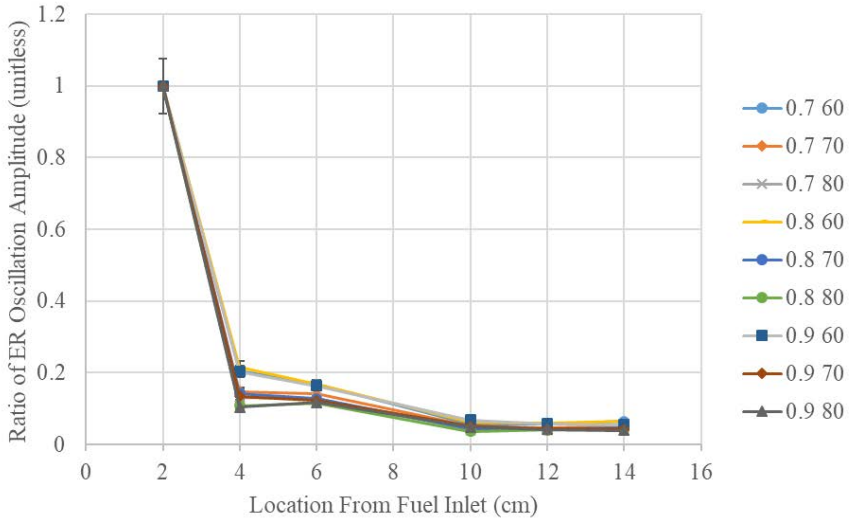

Figure 43. ER oscillation ratio of initial location to each location and operating condition at 500 Hz

In summary, the results for the initial cold flow study focusing on the combined radial and axial mixing in the combustor indicated that ER oscillations drop through the swirl combustor based on frequency. The higher frequency acoustic forcing increased the mixing upstream of the swirler more rapidly than the lower frequency cases. Furthermore, the results show that the acoustic forcing in general aided the mixing as can be observed from the unforced case to forced cases. Each frequency exhibited better mixing by location 3 than the unforced condition.

In order to isolate the effects of axial mixing, the fuel and air must be homogeneously mixed in the radial direction. Therefore, the fuel inlet was relocated to the base of the burner to allow time for radial mixing to occur upstream of the first measurement location, and the tests described above were repeated.

For these tests, the fuel inlet location was moved to a location 12 cm lower than the previous experiments. The measurement locations then correspond to 14 cm, 16 cm, 18 cm, 22 cm, 24 cm, and 26 cm from the fuel inlet. The sintered disc was not inserted to increase the effect of acoustic forcing in the fuel and air lines for the acoustically forced cases. Measurements were made under unforced and forced conditions. For the acoustically forced cases, the forcing amplitude was held constant and the forcing frequency were 300 Hz, 400 Hz, and 500 Hz. The total air flow rate and global ER for these tests were 60, 70, and 80 SLM and 0.7, 0.8, and 0.9, respectively. This set of tests is summarized in Table 5. The Reynolds number and Strouhal number for each of these cases is shown in Appendix IV.

Table 5. Axial mixing cold flow study test conditions

Test Variable	Values Tested
Total Flowrate (SLM)	60, 70, 80
Driving Frequency (Hz)	300, 400, 500
Global ER	0.7, 0.8, 0.9

The results for this cold flow analysis are shown below in Figure 44. Measurements without forcing are nearly constant indicating that the fuel and air were well-mixed upstream of the first measurement location. This provides verification that the local measurement from the IRAS can be assumed to be the global value. With these conditions, the global ER oscillations in the forced cases averaged 3% of the nominal ER supplied by the MFCs. This corresponds to the magnitude of the first location and the value that the results are normalized against. Results for the forced cases indicated that the amplitude of the ER oscillations dropped prior to the swirler with addition of any acoustic forcing. The ER oscillations decreased by about 16% for all forced cases upstream of the swirler. However, the results downstream of the swirler were much less consistent and do not show a consistent drop in ER. One possible factor involved with this trend could be that that swirler has reduced the ER oscillations as much as possible due to the axial flow component. Furthermore, the forced cases also show that the largest drop in equivalence ratio oscillations occur between locations 3 and 4 which corresponds to the location of the swirler. This indicates that the swirler causes significant axial mixing and hence a reduction in the amplitude of the ER oscillations. To further investigate these trends, the same locations were measured using the MFCs to oscillate the ER.

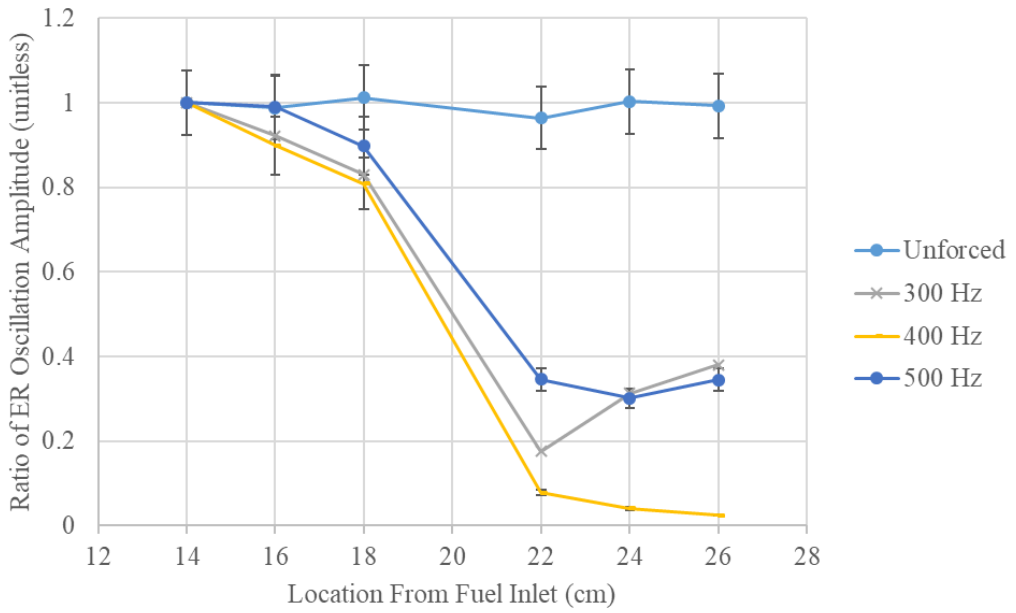

Figure 44. Percentage change in peak equivalence ratio oscillations vs location from fuel inlet at each frequency for the fuel inlet at the base of the burner

To further provide information about the way in which ER oscillations propagate through the combustor, experiments were conducted using the MFCs to provide a time varying ER. Due to the relatively slow time response of the MFC's, the frequency of the provided ER oscillation was limited to less than 5 Hz. However, the MFC's are capable of providing much larger ER oscillations than observed in the acoustically forced cases above. For these tests, the MFC's were operated at a nominal global ER of 1.1 with an ER oscillation amplitude and frequency of 0.23 at 2 Hz, respectively. The fuel inlet was located at the base of the burner so that the locations for the IRAS measurement corresponded to 14, 16, 18, 22, 24, and 26 cm from the fuel injection. The results for this test are shown below in Figure 45. These measurements indicate the ER oscillation amplitude is nearly constant from location 1 to 3, but the ER oscillation amplitude drops by 25% across the swirler which is 21 cm from the fuel injection point. Furthermore, these results show that the ER oscillation amplitude remains fairly constant in the combustion chamber.

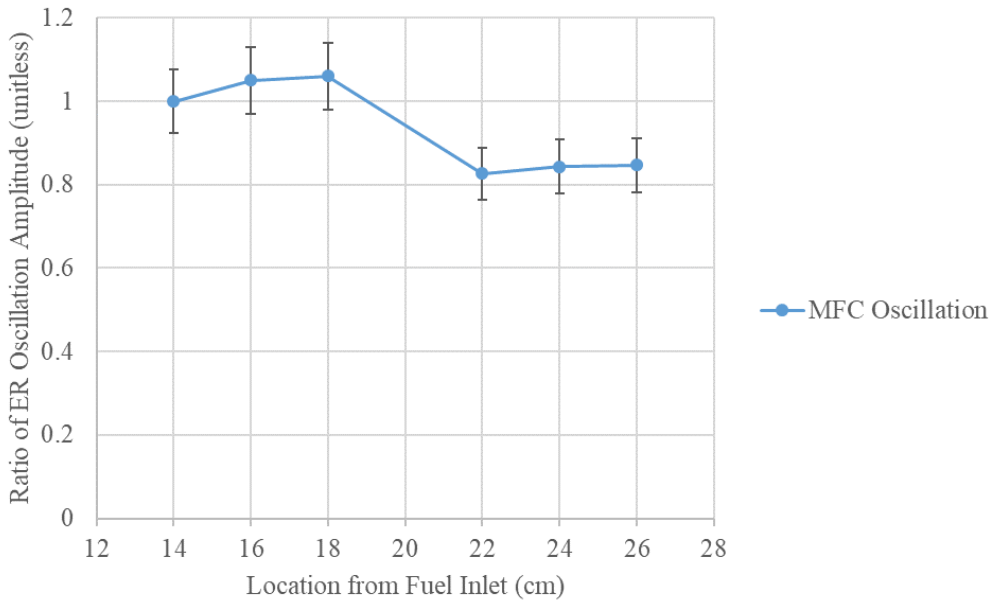

Figure 45. Percentage change in peak equivalence ratio oscillations vs location from inlet at each frequency for the MFC oscillations study

Comparing these results with the acoustically forced cases, the acoustically forced cases dropped 75% across the swirler whereas the MFC oscillation cases only dropped 25%. This indicates that there is some relation between the impact that the acoustic forcing and the swirler have on the equivalence ratio oscillations. One cause of this relation could be the significant difference in pressure oscillations within the chamber under the two scenarios.

It should be noted that while the MFC's provide significant ER oscillations, the acoustic pressure oscillation amplitude in this case was only 238 Pa, which is small compared to the 7200 Pa acoustic pressure amplitude for the acoustically forced cases. Therefore, the observed decrease in ER oscillation amplitude for the MFC cases is due primarily to axial mixing caused by inherent flow instabilities in the axial direction. The swirler causes the flow to be highly three-dimensional compared to the flow field in the constant area premixing duct and combustion chamber resulting in significant reduction in the ER oscillation amplitude across the swirler.

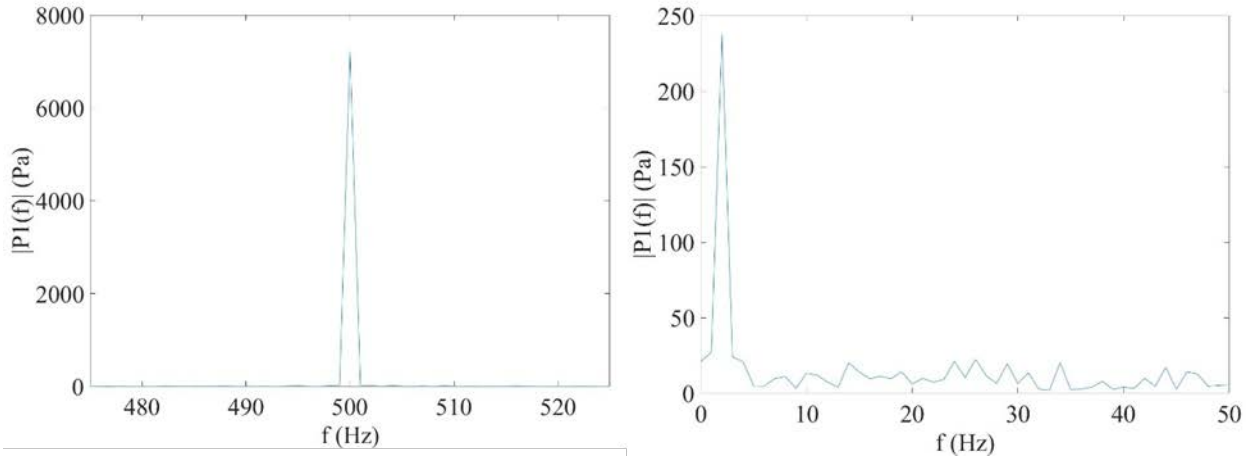

Figure 46. a) Pressure spectrum for acoustic forcing at 500 Hz b) Pressure spectrum for MFC at 2 Hz

In summary, the results indicate that the equivalence ratio oscillation amplitude in the premixing duct were reduced by 16% with acoustic forcing. This was not observed in the MFC forced case due to the very low acoustic pressure amplitude. The ER oscillation amplitude was nearly constant in the combustion chamber downstream of the swirler for both the acoustically and MFC forced cases. However, the ER oscillation amplitude dropped significantly for both the acoustically and MFC forced cases across the swirler. This corresponded to a change from a 25% reduction with the MFC case to 75% under acoustic forcing. This drop was much greater in the acoustically forced cases due to the high amplitude acoustic forcing enhancing the axial mixing. These results indicate that the relatively high amplitude acoustic forcing significantly enhances the axial mixing caused by the swirler. The results also indicate that at all locations, the effect is not significantly dependent on forcing frequency. Overall, these results indicate that acoustic forcing increases the rate of axial mixing and reduces the amplitude of the ER oscillations.

6.2 PMT Equivalence Ratio Study

This section describes tests aimed at evaluating the usefulness of the PMT based ER oscillation measurement technique described previously in Chapter 2. Although the method has been used previously to measure ER oscillations, little has been done correlate this measurement

with ER measurements upstream of the flame. To conduct this study, first the calibration procedure for the chemiluminescence is discussed. Next, static and forced ER oscillation data is measured to verify that the measurement is an accurate measure of ER oscillations in the flame. Finally, a series of experiments were conducted to assess the usefulness of this experimental procedure.

6.2.1 PMT Calibration

To verify the flame spectrum for the propane flame, a full range spectrometer was used to measure the flame's emitted spectrum. A representative spectrum for a flowrate of 55 SLM and ER of 0.7 is shown in Figure 47. This spectrum shows the expected spike at 430 nm for CH*, 515 nm for C2*, and a small peak for OH* at 315 nm. This indicated that C2* and CH* would be good indicators of the strength of the flame. The OH* radical intensity was very small on these spectrometer results which prompted the hypothesis that C2*/CH* would be a better indicator of the ER rather than OH*/CH* which is used commonly with methane flames.[33], [34]

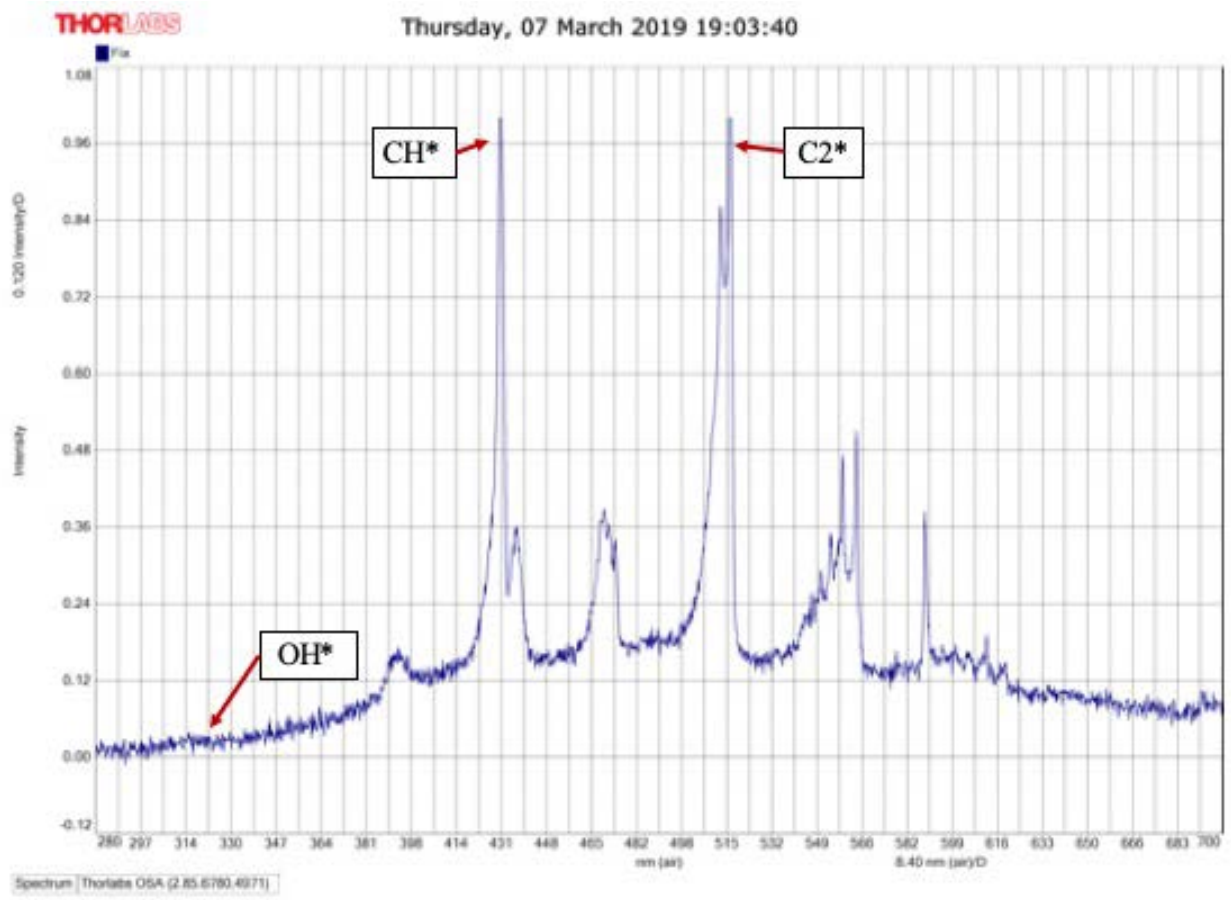

Figure 47. Light spectrum for flow of 55 SLM and equivalence ratio of 0.7

The spectrometer results require an integration time of 2 seconds. Since oscillations within a flame are substantially faster than this, a slow, full-spectrum spectrometer is not viable for ER measurements. Alternatively, PMT's may acquire data at a much faster rate, and thus represent a viable measurement technique. Consequently, three PMTs were setup with bandpass filters for 310 nm, 430 nm, and 515 nm. To obtain a correlation between these measurements and the ER, a calibration set was made. This was done by choking the inlet conditions as described in Chapter 5 to ensure as little natural ER oscillations as possible. Three flowrates were chosen for this calibration series of 50 SLM, 70 SLM, and 90 SLM and equivalence ratios from 0.55 to 1.2. The results for these measurements were fit with a third order polynomial. It should be noted that

previous studies on methane flames used CH*/OH* ratios to measure equivalence ratio and used a linear curve fit.[28], [33], [34] Our results showed that for the propane-air flame C2*/CH* provided a better measure of ER but required using a polynomial curve fit. These data are shown in Figure 48 with the line of best fit plotted over the points. C2*/CH* was chosen because it was the best ratio that correlated well with the ER measurements. As discussed previously, CH*/OH* is the common ratio used when measuring methane flames. However, this ratio does not trend as well for propane flames. This was due to the fact that OH* was so small compared with the CH* and C2* emissions as observed on Figure 47 and could not be distinguished from the background noise in most cases.

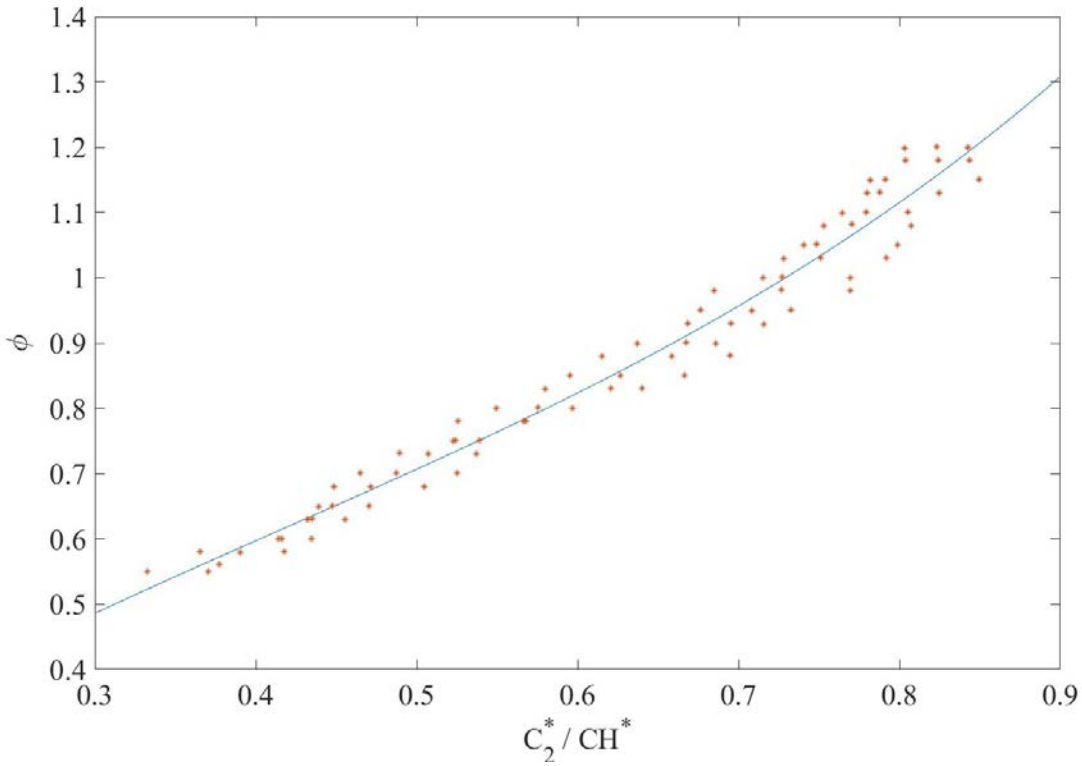

Figure 48. C2*/CH* Calibration data at multiple equivalence ratios and flowrates

6.2.2 PMT Steady State Data

With the correlation from the calibration data, the ratio of C2*/CH* could be used to determine the ER. This was verified with multiple steady state cases to ensure the validity of this measurement. Similar to the IRAS verification, the inlet flows were premixed and then choked with a needle valve. This ensured that natural instabilities or pressure oscillations within the flame would not cause undesired equivalence ratio oscillations during these tests. The results for a case at an ER of 0.7 and flowrate of 70 SLM is shown in Figure 49. Although the PMT data oscillates, it has a mean value of 0.9189 for the desired ER of 0.9.

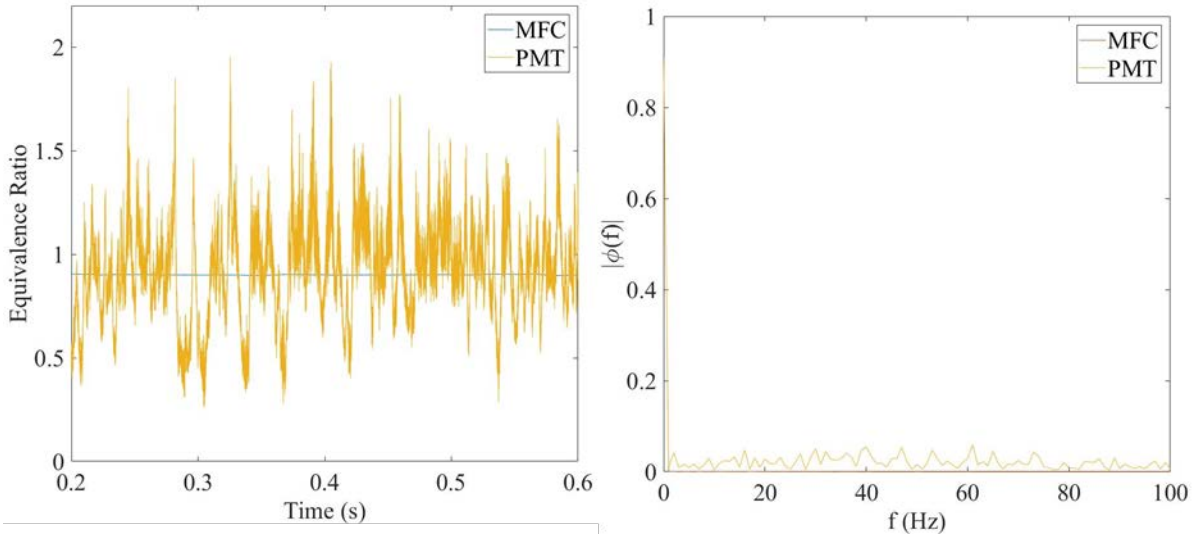

Figure 49. Steady state validation for PMT equivalence ratio at flowrate of 70 SLM, equivalence ratio of 0.7 a) Time domain data b) ER spectrum for data

6.2.3 PMT Dynamic Validation Data

This section describes a series of experiments to investigate whether dynamic C2*/CH* ratio measurements provide a useful measure of ER oscillations within the flame. These tests were conducted using the MFCs to provide equivalence ratio oscillations upstream of the flame as discussed above in regard to the IRAS verification. The nominal equivalence ratio was 1.1 for these tests with ER oscillation amplitude and frequency of 0.1 at 4 Hz, respectively. The ER

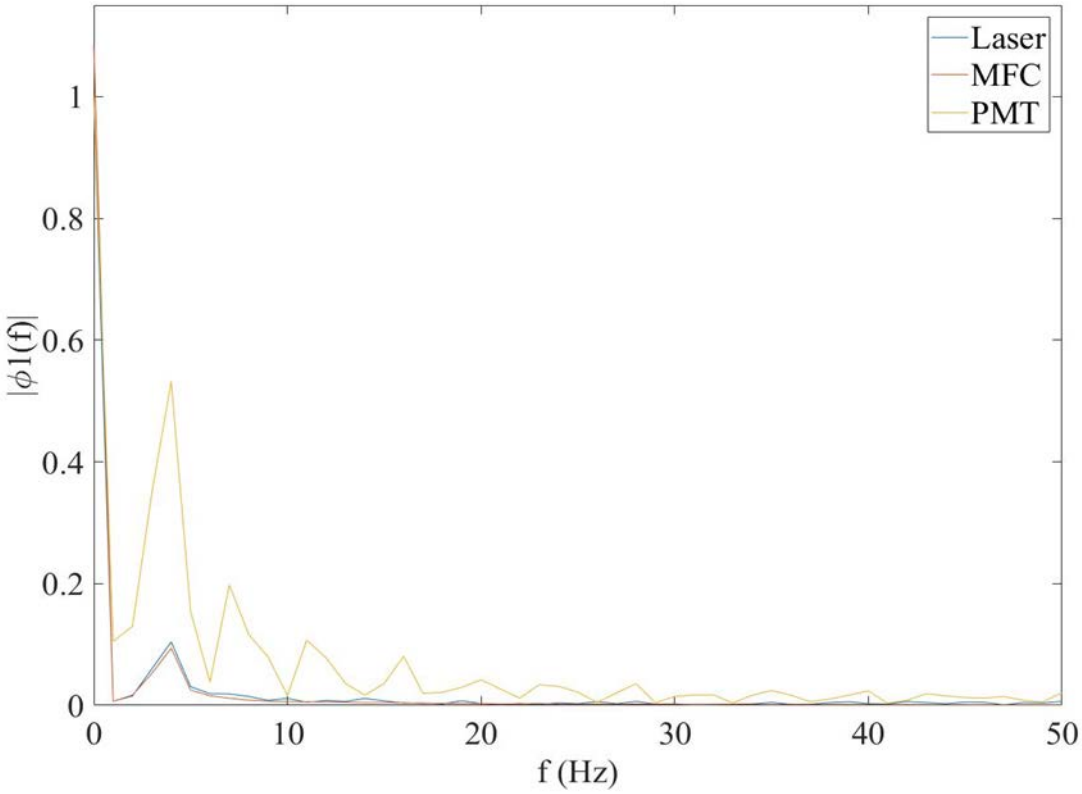

Figure 50. PMT dynamic validation with ER of 1.1 and oscillations of 0.3 at 4 Hz

amplitude spectrum plot for this test is shown in Figure 50. It indicates that the PMT measurement overestimates how much fuel is in the flame. This seemed to occur when the flame moved toward very rich limits. Thus, based on the steady state data and the fact that the tests would be conducted under lean conditions, the probe was deemed acceptable to use in the following study.

6.2.4 Equivalence Ratio Study

This study aims to investigate the relation between the IRAS used in the previous section to the PMT measurement for ER. The goal was to determine if the PMT measurement was capable of measuring oscillations in equivalence ratio at frequencies up to 500 Hz. The test matrix for this study consisted of flowrates of 60 SLM, 70 SLM, and 80 SLM, equivalence ratios of 0.7, 0.8, and 0.9, and acoustic forcing of 150 Hz, 400 Hz, and 500 Hz. This set of tests is summarized in Table 6.

Table 6. PMT study test conditions

Test Variable	Values Tested
Total Flowrate (SLM)	60, 70, 80
Driving Frequency (Hz)	150, 400, 500
Global ER	0.7, 0.8, 0.9

The PMT fiber optic probe was mounted 1 cm above the dump plane, which corresponds to location 4 in the cold flow study cases, and 1 cm away from the combustion chamber quartz tube. Fuel was injected 14 cm above the base of the burner resulting in significant local ER oscillations.

The results at an air flow rate of 80 SLM and nominal global ER of 0.7 is shown in Figure 51, and the equivalence ratio spectrum for this condition is shown below in Figure 52. This figure shows that there is a broad spectrum of low amplitude equivalence ratio oscillations. The spectrum in Figure 52 indicates that the PMT and IRAS match and show a broad spectrum of ER oscillations. Due to the lack of clarity at the largest amplitude oscillation on this plot, a focus is made on 36 Hz to show that both laser and PMT system measure the same ER oscillations. This showed promising results for the measurement as both the laser measurement and the PMT measurement matched and also agreed with the nominal ER.

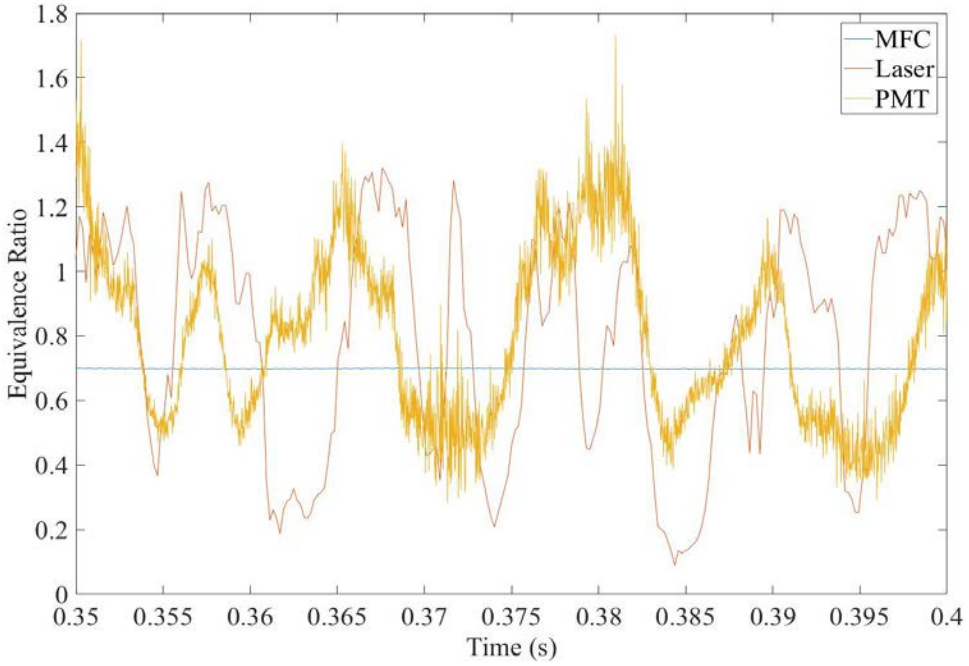

Figure 51. Equivalence ratio for unforced burning at flowrate of 80 SLM and equivalence ratio of 0.7

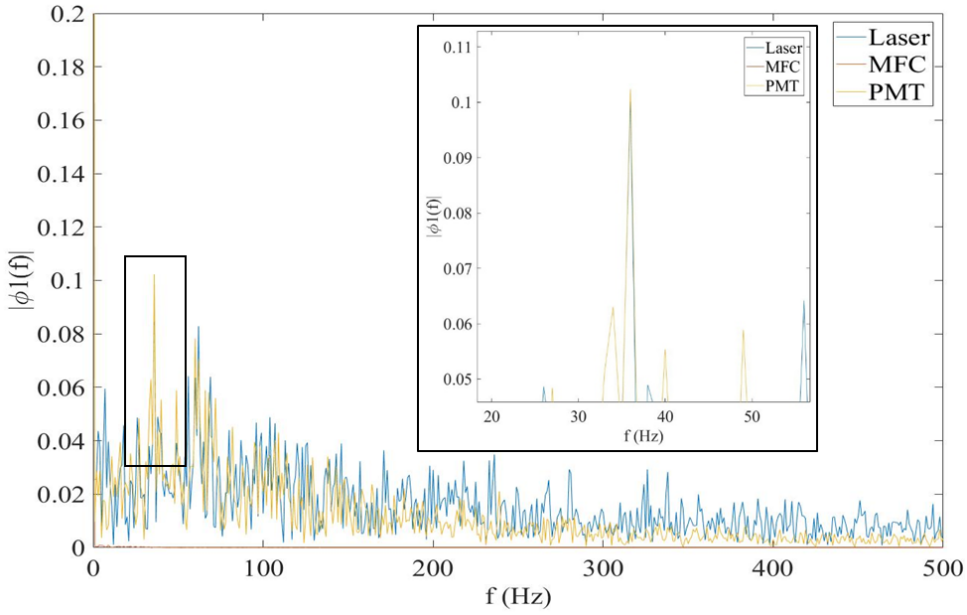

Figure 52. FFT for unforced burning at flowrate of 80 SLM and equivalence ratio of 0.7

Next, the forced cases were analyzed to determine the impact that acoustic forcing had on the measurements. First, a low power acoustically forced test at 150 Hz with a flowrate of 60 SLM and global ER of 0.7 was analyzed and is shown in Figure 53. As stated previously, the fuel was injected at the initial condition that was 14 cm above the base of the burner. Consequently, these measurements are compared with the initial measurements from the cold flow study. For this test, the IRAS measured at location 1 from the cold flow study and the PMT probe was measured at location 4. The IRAS measured an ER oscillation of 0.2385 while the PMT measured oscillations of 0.03123. Based on the findings of the cold flow study in this operating condition, it is expected that the oscillations drop by 88.8% from location 1 to location 4. These results correspond to a drop of 86.9%. These findings show that the PMT equivalence ratio is in good agreement with the expected value in this test case.

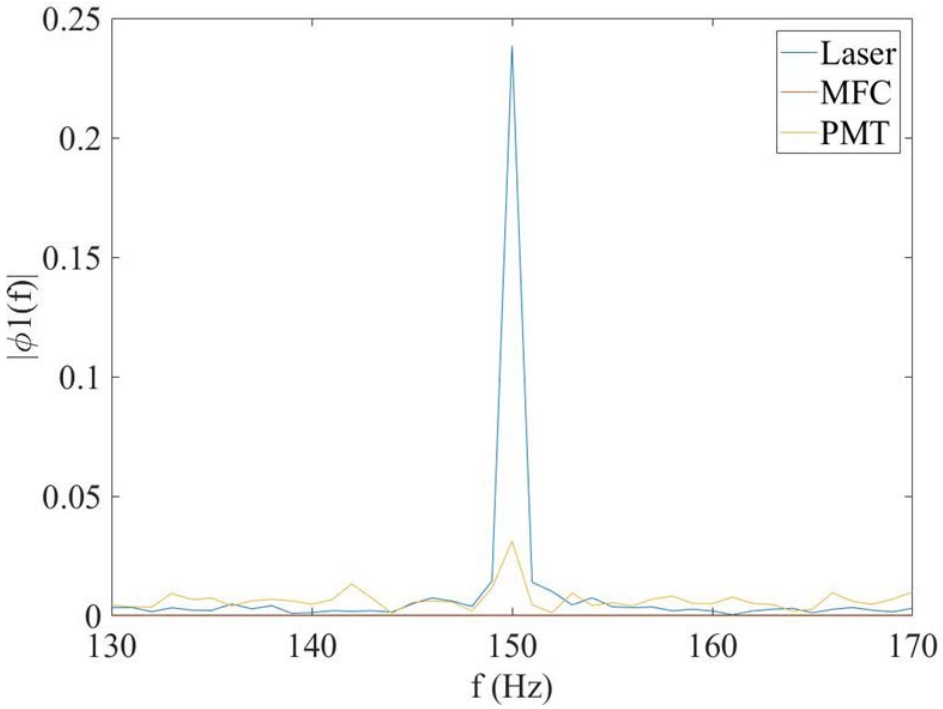

Figure 53. PMT test case with flowrate of 60 SLM, equivalence ratio of 0.7, and acoustically forced at 150 HZ

Following the low power test case, a higher power test case was analyzed. This test was operated at a flowrate of 80 SLM with a global ER of 0.7 and acoustic forcing at 150 Hz. The IRAS measurement was located at location 3 for this test and the PMT probe remained at location 4. The spectrum for this test is shown below in Figure 54. The laser measured a local ER oscillation of 0.1172 while the PMTs measured oscillations of 0.09063. This corresponds to a 20% reduction in ER oscillations. However, results from the cold flow study indicated that this condition should drop by 40%. This meant that the PMT measurement overestimated the ER

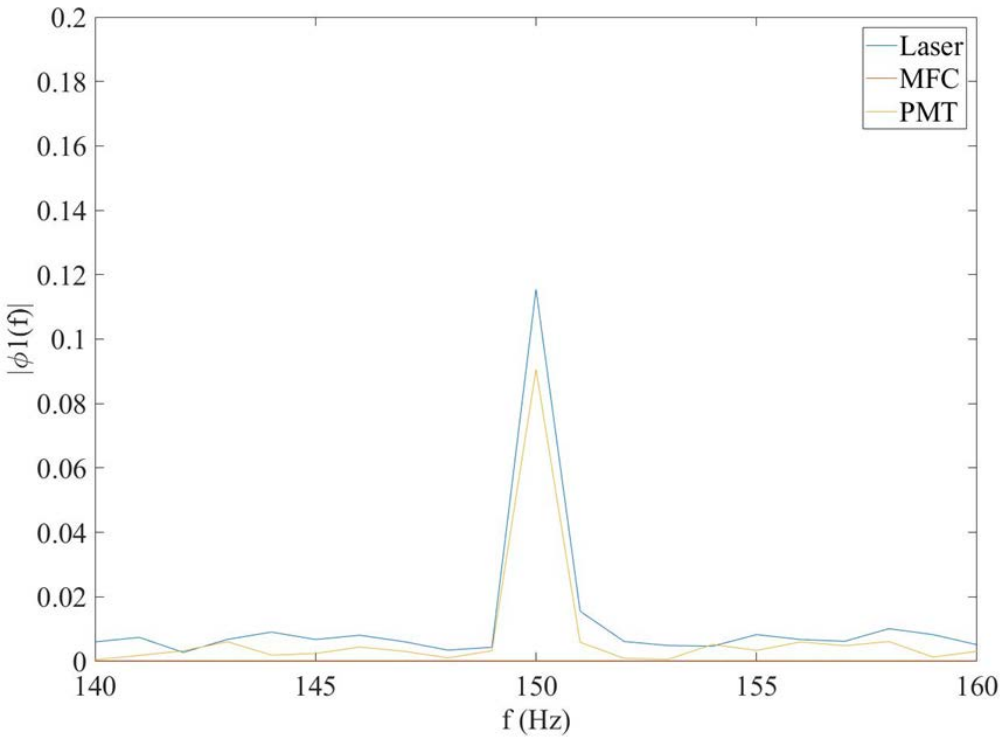

Figure 54. FFT for burning case forced at 150 Hz with flowrate of 80 SLM and equivalence ratio 0.7

oscillations within the flame. This could be due to the change from cold flow to burning as well as an overestimation by the PMT technique.

Finally, an operating condition corresponding to a natural instability was tested. It was found that the burner would go unstable near a flowrate of 90 SLM and global ER of 0.98. The ER spectrum results for this case are shown in Figure 55 with the pressure spectrum in the cutout. The ER shows a large spike at 337 Hz, which is promising as it aligns well with the pressure measurements observed within the combustor. However, again the PMT measurement

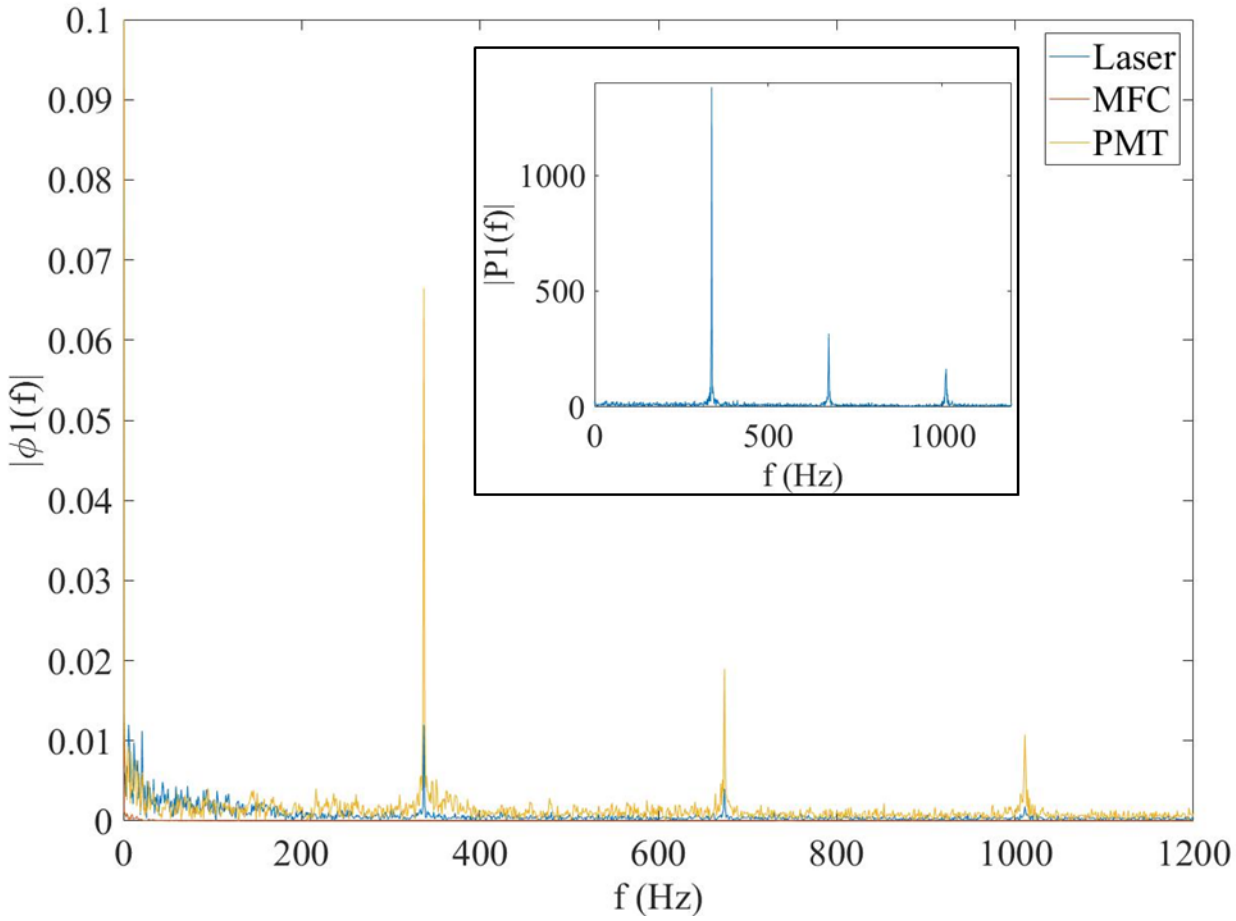

Figure 55. FFT for natural instability burning condition with flowrate of 90 SLM and equivalence ratio of 0.98

far overestimates the ER within the flame. Consequently, this measurement needs more validation before it can confidently predict measurements for equivalence ratio oscillations.

In summary, the PMT ER study seems to indicate promising results for measuring ER within the flame but has more verification required to develop the measurement. The measurement technique showed promising results for steady state ER cases. However, under certain acoustically forced cases and in the MFC oscillation case, the measurement overestimated the ER. This could be due to a number of reasons that impact the light emissions for these wavelengths. Regardless, the technique needs further verification.

Chapter 7: Conclusions

This investigation focused on measuring equivalence ratio oscillations within a lean premixed combustor and analyzing how they propagate downstream from the inlet conditions. This required the development of a combustor that could be operated in multiple configurations and with optical access for diagnostics. This led to the combustor discussed that was capable of operating in a standard burner operation as well as in a swirl burner configuration. This experimental setup was tested and verified to operate at unstable and stable conditions through the use of flow control and acoustic forcing. Next the development of a HeNe laser optical probe to measure the equivalence ratio of a premixed fuel and oxidizer flow based on the work of previous researchers was conducted. This measurement technique proved accurate in measuring equivalence ratios under a variety of both static and dynamic conditions. Finally, a PMT probe to measure the intensity of various radicals within the flame was developed. The relationship between the intensities was used to determine the equivalence ratio within the flame itself. This diagnostic proved less conclusive than the laser equivalence ratio measurement.

The experimental setup was then utilized to conduct studies that analyzed the way in which equivalence ratio oscillations propagated through the burner. The first study was conducted under cold flow conditions to limit the impact that the flame had on the oscillations. The results from this study indicated that the acoustic forcing frequency aided the overall mixing that was occurring within the mixing chamber. This impact was frequency dependent as the higher frequencies exhibited faster mixing in the chamber. Following this, the axial mixing was isolated to understand the impact that the forcing had on reducing equivalence ratio oscillations along the flow path through the combustor. These results showed that the most significant reduction in equivalence ratio oscillations occurred across the swirler. This reduction was

increased by the existence of acoustic forcing but was not frequency dependent. Furthermore, these results showed that the addition of acoustic forcing reduced the equivalence ratio oscillations prior to the swirler but did not show this trend downstream. Next a PMT equivalence ratio study was conducted to evaluate the validity of using chemiluminescence measurements to determine equivalence ratio oscillations. This study found that under steady state and lean conditions this probe measured the equivalence ratio accurately. Furthermore, in some acoustically forced cases the PMT measurement followed the expected trends from the previous cold flow study. However, under certain operating conditions that corresponded to richer burning the measurement began overestimating the equivalence ratio. Consequently, the probe needs further verification.

This study accomplished building and testing a swirl combustor that was successful in providing a test bed for the IRAS probe and the PMT system. The work conducted with the IRAS and the PMT system to measure equivalence ratio oscillations through the combustor can provide information about the way in which oscillations propagate through a mixing chamber and across a swirler. This work can be continued to further verify the PMT system so that it can become a useful diagnostic technique for analyzing combustion instabilities.

7.1 Future Work

This experimental setup and resulting information could be used to provide in-depth information about the way in which equivalence ratio oscillations propagate through a burner. This information and testbed could be used to study fuel line tuners, geometry changes within mixing chambers, or various types of swirlers. Questions about the effectiveness of passive and active fuel line tuners could be analyzed with this experimental system. Further analysis could provide information into the power of the acoustic forcing and its effect on the equivalence ratio

oscillations. This would be useful in determining the goal in which to achieve acceptable damping with equivalence ratio oscillations. Furthermore, the PMT probe could be verified to prove its accuracy under nonstandard operating conditions.

Furthermore, this experimental setup has the capability to measure equivalence ratio, heat release through the CH* emissions, and pressure oscillations. These pieces of information are utilized to create flame transfer functions and heat release transfer functions for combustors. This type of work could lead to improved modeling of combustors and lead to better designs in the future of gas turbine engines.

References

[1] "AERODERIVATIVE AND HEAVY DUTY GAS TURBINES." [Online]. Available: https://www.ge.com/power/gas/gas-turbines.

[2] "BREAKING THE POWER PLANT EFFICIENCY RECORD." .

[3] A. H. Lefebvre, *Gas Turbine Combustion*, 2nd ed. London, UK: Taylor and Francis, 1998.

[4] D. E. Scarborough, "Personal Communication." .

[5] S. Candel, "COMBUSTION DYNAMICS AND CONTROL: PROGRESS AND CHALLENGES," *Proc. Combust. Inst.*, vol. 29, pp. 1–28, 2002.

[6] M. Fleifil, A. M. Annaswamy, Z. A. Ghoneim, and A. F. Ghoniem, "Response of a laminar premixed flame to flow oscillations: A kinematic model and thermoacoustic instability results," *Combust. Flame*, vol. 106, no. 4, pp. 487–510, 1996.

[7] R. KEANINI, A. TROUVE, J. DAILY, K. YU, and L. BAUWENS, "Low frequency pressure oscillations in a model ramjet combustor - The nature of frequency selection," in *27th Aer*, 1989.

[8] K. C. Schadow and E. Gutmark, "Combustion instability related to vortex shedding in dump combustors and their passive control," *Prog. Energy Combust. Sci.*, vol. 18, no. 2, pp. 117–132, 1992.

[9] T. Schuller, D. Durox, and S. Candel, "Dynamics of and noise radiated by a perturbed impinging premixed jet flame," *Combust. Flame*, vol. 128, no. 1–2, pp. 88–110, 2002.

[10] B. . Ayoola, R. Balachandran, E. Mastorakos, C. F. Kaminki, and A. P. Dowling, "Experimental investigation of the nonlinear response of turbulent premixed flames to imposed inlet velocity oscillations," *Combust. Flame*, vol. 143, pp. 37–55, 2005.

[11] B. D. Bellows, Y. Neumeier, and T. Lieuwen, “Forced Response of a Swirling, Premixed Flame to Flow Disturbances,” *J. Propuls. Power*, vol. 22, no. 5, pp. 1075–1084, 2008.

[12] K. T. Kim, J. G. Lee, B. D. Quay, H. J. Lee, and D. A. Santavicca, “Characterization of Forced Flame Response of Swirl-Stabilized Turbulent Lean-Premixed Flames in a Gas Turbine Combustor,” *J. Eng. Gas Turbines Power*, vol. 132, no. 4, p. 041502, 2010.

[13] T. Lieuwen and B. T. Zinn, “The role of equivalence ratio oscillations in driving combustion instabilities in low NOx gas turbines,” *Symp. Combust.*, vol. 27, no. 2, pp. 1809–1816, 1998.

[14] J. G. Lee, K. Kim, and D. A. Santavicca, “MEASUREMENT OF EQUIVALENCE RATIO FLUCTUATION AND ITS EFFECT ON HEAT RELEASE DURING UNSTABLE COMBUSTION,” *Proc. Combust. Inst.*, vol. 28, pp. 415–421, 2000.

[15] T. Lieuwen, H. Torres, C. Johnson, and B. T. Zinn, “A Mechanism of Combustion Instability in Lean Premixed Gas Turbine Combustors,” *J. Eng. Gas Turbines Power*, vol. 123, no. 1, p. 182, 2001.

[16] J. H. Cho and T. Lieuwen, “Laminar premixed flame response to equivalence ratio oscillations,” *Combust. Flame*, vol. 140, no. 1–2, pp. 116–129, 2005.

[17] J. W. Strutt and B. Rayleigh, *The Theory of Sound*, 2nd ed. Macmillan, 1894.

[18] D. Jaynes and B. Beam, “Hydrocarbon Gas Absorption by a HeNe Laser Beam at a 3.39-μ Wavelength,” *Appl. Opt.*, vol. 8, no. 8, pp. 1741–1742, 1969.

[19] T. Tsuboi, K. Inomata, Y. Tsunoda, A. Isobe, and K. Nagaya, “Light Absorption by Hydrocarbon Molecules at 3.392 um of He-Ne Laser,” *Jpn. J. Appl. Phys.*, vol. 24, no. 1, pp. 8–13, 1985.

[20] R. Mongia, R. Dibble, and J. Lovett, “Measurement of Air-Fuel Ratio Fluctuations Caused

by Combustor Driven Oscillations," in *Volume 3: Coal, Biomass and Alternative Fuels; Combustion and Fuels; Oil and Gas Applications; Cycle Innovations*, 1998, no. 2, p. V003T06A026.

[21] K. T. Kim, J. G. Lee, B. D. Quay, and D. Santavicca, "Experimental Investigation of the Nonlinear Response of Swirl-Stabilized Flames to Equivalence Ratio Oscillations," *J. Eng. Gas Turbines Power*, vol. 133, no. 2, p. 021502, 2011.

[22] J. A. Ranalli, C. R. Martin, P. R. Black, U. Vandsburger, and R. West, "Measurement of Flame Transfer Functions in Swirl-Stabilized, Lean-Premixed Combustion," *J. Propuls. Power*, vol. 25, no. 6, pp. 1350–1354, 2009.

[23] Y. Ikeda, J. Kojima, T. Nakajima, F. Akamatsu, and M. Katsuki, "Measurement of the local flamefront structure of turbulent premixed flames by local chemiluminescence," *Proc. Combust. Inst.*, vol. 28, no. 1, pp. 343–350, 2000.

[24] B. Higgins, M. Q. McQuay, F. Lacas, J. C. Rolon, N. Darabiha, and S. Candel, "Systematic measurements of OH chemiluminescence for fuel-lean, high-pressure, premixed, laminar flames," *Fuel*, vol. 80, no. 1, pp. 67–74, 2001.

[25] R. Layeka, A. Dattaa, R. Palb, and E. R. Dougherty, "Diagnostic techniques for the monitoring and control of practical flame," *Prog. Energy Combust. Sci.*, vol. 36, pp. 375–411, 2010.

[26] Y. Hardalupas, C. S. Panoutsos, and A. M. K. P. Taylor, "Spatial resolution of a chemiluminescence sensor for local heat-release rate and equivalence ratio measurements in a model gas turbine combustor," *Exp. Fluids*, vol. 49, no. 4, pp. 883–909, 2010.

[27] S. Sardeshmukh, M. Bedard, and W. Anderson, "The use of OH* and CH* as heat release markers in combustion dynamics," *Int. J. Spray Combust. Dyn.*, vol. 9, no. 4, pp. 409–423,

2017.

[28] Y. Hardalupas *et al.*, “Chemiluminescence sensor for local equivalence ratio of reacting mixtures of fuel and air (FLAMESEEK),” *Appl. Therm. Eng.*, vol. 24, no. 11–12, pp. 1619–1632, 2004.

[29] N. Docquier, F. Lacas, and S. Candel, “Closed-loop equivalence ratio control of premixed combustors using spectrally resolved chemiluminescence measurements,” *Proc. Combust. Inst.*, vol. 29, no. 1, pp. 139–145, 2002.

[30] T. S. Cheng, C. Y. Wu, Y. H. Li, and Y. C. Chao, “Chemiluminescence measurements of local equivalence ratio in a partially premixed flame,” *Combust. Sci. Technol.*, vol. 178, no. 10–11, pp. 1821–1841, 2006.

[31] C. S. Panoutsos, Y. Hardalupas, and A. M. K. P. Taylor, “Numerical evaluation of equivalence ratio measurement using OH*and CH*chemiluminescence in premixed and non-premixed methane-air flames,” *Combust. Flame*, vol. 156, no. 2, pp. 273–291, 2009.

[32] M. Orain and Y. Hardalupas, “Influence du combustible sur la mesure de richesse par chimiluminescence dans les flammes prémélangées,” *Comptes Rendus - Mec.*, vol. 338, no. 5, pp. 241–254, 2010.

[33] Y. Hardalupas and M. Orain, “Local measurements of the time-dependent heat release rate and equivalence ratio using chemiluminescent emission from a flame,” *Combust. Flame*, vol. 139, no. 3, pp. 188–207, 2004.

[34] T. M. Muruganandam *et al.*, “Optical equivalence ratio sensors for gas turbine combustors,” *Proc. Combust. Inst.*, vol. 30, no. 1, pp. 1601–1608, 2005.

[35] “Fused Silica/Quartz Glass - Properties and Applications of Fused Silica/Quartz Glass by Goodfellow Ceramic & Glass Division,” *AZO Materials*. .

[36] “PMM01 Amplified Photomultiplier Tube User Guide.” Thorlabs, p. 4.

[37] R. H. Dieck, *Measurement Uncertainty: Methods and Applications*, 4th Editio. ISA, 2007.

Appendix I

LabVIEW Control Panel

Appendix II

Repeatability Results

				Test Iteration								
Measurement Location	Frequency	Equivalence Ratio	Flowrate (SLM)	1	2	3	4	5	AVG	St Dev	%	Avg St Dev
1	0	0.7	60	0.650	0.655	0.656	0.659	0.650	0.654	0.00395	0.6%	0.64%
1	0	0.7	80	0.678	0.685	0.689	0.693	0.694	0.688	0.00642	0.9%	
1	0	0.9	60	0.887	0.893	0.898	0.896	0.898	0.894	0.00471	0.5%	
1	0	0.9	80	0.869	0.879	0.881	0.877	0.874	0.876	0.00451	0.5%	
1	150	0.7	60	0.030	0.029	0.031	0.031	0.029	0.030	0.00103	3.4%	2.78%
1	150	0.7	80	0.033	0.033	0.033	0.032	0.030	0.032	0.00098	3.0%	
1	150	0.9	60	0.042	0.041	0.040	0.040	0.040	0.040	0.00073	1.8%	
1	150	0.9	80	0.038	0.037	0.037	0.039	0.036	0.037	0.00106	2.8%	
1	500	0.7	60	0.026	0.026	0.025	0.025	0.025	0.025	0.00037	1.5%	1.42%
1	500	0.7	80	0.026	0.026	0.027	0.026	0.026	0.026	0.00044	1.7%	
1	500	0.9	60	0.034	0.034	0.033	0.033	0.033	0.033	0.00058	1.7%	
1	500	0.9	80	0.033	0.033	0.033	0.033	0.033	0.033	0.00025	0.8%	
1	1.1 ~ 0.2 at 2 Hz		80	0.151	0.149	0.145	0.147	0.151	0.149	0.00248	1.7%	1.7%
4	0	0.7	60	0.669	0.676	0.676	0.675	0.671	0.674	0.00315	0.5%	0.56%
4	0	0.7	80	0.675	0.678	0.679	0.674	0.671	0.675	0.00313	0.5%	
4	0	0.9	60	0.851	0.857	0.855	0.850	0.842	0.851	0.00575	0.7%	
4	0	0.9	80	0.828	0.834	0.835	0.828	0.822	0.829	0.00523	0.6%	
4	150	0.7	60	0.025	0.023	0.022	0.025	0.023	0.023	0.00120	5.1%	3.14%
4	150	0.7	80	0.024	0.024	0.025	0.024	0.025	0.024	0.00057	2.3%	
4	150	0.9	60	0.029	0.029	0.030	0.028	0.028	0.029	0.00074	2.6%	
4	150	0.9	80	0.029	0.030	0.031	0.029	0.029	0.029	0.00075	2.6%	
4	500	0.7	60	0.008	0.008	0.008	0.008	0.008	0.008	0.00019	2.3%	2.46%
4	500	0.7	80	0.008	0.009	0.009	0.008	0.008	0.008	0.00030	3.6%	
4	500	0.9	60	0.011	0.011	0.011	0.011	0.010	0.011	0.00029	2.7%	
4	500	0.9	80	0.010	0.011	0.011	0.010	0.011	0.011	0.00013	1.2%	
4	1.1 ~ 0.2 at 2 Hz		80	0.113	0.122	0.123	0.120	0.119	0.119	0.00427	3.6%	3.6%

Appendix III

Error Analysis

An error analysis was conducted on the process used to calculate the ER from the absorption measurements in the experiment. This was conducted with the Taylor Series uncertainty propagation method.[37] As stated in Chapter 4, the equation used to calculate the mole fraction of fuel follows:

$$x_f = \frac{\ln\left(\frac{I}{I_0}\right)}{-\alpha \cdot L \cdot P} \tag{7.1}$$

The equation to calculate the equivalence ratio with this mole fraction is:

$$\phi = \frac{23.9 \cdot x_f}{1 - x_f} \tag{7.2}$$

The error from these combined equations follows using the Taylor Series uncertainty propagation method:

$$\varepsilon^2 = \left(\frac{\partial \phi}{\partial x_f}\frac{\partial x_f}{\partial I}\delta I\right)^2 + \left(\frac{\partial \phi}{\partial x_f}\frac{\partial x_f}{\partial I_0}\delta I_0\right)^2 + \left(\frac{\partial \phi}{\partial x_f}\frac{\partial x_f}{\partial \alpha}\delta \alpha\right)^2 + \left(\frac{\partial \phi}{\partial x_f}\frac{\partial x_f}{\partial L}\delta L\right)^2 + \left(\frac{\partial \phi}{\partial x_f}\frac{\partial x_f}{\partial P}\delta P\right)^2 \tag{7.3}$$

The sensitivity coefficients follow as:

$$\frac{\partial \phi}{\partial x_f} = \frac{23.9}{\left(1 - x_f\right)^2} \tag{7.4}$$

$$\frac{\partial x_f}{\partial I} = \frac{1}{-\alpha \cdot L \cdot P} \cdot \frac{1/I_0}{I/I_0} = \frac{1}{-\alpha \cdot L \cdot P \cdot I} \tag{7.5}$$

$$\frac{\partial x_f}{\partial I_0} = \frac{1}{-\alpha \cdot L \cdot P} \cdot \frac{-I/I_0^{\,2}}{I/I_0} = \frac{1}{\alpha \cdot L \cdot P \cdot I_0} \tag{7.6}$$

$$\frac{\partial x_f}{\partial \alpha} = \frac{\ln\left(I/I_0\right)}{\alpha^2 \cdot L \cdot P} \tag{7.7}$$

$$\frac{\partial x_f}{\partial L} = \frac{\ln\left(I/I_0\right)}{\alpha \cdot L^2 \cdot P} \tag{7.8}$$

$$\frac{\partial x_f}{\partial P} = \frac{\ln\left(I/I_0\right)}{\alpha \cdot L \cdot P^2} \tag{7.9}$$

The coefficients were calculated for the ranges of the intensity measurements typically measured in the experiments. This included I from 0.05 to 0.15 and I0 from 0.10 to 0.20. The sensitivity values for the changing intensity measurement I follow in Figure 56 and the values for changing I0 are in Figure 57

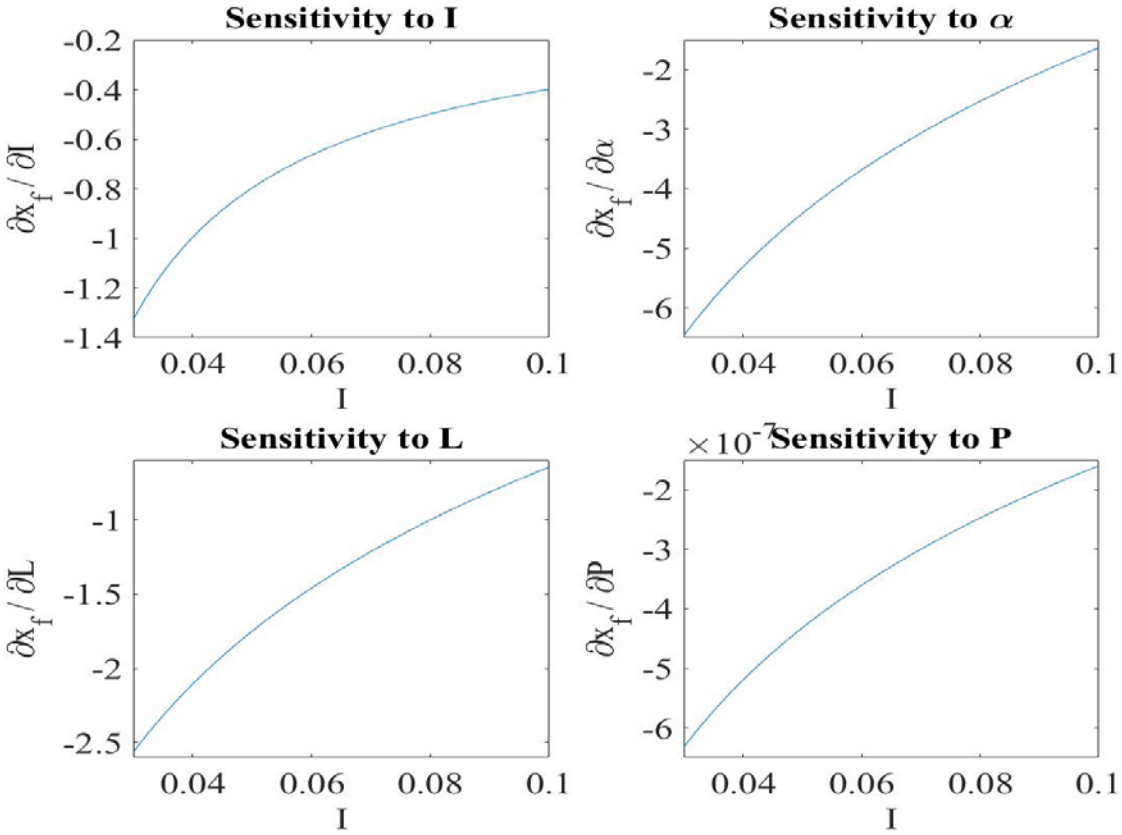

Figure 56. Sensitivity coefficients in relation to I

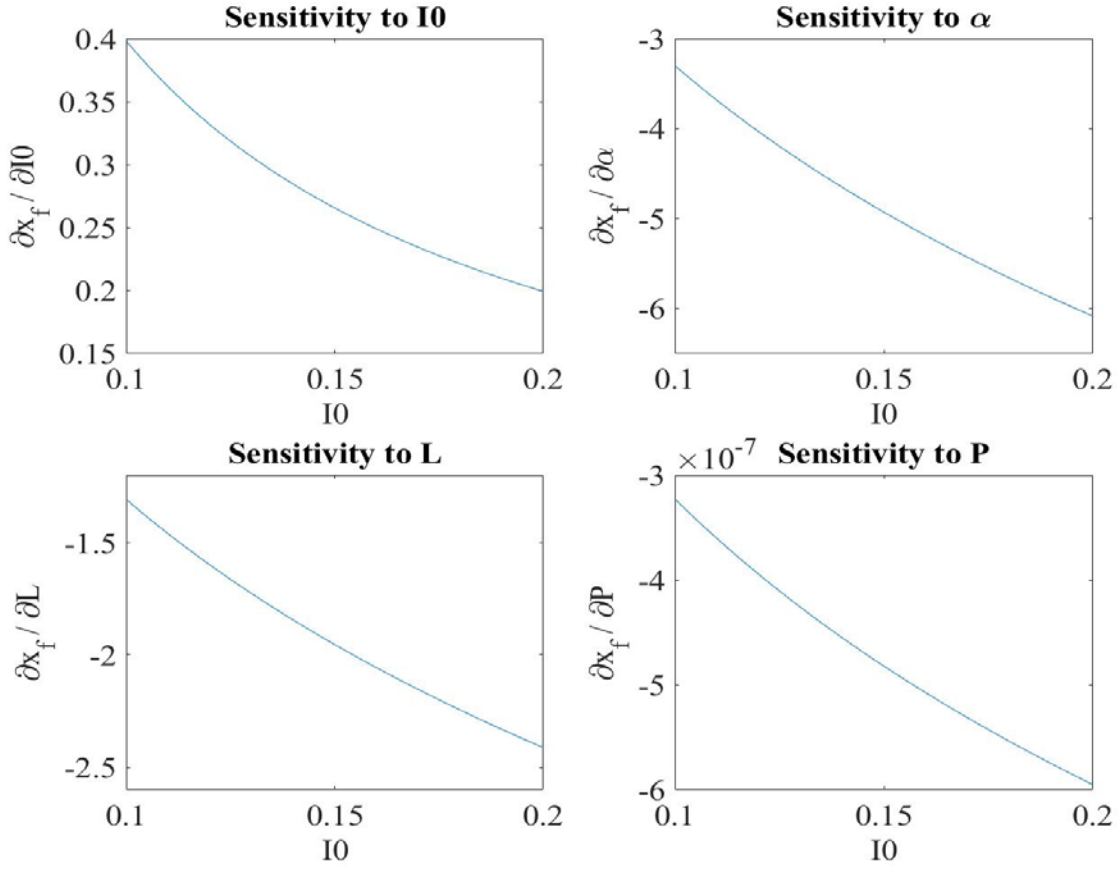

Figure 57. Sensitivity coefficients in relation to I0

Next, the values for standard conditions were analyzed to calculate the total error observed in the measurement. To do this, an error will be assumed for each variable of 3% based on the random error observed in the repeatability study and bias error expected from the measurements. This resulted in an error of 0.06120 which corresponds to a percent error of measured value of 7.6%.

Appendix IV

Reynolds Numbers

Total Flowrate (SLM)	Phi	Air Flowrate (SLM)	Fuel Flowrate (SLM)	Air Velocity (m/s)	Fuel Velocity (m/s)	Air Re #	Fuel Re #
60	0.7	56.62	3.38	2.89	3.44	3896	3606
60	0.8	57.02	2.98	2.91	3.03	3924	3177
60	0.9	57.33	2.67	2.92	2.71	3945	2840
70	0.7	66.05	3.95	3.37	4.01	4545	4207
70	0.8	66.52	3.48	3.39	3.53	4578	3707
70	0.9	66.89	3.11	3.41	3.16	4603	3313
80	0.7	75.49	4.51	3.85	4.58	5195	4807
80	0.8	76.02	3.98	3.88	4.04	5232	4236
80	0.9	76.45	3.55	3.90	3.61	5261	3787

Propane		Air	
ρ (kg/m^3)	1.84	ρ (kg/m^3)	1.20
μ (kg/m-s)	8.02E-06	μ (kg/m-s)	1.82E-05
L (m)	0.0046	L (m)	0.0204
A (m^2)	1.64E-05	A (m^2)	3.27E-04

Strouhal Numbers

Frequency (Hz)	Total Flowrate (SLM)	Flow Velocity (m/s)	Strouhal #
0	60	2.04	0.00
0	70	2.38	0.00
0	80	2.72	0.00
100	60	2.04	1.23
100	70	2.38	1.05
100	80	2.72	0.92
150	60	2.04	1.84
150	70	2.38	1.58
150	80	2.72	1.38
300	60	2.04	3.68
300	70	2.38	3.16
300	80	2.72	2.76
400	60	2.04	4.91
400	70	2.38	4.21
400	80	2.72	3.68
500	60	2.04	6.14
500	70	2.38	5.26
500	80	2.72	4.60